Ph. D. thesis

Quantum Phase Transitions in Correlated Systems

Ákos Rapp

Supervisor: Prof. Gergely Zaránd
Department of Theoretical Physics
Budapest University of Technology and Economics

BUTE
2008

Gergőnek, Dávidnak és édesapámnak.

Köszönetnyilvánítás

Ez a dolgozat nem jöhetett volna létre számos ember munkája és áldozata nélkül, akiknek ezért sok köszönettel tartozom. Nagyon köszönöm Prof. Zaránd Gergelynek a közös munkát és irányítását, ezek a munkám alapját jelentették. Köszönöm a hitvesemnek megértését és türelmét, édesanyámnak minden áldozatát. Nagyon hálás vagyok Prof. Kertész Jánosnak és különösen Prof. Zawadowski Alfrédnek tanácsaikért és állandó támogatásukért. Nagyon nagyra értékelem Dr. Borda László segítségét. Köszönöm Dr. Varga Imrének a dolgozattal kapcsolatos javaslatait. Örülök, hogy az elmúlt éveket az Elméleti Fizika Tanszéken tölthettem, ahol kedves és segítőkész munkatársakkal dolgozhattam együtt. Munkámat az OTKA a NF061726, T046303, T046267, T049571 és a NI70594 számú pályázatokon keresztül támogatta.

Contents

Chapter 1

Introduction

In this thesis we shall investigate the properties of systems with strong correlations. Correlations are present even in ideal gases: at low temperatures, quantum statistics manifest in entirely different behavior of bosons and fermions. The situation gets more interesting and also more involved when interactions are present. In contrast to ideal gases, the general theoretical description of interacting systems is not possible, furthermore, only a minor fraction of models could have been solved exactly. Interactions present the possibility of new types of collective behavior, and the system can evolve to a more complex level of existence.

In the first chapter, we shall review some general concepts about second order quantum phase transitions. First we shall briefly discuss how the effects of zero temperature phase transitions appear in experiments. Then we shall turn our attention to the theory of the probably simplest model exhibiting quantum critical behavior, the Ising chain in a transversal magnetic field.

In the second chapter, we shall investigate the dynamical properties of the quantum Potts model in one dimension at low temperatures. The discussion involves both the quantum critical region in the $Q = 3$ case and the gapped phases, where a semiclassical approximation shall be applied. As a generalization of the semiclassical method, we shall also discuss dynamical correlations in other gapped one-dimensional spin models.

In the third chapter, we shall briefly review the basic properties of ultracold atomic systems. This discussion will serve as a motivation for the study of the three component attractive Hubbard model. We shall see that the ground state in infinite dimensions can be approximated by a Gutzwiller variational wave function. We shall present the details of this calculation and discuss some generalizations to realistic systems.

I shall summarize my scientific results in thesis points in the Summary. These thesis points are the conclusions of the calculations presented in Sections 2.3.3, 2.4.2- 2.4.5, 2.5.3 - 2.5.5, and 3.3.3 - 3.3.6. Some of the more technical derivations have been transferred to the appendices.

1.1 Phase transitions

The materials in the surrounding world can be found in different phases, which are usually characterized by certain macroscopic quantities. Phase transitions take

place when some control parameter is tuned through a transition point. These transitions are associated with the singularities of thermodynamic quantities and, accordingly, can be traditionally classified as first-order or second-order transitions. In experiments, control parameters can be temperature, pressure, magnetic and electric fields or doping. When the phase transition is happening between an ordered and a disordered phase, it is possible to construct an order parameter compatible with the symmetries of the system, vanishing in the disordered phase while being finite in the ordered phase. Although for a ferromagnetic - paramagnetic transition the choice of this order parameter is usually obvious, there are also systems with hidden order, where the nature of the order parameter is unknown. It is possible to define the correlation function of the order parameter. Far away from a phase transition, these correlations decay usually exponentially, defining the characteristic length- and timescale, ξ and τ, respectively.

The most common phase transitions are first order phase transitions. The phases coexist at the transition point and the order parameter jumps at the phase boundary. Latent heat is disengaged at the phase transition as a signature of a discontinuity in the entropy. The correlation length ξ is finite at the transition.

At second order transitions, the order parameter vanishes continuously at $T = T_C$, when increasing the temperature. The correlation length diverges as $\xi \sim |T - T_C|^{-\nu}$ and the correlation time as $\tau \sim |T - T_C|^{-z\nu}$, where z is the dynamical critical exponent. Usually, there exists an upper critical dimension d_c for a given phase transition, so that the fluctuations do not play an essential role and mean field approximations become exact close to the transition point for a system with dimension $d > d_c$. There is a number of physical systems, however, where the upper critical dimension is $d_c \geq 4$ and fluctuations become important close to the transition temperature.

Spontaneous breaking of symmetry is also an important signature of a phase transition: the disordered phase typically exhibits the symmetries of the microscopic model. This manifests also in the vicinity of the global minimum of the thermodynamic potential, which usually also has large symmetry in the disordered phase. The second order transition shifts the global minimum in a direction chosen spontaneously to a point of reduced symmetry in parameter space.

1.2 Quantum phase transitions

As the correlation length diverges in second order phase transitions, universal *classical* behavior can be observed in a region close to the phase boundary at finite temperatures. Would this mean that all critical theories are classical? This question was first investigated by Hertz [Her76] in the context of itinerant ferromagnets, and was extended by Millis [Mil93].

The answer to the question how quantum mechanics can play any important role in second order phase transitions lies in the fact that the critical temperature T_C also depends on other parameters, e. g., pressure or doping. By changing these quantities, the transition temperature can be modified. In principle, there is no lower bound where it should saturate and in some cases, it is possible to suppress it down to $T_C = 0$. When $T_C > 0$, thermal fluctuations are driving the transition and as the correlation length diverges, there is a threshold where classical behavior emerges. For $T_C = 0$, however, thermal fluctuations are absent, and the order is destroyed entirely by quantum fluctuations. Most importantly, this zero tem-

perature transition can have a major impact on the behavior of the system for a relatively large temperature region.

We are also able to sketch the generic phase diagrams of these system as a function of temperature and some control parameter g, which can be associated with pressure, doping concentration, or magnetic fields. For a class of materials, a continuous phase transition happens at finite temperature, as shown in Fig. 1.1. The transition temperature can be tuned to zero by the control parameter at $g = g_c$. At $T = 0$ for $g > g_c$, a disordered phase can be found with long-range order destroyed by quantum fluctuations in the ground state. Anomalous behavior can be observed in a region $T > T^-$ and $T > T^+$ where the scaling properties of static quantities are also affected by the dynamical scaling exponent z of the quantum phase transition. The crossover temperatures $T^{\pm}$ scale with $|g - g_c|$. The quantum critical region reaches up to relatively large temperatures, while the region with classical scaling behavior can be observed only in the vicinity of the second order phase transition line. For certain systems, long-range order may be absent for finite temperatures, however, they can have an ordered ground state and a $T = 0$ temperature continuous phase transition. These belong to the other class of materials, shown on the other phase diagram in Fig. 1.1.

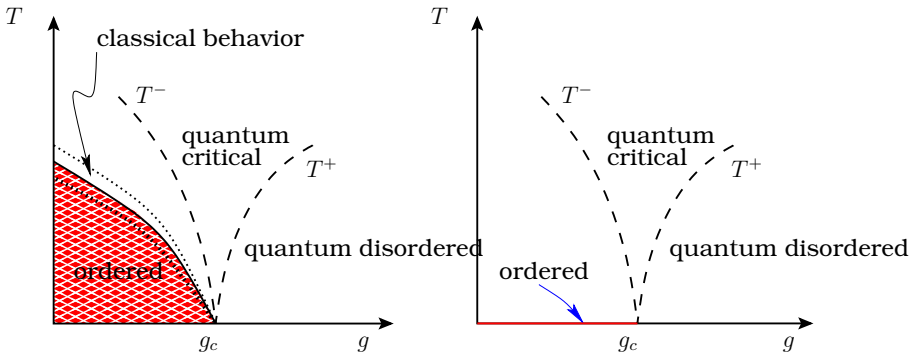

Figure 1.1: Generic phase diagrams around a quantum critical point at $T = 0$, $g = g_c$.

We remark that quantum critical transitions can happen between phases with distinct order parameters. There is a quantum phase transition in two-dimensional antiferromagnets between different ordered phases. This transition is beyond the Ginzburg-Landau-Wilson paradigm of second-order phase transitions at finite temperatures [Sen04a, Sen04b].

Let us now focus on experimental systems, where quantum critical behavior has been observed. We selected a handful of materials to show that continuous quantum phase transitions appear in numerous systems, ranging from $d = 0$ dimensional quantum dots to $d = 3$ dimensional materials.

Heavy fermion materials

There is a large number of heavy fermion materials that show quantum critical behavior, however, the dynamical properties have not been studied extensively. An important observation of the effects of a quantum phase transition was made on $CeCu_6$ doped by Au [Loh94].

For small dopings, this compound shows typical "heavy fermion" behavior. The Landau theory of Fermi-liquids predicts that the electronic specific heat of metallic materials is proportional to temperature, determining the Sommerfeld coefficient. In $CeCu_6$ with small concentrations $x \ll 1$ of Au, this coefficient saturates at low temperatures to a value which is three orders of magnitude larger than in simple metals. The heavy fermion nomination comes from the increased effective mass, which is proportional to the Sommerfeld coefficient in a Fermi-liquid.

As the doping is increased, the Sommerfeld ratio diverges at $x_c \approx 0.1$ within experimental accuracy. At this critical doping, the resistivity also shows anomalous behavior and increases linearly with temperature. For a normal metal, a quadratic $\sim T^2$ behavior is expected due to quasiparticle scattering in the Fermi-liquid.

For $x \geq 0.2$, antiferromagnetic order develops below the Neél temperature $T_N \leq 1$ K, which increases linearly with the doping concentration. The anomalous behavior is visible up to the temperature range $T \approx 1$K.

On the matter of quantum critical behavior and heavy fermions, we would also like to turn the attention of the Reader to a recent review by Coleman and Schofield [Col05].

Bilayer ^{3}He

Very recently, a continuous quantum phase transition in a bilayer of ^{3}He was observed [Neu07]. This system is an example of $d = 2$ dimensional systems exhibiting quantum critical behavior. In the experiment, ^{3}He was absorbed on a bilayer of solid ^{4}He on a graphite substrate. As a function of the coverage (atoms over a unit area), a first, and then a second layer of ^{3}He was formed. Initially, the second layer behaved like a Fermi-liquid, exhibiting large effective mass, i.e., heavy fermion behavior, at temperatures $T < T_0$. The Fermi-liquid temperature scale T_0 decreased as a function of the coverage and finally vanished at the quantum critical point.

"A model magnet" - $LiHoF_4$

In Section 1.3, we shall discuss the probably simplest model with a quantum critical point, the Ising chain in a transversal magnetic field. This model can be realized using $LiHoF_4$. This material is a uniaxial material, where Ho ions are well described by the Ising model at low temperatures. By applying a magnetic field perpendicular to the easy axis, Bitko et. al. demonstrated that a quantum phase transition happens at a certain magnetic field strength, where the ferromagnetic order is destroyed [Bit96].

A second important observation was also made. Being an Ising material, the upper critical dimension for the classical ferromagnetic transition is $d_c = 4$. Bitko and colleagues observed an unusual phenomenon: in the quantum critical region, the material behaved as if it was a $D = d + z \geq d_c$ dimensional system, i.e., it showed mean field behavior.

The two-channel Kondo effect in a single electron transistor

In the single-channel Kondo model a single impurity is coupled to a bath of electrons. At very low temperatures $T \leq T_K$, the impurity spin forms a singlet with the conduction electrons. In a metal with magnetic impurities this leads to an increase in the resistivity at low temperatures. An analogous effect can be observed also in

$d = 0$ dimensional quantum dots. These quantum dots can be manufactured by attaching specific electrodes to a semiconductor heterostructure, and the Kondo effect manifests as an increase of the conductance at low temperature for dots having odd number of electrons [Gol98].

In the two channel Kondo model [Noz80, Zaw80], an $S = 1/2$ impurity spin interacts with two independent baths of electrons, thus there is a competition between the two couplings. For large asymmetry, the stronger coupling (having a larger Kondo-temperature T_K) wins, and a one-channel Kondo effect appears. When the difference in the couplings is small, however, a two-channel Kondo effect emerges showing non-Fermi-liquid behavior. This exotic region can be interpreted as a quantum critical region, and was recently realized and observed by the group of Goldhaber-Gordon [Poto07].

Ultracold atoms in magnetic traps and optical lattices

A relatively new field in experimental physics investigates atomic vapors cooled to the quantum degenerate limit. By now, both bosonic and fermionic systems can be trapped and manipulated routinely. In these systems, external "static potentials", interactions and even disorder can be tuned in a flexible way, thus ultracold gases offer a new possibility for simulating the properties of correlated condensed matter systems. The realization of bosonic Mott insulators and the observation of the fermionic BEC-BCS transition are among the most famous achievements of this field. We shall dedicate a longer introduction to ultracold atomic systems in Section 3.1.

The previous selection of materials shows that second order quantum phase transitions can be observed in many interesting correlated systems. Before we discuss the simplest theoretical model exhibiting quantum critical behavior, the transverse field Ising model, we shall predefine some variables and declare some conventions for clarity. The physical dimension of a model will be noted by d, while for the number of sites in a lattice, we shall use N. If not noted otherwise, temperatures (T) and frequencies (ω) will be measured in units of energy, by setting Boltzmann's and Planck's constants to unity: $k_{\mathrm{B}} = 1$; $\hbar = 1$. The inverse temperature therefore shall be given by $\beta = 1/T$. Quantummechanical operators shall be noted by hats, or in special cases, by tildes.

1.3 The Ising chain in a transverse field

Possibly the simplest model exhibiting a quantum phase transition is the Ising chain in a transverse magnetic field, defined by the Hamiltonian

$$\hat{H}_I = -J \sum_i \hat{\sigma}_i^z \hat{\sigma}_{i+1}^z - Jg \sum_i \hat{\sigma}_i^x \ . \tag{1.1}$$

Here the operators $\hat{\sigma}$ are represented by the corresponding Pauli matrices, $J > 0$ is a ferromagnetic coupling between the Ising spins and the control parameter g is proportional to the strength of the transverse magnetic field.

The model defined by Eq. (1.1) can be shown to exhibit a phase transition in the ground state. If g is small, the energy is minimized by aligning the spins parallel leading to a ferromagnetic ground state. However, for large g, the magnetic field

turns the spins to a perpendicular direction. The competition between the two terms in the Hamiltonian leads to a phase transition at $T = 0$ [Sac99].

The limits $g \ll 1$ and $g \gg 1$ can be analyzed following simple perturbation theory. This will be given in the context of the quantum Potts model in Chapter 2 as a possible generalization of the Ising model in a transverse field. However, due to its structure, the Hamiltonian of the Ising model in a transverse magnetic field can be diagonalized in terms of fermionic variables, giving the exact quasiparticle spectrum, as shown in the next subsection.

1.3.1 Exact spectrum

To obtain the exact spectrum of the transverse field Ising model, we observe that the eigenstates of $\hat{\sigma}^z$ can be mapped to the Fock space of spinless fermions. However, the Pauli matrices obey commutation rules, while fermionic creation operators are anticommuting. This discrepancy can be avoided using a Jordan-Wigner transformation

$$\hat{\sigma}_i^x = 1 - 2\hat{c}_i^+ \hat{c}_i \tag{1.2}$$

$$\hat{\sigma}_i^z = -\prod_{j<i}(1 - 2\hat{c}_j^+ \hat{c}_j\,)(\hat{c}_i\ + \hat{c}_i^+), \tag{1.3}$$

where the fermionic operators obey the anticommutation relations $\{\hat{c}_i, \hat{c}_j^+\} = \delta_{ij}$, $\{\hat{c}_i, \hat{c}_j\} = \{\hat{c}_i^+, \hat{c}_j^+\} = 0$. Note that this transformation is a non-local mapping from the spin Hilbert space to the fermionic Fock space. Substitution of Eqs. (1.2) and (1.3) into the Hamiltonian in Eq. (1.1) gives the expression

$$\hat{H}_I = -J\sum_i \left(\hat{c}_i^+ \hat{c}_{i+1} + \hat{c}_{i+1}^+ \hat{c}_i + \hat{c}_i^+ \hat{c}_{i+1}^+ + \hat{c}_i \hat{c}_{i+1} - 2g\hat{c}_i^+ \hat{c}_i - g\right)\ , \tag{1.4}$$

which is quadratic in the fermionic variables. To diagonalize Eq. (1.4), we first apply a Fourier transformation in coordinate space. For a chain of N sites, we introduce $\hat{c}_i = \frac{1}{\sqrt{N}}\sum_k e^{ikx_i}\hat{c}_k$, which gives

$$\hat{H}_I = J\sum_k \left(2[g - \cos ka]\hat{c}_k^+ \hat{c}_k - i\sin ka[\hat{c}_{-k}^+ \hat{c}_k^+ + \hat{c}_{-k}\hat{c}_k] - g\right)\ , \tag{1.5}$$

where a is the lattice spacing, $x_i = ia$ is the position of site i and $k = \frac{2\pi}{Na}n$ ($n = -\frac{N}{2}\ldots\frac{N}{2}$) is the wave number. Next, we proceed with Eq. (1.5) using a Bogoliubov transformation within the Nambu blocks $(\hat{c}_k^+, \hat{c}_{-k})$. To this end, we regroup terms as

$$\hat{H}_I = J\sum_k (\hat{c}_k^+, \hat{c}_{-k}) \begin{pmatrix} g - \cos ka & i\sin ka \\ -i\sin ka & -(g - \cos ka) \end{pmatrix} \begin{pmatrix} \hat{c}_k \\ \hat{c}_{-k}^+ \end{pmatrix} - J\sum_k \cos ka\ . \tag{1.6}$$

The block matrix can then be diagonalized by the unitary matrix

$$\mathcal{U}_k = \begin{pmatrix} \cos(\theta_k/2) & i\sin(\theta_k/2) \\ i\sin(\theta_k/2) & \cos(\theta_k/2) \end{pmatrix}\ , \tag{1.7}$$

with $\tan\theta_k = \frac{\sin ka}{\cos ka - g}$. The Hamiltonian after the transformation simply reads

$$\hat{H}_I = \sum_k \epsilon_k(\hat{a}_k^+ \hat{a}_k - 1/2)\ , \tag{1.8}$$

with

$$\hat{a}_k = \cos(\theta_k/2)\ \hat{c}_k - i\sin(\theta_k/2)\ \hat{c}^+_{-k}\ , \tag{1.9}$$

the annihilation operator of a quasiparticle, and

$$\epsilon_k = 2J\sqrt{1+g^2-2g\cos ka} \tag{1.10}$$

its energy.

As we can see, $\epsilon_k \geq 0$, and therefore the ground state of the Ising model in an arbitrary transverse magnetic field is equivalent to the vacuum state of a spinless fermionic system. The quasiparticles have a gap at $k = 0$, given by

$$|\Delta(g)| = 2J|1-g|\ , \tag{1.11}$$

and the gap vanishes for the critical value $g = g_c = 1$. At this point of the parameter space, long wavelength excitations are possible with arbitrary small energies, which leads to an anomalous, quantum critical behavior in the region $J > T \gg |\Delta(g)|$. The dynamical properties of this region shall be discussed in the next subsection.

Although it is hard to visualize the quasiparticles in terms of the spin operators for general g, in the limiting cases they can be interpreted as follows. For $g \ll 1$, the ground state is a ferromagnet (although long-range order is immediately destroyed at finite temperatures), and the quasiparticles can be visualized as domain walls. For $g \gg 1$, where the spins are polarized in the $+x$ direction in the ground state, excitations are spins flipped to $-x$. These quasiparticles can propagate along the chain for finite values of g in both phases [Sac99].

1.3.2 Quantum critical region

As we have seen in the last subsection, soft, long wavelength modes exist for temperatures $J > T \gg |\Delta(g)|$, which also dominate the thermodynamic behavior. We construct a continuum Hamiltonian to get rid of the short wavelength degrees of freedom, which do not play a relevant role in the critical behavior.

To achieve this goal, we start from Eq. (1.4). First, we replace the fermionic operators by the continuum field operators

$$\hat{\Psi}(x_i) = \frac{1}{\sqrt{a}}\hat{c}_i\ , \tag{1.12}$$

which obey in the limit $a \to 0$ the continuum relation $\{\hat{\Psi}(x), \hat{\Psi}^+(x')\} = \delta(x-x')$. Substituting Eq. (1.12) into the Hamilton operator Eq. (1.4) and expanding it in first order in the gradients gives the expression

$$\hat{H}_I = E_0 + \int dx \left[\frac{c}{2}(\hat{\Psi}^+\partial_x\hat{\Psi}^+ - \hat{\Psi}\partial_x\hat{\Psi}) + \Delta\hat{\Psi}^+\hat{\Psi}\right] + \mathcal{O}(a)\ , \tag{1.13}$$

where $c = 2Ja$, and $\Delta = 2J(1-g)$. The continuum limit $a \to 0$ is taken while keeping Ψ, c and Δ fixed. Thus the continuum limit implies both $J \to \infty$ and $g \to 1$. In the same limit, the quasiparticle energy has the relativistic form $\epsilon_k = \sqrt{\Delta^2 + c^2k^2}$.

Using Eq. (1.13), we can write the partition function in a path integral representation, following Ref. [Neg98], as

$$\mathcal{Z} = \int \mathcal{D}\Psi\mathcal{D}\bar{\Psi}\ \exp\left\{-\int_0^{T^{-1}} d\tau \int dx\ \mathcal{L}_I\right\}\ , \tag{1.14}$$

with the Lagrange density

$$\mathcal{L}_I = \bar{\Psi}\partial_\tau \Psi + \frac{c}{2}(\bar{\Psi}\partial_x \bar{\Psi} - \Psi \partial_x \Psi) + \Delta \bar{\Psi}\Psi \ , \tag{1.15}$$

where the field operators $\hat{\Psi}$ have been replaced by the complex Grassmann variables Ψ.

This Lagrangian has three important symmetries: (A) Lorentz invariance manifests in the symmetry with respect to the transformation

$$\begin{pmatrix} c\tau' \\ x' \end{pmatrix} = \begin{pmatrix} \cosh(\theta) & -\sinh(\theta) \\ -\sinh(\theta) & \cosh(\theta) \end{pmatrix} \begin{pmatrix} c\tau \\ x \end{pmatrix} \tag{1.16}$$

and $\Psi(x,\tau) = \Psi'(x',\tau')$, where θ is the rapidity of the Lorentz-boost [Sac99]. (B) Also rescaling the space-time variables and the field by a logarithmic scale l

$$\begin{aligned} x' &= x e^{-l} \ , \\ \tau' &= \tau e^{-zl} \ , \\ \Psi' &= \Psi e^{-l/2} \ . \end{aligned} \tag{1.17}$$

does not change the action at $\Delta = T = 0$ [Sac99]. (C) The scale invariance at the quantum critical point is part of a larger conformal invariance at $\Delta = 0$: If w is a conformal mapping of the complex plane, then the transformation

$$c\tau' + ix' = w(c\tau + ix) \tag{1.18}$$

leaves the action invariant [Car96].

Using these symmetries, we can calculate the dynamic correlation function for the critical theory at $\Delta = 0$, which is in general defined by

$$C^{\mathrm{Ising}}(x = na, 0) = \langle \hat{\sigma}^z_n \hat{\sigma}^z_0 \rangle \ . \tag{1.19}$$

We first start by calculating the *equal-time* correlation function *at the quantum critical point*, $T = 0$ and $\Delta = 0$. The correlation function then can be evaluated by expressing the spin operators with the fermionic variables and then make use of the fact that the fermionic Hamiltonian is quadratic [McC68]. A different approach is that one can prove that the scaling dimension of $\hat{\sigma}^z$ is $\dim[\hat{\sigma}^z] = 1/8$ [Sac99]. Scale invariance then gives

$$C^{\mathrm{Ising}}(x, 0) = \frac{\tilde{Z}}{(|x|/c)^{1/4}} \text{ at } T = 0, \Delta = 0, \tag{1.20}$$

where $\tilde{Z}$ is a non-universal constant factor. From Lorentz invariance, we can obtain the zero temperature *imaginary time* correlation function:

$$C^{\mathrm{Ising}}(x,\tau)_{T=0,\Delta=0} = \frac{\tilde{Z}}{(\tau^2 + x^2/c^2)^{1/8}} \ . \tag{1.21}$$

Translation invariance implies

$$\begin{aligned} C^{\mathrm{Ising}}\left(x = \mathrm{Im}(z_1 - z_2), \tau = \mathrm{Re}(z_1 - z_2)/c\right)_{T=0,\Delta=0} \\ = \frac{\tilde{Z}}{(z_1 - z_2)^{1/8}(\bar{z}_1 - \bar{z}_2)^{1/8}} \ . \end{aligned} \tag{1.22}$$

We can compute the finite temperature correlation function using the conformal mapping to the $T = 0$ correlation function, defined by the transformation

$$z' = w(z) = c/(\pi T)\mathrm{ctg}(\pi T z/c) \; , \tag{1.23}$$

which maps the finite strip $\mathrm{Re}z \in [0, c/T]$ to $\mathrm{Re}z' \in \mathcal{R}$. According to Ref. [Car96], the correlation function transforms as

$$\begin{aligned}\langle \hat{\sigma}^z(z_1, \bar{z}_1)\hat{\sigma}^z(z_2, \bar{z}_2)\rangle = [w'(z_1)\bar{w}'(z_1)w'(z_2)\bar{w}'(z_2)]^{1/8} \\ \langle \hat{\sigma}^z(z_1', \bar{z}_1')\hat{\sigma}^z(z_2', \bar{z}_2')\rangle \; .\end{aligned} \tag{1.24}$$

After some algebra, the finite temperature correlation function takes on the following form:

$$C^{\mathrm{Ising}}(x, \tau)_{\Delta=0} = \frac{\tilde{Z}T^{1/4}}{[\sin(\pi T(\tau + ix/c))\sin(\pi T(\tau - ix/c))]^{1/8}}. \tag{1.25}$$

In Ref. [Sac99], this expression is also obtained by an alternative approach: the bosonization of the fermionic field theory.

To describe the real-time dynamics of the system, the imaginary time correlation function has to be Fourier transformed

$$C(k, \omega_n) = \int_0^{1/T} d\tau \int dx \; e^{i\omega_n \tau - ikx} C(x, \tau) \; . \tag{1.26}$$

This Fourier transform is defined at the Matsubara frequencies, and has to be continued analytically to the real axis $i\omega_n \to \omega + i\delta$ to obtain the real-time dynamics. At $\Delta = 0$. this can be done analytically, and according to Refs. [Sac94, Sac99], the procedure gives the following dynamical susceptibility:

$$\chi(k, \omega) \sim \frac{1}{T^{7/4}} \frac{\Gamma(7/8)}{\Gamma(1/8)} \frac{\Gamma\left(\frac{1}{16} - i\frac{\omega + ck}{4\pi T}\right)\Gamma\left(\frac{1}{16} - i\frac{\omega - ck}{4\pi T}\right)}{\Gamma\left(\frac{15}{16} - i\frac{\omega + ck}{4\pi T}\right)\Gamma\left(\frac{15}{16} - i\frac{\omega - ck}{4\pi T}\right)} \; . \tag{1.27}$$

The correlation function above has clearly the scaling form expected in a critical region. A thorough discussion of the properties of this susceptibility can be found in Ref. [Sac99].

So far we discussed the dynamics at $\Delta = 0$, however, scaling analysis shows that Δ is also a relevant coupling with scaling dimension $\dim[\Delta] = 1$ [Sac99]. Therefore the leading universal contribution to the correlation function assumes the form

$$C(x, \tau) = \tilde{Z}T^{1/4}\Phi_I(Tx/c, T\tau, \Delta/T) \; , \tag{1.28}$$

where Φ_I is a universal scaling function of its arguments. The calculation of this function is a difficult problem, and the discussion is beyond the scope of the introduction presented here.

1.3.3 Summary

We discussed the transverse field Ising model as an example of a system exhibiting quantum critical behavior. The model could be diagonalized by simple transformations, nevertheless, we found interesting physics. For more general spin models and for itinerant particle systems, the identification of the quantum critical transition is usually a major theoretical problem in itself, let alone developing a theory for the behavior in the quantum critical region.

Chapter 2

The Q-state quantum Potts model

2.1 Introduction

In this chapter we shall study the finite temperature dynamical correlations of the Q-state quantum Potts model in one dimension. The investigation of one-dimensional systems has a long history. The field is living its renaissance, as a consequence of recent experimental and theoretical developments. These one-dimensional systems can exhibit quantum phase transitions and provide the simplest examples of spin liquid systems. Among one-dimensional systems, spin chains have been playing a rather special role since the dawn of modern physics. In 1931, Bethe solved the S=1/2 antiferromagnetic Heisenberg model, and showed that its spectrum is gapless [Bet31]. Since then, the zero temperature behavior and static properties at finite temperatures have been studied extensively, while the dynamics in gapped systems at finite temperatures is not fully understood yet. The quantum Potts model both exhibits a quantum phase transition and has gapped phases where quasiparticles have discrete quantum numbers. These properties are rather unique among one-dimensional spin systems.

2.2 Model

The one-dimensional Q-state quantum Potts model is defined by the following Hamiltonian:

$$\hat{H}_P = -J \sum_i \sum_\mu \hat{P}_i^\mu \hat{P}_{i+1}^\mu - Jg \sum_i \hat{P}_i \ . \tag{2.1}$$

In this expression, the operator $\hat{P}_i^\mu$ projects on the μth component of an orthonormal complete set of states $|\mu\rangle_i$ of the local Q-dimensional Hilbert space at site $i = 1, \ldots, N$. In this basis, the operator $\hat{P}_i$ projects on the "corner state"

$$|C\rangle_i \equiv \sum_\mu \frac{1}{\sqrt{Q}} |\mu\rangle_i \ . \tag{2.2}$$

The coupling $J > 0$ is "ferromagnetic", i.e., it tries to align all Potts spins in one of the directions. This interaction competes with the second term in the Hamiltonian,

which mixes all of the components. As we shall see, the Potts model exhibits a $T = 0$ temperature phase transition between two phases governed by these two terms of the Hamiltonian. The transition is controlled by the parameter g, which plays the role of the transverse field in the transverse field Ising model, discussed already in Section 1.3.

In the following, we shall find it more convenient to replace the projectors by traceless operators,

$$\tilde{P}^{\mu} = \hat{P}^{\mu} - \frac{1}{Q} \text{ and } \tilde{P} = \hat{P} - \frac{1}{Q} \, . \tag{2.3}$$

This transformation shifts the energies by a constant which shall be omitted from now on.

For $Q = 2$, the operators can be represented as

$$\tilde{P}^{\sigma} = \frac{1}{2}\sigma\hat{\sigma}^{z} \text{ and } \tilde{P} = \frac{1}{2}\hat{\sigma}^{x} \, , \tag{2.4}$$

and the $Q = 2$ quantum Potts model reduces to the Ising model in a transverse magnetic field with $J_{\text{Potts}} = 2J_{\text{Ising}}$.

2.2.1 Symmetries

It is instructive to discuss the symmetries of the quantum Potts model before performing a perturbative analysis to gain insight about the behavior of this system.

Permutation symmetry

We can see that a permutation $\mathcal{P} \in S_Q$ of the basis states $|\mu\rangle$ on every site leaves the Hamiltonian invariant. This global symmetry can be spontaneously broken in $d = 1$ dimension at $T = 0$. Furthermore, for $Q \geq 3$, the symmetric group S_Q is non-Abelian, e.g., there exists a $(Q-1)$- dimensional irreducible representation. Therefore quasiparticles have (discrete) quantum numbers, which leads to interesting dynamics.

Translational invariance

In the thermodynamic limit $N \to \infty$, a shift by a multiple of the lattice constant leaves the Hamiltonian invariant. As a consequence, the states can be characterized by their lattice momentum $k \in [-\pi/a, \pi/a]$. As the Hamiltonian is time independent (i.e. invariant for translations in time), energy is also conserved. These symmetries have far-reaching consequences in one-dimensional systems. Let's assume that there are well defined quasiparticles in the system. Then in a normal (not umklapp) scattering of two quasiparticles, energy and momentum conservation implies that the incoming momenta and energies are pairwise the same as the outgoing momenta and energies.

2.2.2 Perturbative analysis in the $g \ll 1$ limit

The generic properties of the quantum Potts model can be captured in the limits $g \ll 1$ and $g \gg 1$ perturbatively. First we discuss the eigenstates of the first term of

Hamilton operator in Eq. (2.1),

$$\hat{H}_0 = -J \sum_i \sum_\mu \tilde{P}_i^\mu \tilde{P}_{i+1}^\mu \ , \tag{2.5}$$

when they are exposed to a small perturbation ($g \ ll 1$),

$$\hat{H}_1 = -Jg \sum_i \tilde{P}_i \ . \tag{2.6}$$

Unperturbed ground state and excitations

The ground state of the Hamiltonian, $\hat{H}_0$ in Eq. (2.5), is Q-fold degenerate and the states with the lowest energies are given by

$$|0\rangle_\mu := \prod_i |\mu\rangle_i \ . \tag{2.7}$$

The ground state energy is $E_0^{(0)} = -J\left(1 - \frac{1}{Q}\right) N$. We assume that as $T \to 0$, the system is in the state polarized to the direction μ. Permutation symmetry is broken in the ground state, which is shown by the non-vanishing expectation value

$${}_\mu\langle 0|\tilde{P}^{\mu'}|0\rangle_\mu = \delta_{\mu,\mu'} - \frac{1}{Q} \ . \tag{2.8}$$

Of course, this finite expectation value also implies long-range order, which is most clearly captured by the correlation function, defined as

$$C^{\mu_1\mu_2}(x = ia, t) = \langle \tilde{P}_i^{\mu_1}(t) \tilde{P}_0^{\mu_2}(0) \rangle \ , \tag{2.9}$$

where $\tilde{P}^\mu(t) = e^{i\hat{H}_P t} \tilde{P}^\mu e^{-i\hat{H}_P t}$ is a Heisenberg operator. For $T = 0$ and $g = 0$, this is can be evaluated simply as

$$C^{\mu_1\mu_2}(x,t)_{T=0,g=0} = \left(\delta_{\mu\mu_1} - \frac{1}{Q}\right)\left(\delta_{\mu\mu_2} - \frac{1}{Q}\right) \ . \tag{2.10}$$

This implies that the dynamic structure factor, defined as the Fourier transform of the correlation function,

$$S^{\mu_1\mu_2}(q,\omega) \equiv \int dx \int dt \ e^{-iqx + i\omega t} C^{\mu_1\mu_2}(x,t) \ , \tag{2.11}$$

has a δ- peak at $q = 0, \omega = 0$ as a characteristic of long-range order. We remark that this long-range order is immediately destroyed at finite temperature $T > 0$. We note that if we average over the orientations μ of the ground states, the expectation value in Eq. (2.8) would vanish, however, the δ-peak in the dynamic structure factor would remain.

The simplest excitations of the ground state are kinks connecting different domains. A state with n "domain walls" or kinks has an energy given by $E_n^{(0)} = E_0^{(0)} + nJ$. These excited states are highly degenerate, which will be lifted by the perturbation. A state with a single domain wall at site i with Potts spin directions μ for $j \leq i$ and μ' for $j' > i$ is given by the product state

$$|\mu, \mu'; i\rangle = \prod_{j \leq i} |\mu\rangle_j \prod_{j' > i} |\mu'\rangle_{j'} \ . \tag{2.12}$$

As we can see, applying any local operator on a state with a single domain wall will allways be orthogonal to the ground state. This implies that in any finite order in perturbation theory, the single-particle Hilbert space shall not mix with the ground state in an infinite system.

We shall find it more convenient to use a new notation for domain walls. We observe that domain wall configurations with different orientations for $i \to -\infty$ shall also not mix in finite orders of perturbation theory. We can consider a subspace/sector of the Hilbert space where the Potts spins point to the direction μ for $i \to -\infty$. From now on in this subsection, this direction μ shall not be displayed explicitly. We observe that a domain wall is allways one of $Q-1$ possible "steps" in the orientation. We therefore define the quantum number θ as the step size modulo Q, and denote the state in Eq (2.12) as

$$|\theta, i\rangle = \prod_{j \leq i} |\mu\rangle_j \prod_{j' > i} |\mu' = (\mu + \theta) \mathrm{mod} Q\rangle_{j'} \ . \tag{2.13}$$

It is straightforward to generalize this notation for multiple domain wall configurations. However, in this subsection we shall not discuss contributions from the multiparticle Hilbert space.

As the subspace with single domain walls is degenerate, we can create linear combinations to construct states which are eigenstates of the lattice translation operator:

$$|\theta, k\rangle = \frac{1}{\sqrt{N}} \sum_j e^{ikja} |\theta, j\rangle \ . \tag{2.14}$$

Note that this definition introduces domain walls propagating like plane waves. As we shall see, these states are also eigenstates of the Hamiltonian in leading order of g.

First order perturbation theory

It is easy to see that there is no first order shift in the ground state energy: $\delta E_0^{(1)} = \langle 0|\hat{H}_1|0\rangle = 0$. However, $\hat{H}_1$ does split the degeneracy of the single-kink excitations, and the first order energies are given by the eigenvalues of the matrix

$$\langle \theta, k|\hat{H}_1|\theta', k'\rangle = -J\frac{2}{Q} g \cos ka \ \delta_{\theta,\theta'}\delta_{kk'} \ . \tag{2.15}$$

Due to the choice of the basis for the unperturbed wave functions, this matrix is simply diagonal. The wave functions $|\theta, k\rangle$ are thus also the eigenfunctions in the first order of perturbation theory. The quasiparticle energies (measured with respect to the ground state energy) are approximately given by:

$$\epsilon_k^\theta = J - J\frac{2}{Q} g \cos ka + \mathcal{O}(g^2) \ . \tag{2.16}$$

To conclude, in first order of perturbation theory, the ground state is stable and the quasiparticles form a finite band. The quasiparticles have internal quantum numbers θ, which describe the step sizes between neighboring domains. The gap for the excitations at $k = 0$ is approximately

$$\Delta \approx J - J\frac{2}{Q} g \ . \tag{2.17}$$

Due to this gap, perturbation theory is expected to be convergent for $g \ll 1$. Therefore all qualitative conclusions made in first order in g should carry over to the ferromagnetic side.

2.2.3 Perturbative analysis in the $g \gg 1$ limit

The case $g \gg 1$ can be also treated perturbatively, in a similar way to the ferromagnetic side $g \ll 1$. In this limit, we investigate the second term of the Hamilton operator in Eq. (2.1),

$$\hat{H}_0' = -Jg \sum_i \tilde{P}_i \ , \tag{2.18}$$

and treat

$$\hat{H}_1' = -J \sum_i \sum_\mu \tilde{P}_i^\mu \tilde{P}_{i+1}^\mu \tag{2.19}$$

as a perturbation.

Unperturbed ground state and excitations

It is clear that the ground state of $\hat{H}_0'$ is a non-degenerate product state,

$$|\mathcal{C}\rangle = \prod_i |C\rangle_i \ . \tag{2.20}$$

The energy of this state is given by $E_0^{(0)} = \langle \mathcal{C}|\hat{H}_0'|\mathcal{C}\rangle = 0$, and there is no spontaneous magnetization, since $\langle \mathcal{C}|\tilde{P}_i^\mu|\mathcal{C}\rangle = 0$. We shall call this region "quantum paramagnetic".

Elementary excitations are local "spin flips", where the energy of a state with n quasiparticles – spin flips at n different sites – is given by $E_n^{(0)} = nJg$. The wave function corresponding to a single excitation at site i can be written as

$$|\lambda, i\rangle = |\lambda\rangle_i \prod_{j \neq i} |C\rangle_j \ , \tag{2.21}$$

where $|\lambda\rangle_i$ is one of the basis vectors of the subspace orthogonal to the "corner state" $|C\rangle_i$.

As in the previous subsection, we can create linear combinations of singleparticle states in Eq. (2.21) by a Fourier transform, which are momentum eigenstates and therefore form a practical basis for perturbation theory:

$$|\lambda, k\rangle = \frac{1}{\sqrt{N}} \sum_j e^{ikja} |\lambda, j\rangle \ . \tag{2.22}$$

First order perturbation theory

Similarly to the ferromagnetic side, there is no first order energy shift in the ground state: $\delta E_0^{(1)} = \langle \mathcal{C}|\hat{H}_1|\mathcal{C}\rangle = 0$, since the operators in $\hat{H}_1$ are traceless.

To calculate the first order shift of the quasiparticle energies, we have to compute the matrix elements

$$\langle \lambda, k|\hat{H}_1|\lambda', k'\rangle = -J\frac{2}{Q} \cos ka \ \delta_{kk'} \delta_{\lambda\lambda'} \ . \tag{2.23}$$

Thus for $g \gg 1$ the quasiparticles have the dispersion relation

$$\epsilon_k^\lambda = Jg\left(1 - \frac{2}{Q}\frac{1}{g}\cos ka + \mathcal{O}(g^{-2})\right) , \tag{2.24}$$

and a gap at $k = 0$, that can be approximated as

$$\Delta \approx Jg - J\frac{2}{Q} . \tag{2.25}$$

Again, similarly to the ferromagnetic side ($g \ll 1$), perturbation theory is convergent.

Let us now compute the correlation function Eq. (2.9) at zero temperature in the limit $g \gg 1$ for low energies. Neglecting multiparticle contributions and keeping only terms up to $\mathcal{O}(1/g)$, a simple calculation at $T = 0$ yields

$$C^{\mu_1\mu_2}(x,t)_{T=0,g\to\infty} = \frac{1}{Q}\left(\delta_{\mu_1\mu_2} - \frac{1}{Q}\right)\frac{1}{N}\sum_k e^{ikx - it\epsilon_k^\lambda} + \dots . \tag{2.26}$$

Hence the dynamic structure factor has no peak at $q = \omega = 0$, rather, there is a quasiparticle pole at $\omega = \epsilon_q^\lambda$:

$$S^{\mu_1\mu_2}(q,\omega)_{T=0,g\to\infty} = \frac{1}{Q}\left(\delta_{\mu_1\mu_2} - \frac{1}{Q}\right)\delta(\omega - \epsilon_q^\lambda) + \dots . \tag{2.27}$$

2.3 Phase transition in the ground state

In the previous subsections we investigated the quantum Potts model in the limits $g \to 0$ and $g \to \infty$. For the former limit, there is a ferromagnetic ground state with long-range order, which breaks the permutation symmetry. In this limit, the excitations are non-local objects, kinks – which behave as quasiparticles with internal quantum numbers θ. For large values of the control parameter g, on the other hand, a non-degenerate quantum paramagnetic ground state was found. The excitations are local spin flips and carry the quantum numbers λ.

As g is tuned continuously, the ground states cannot evolve analytically into each other. As a consequence, there must be a phase transition at $T = 0$ when g changes from 0 to ∞. The phases are separated by a single point in parameter space, which shall be proved in the next subsections.

2.3.1 Quantum-to-classical mapping

To prove the existence of a single phase transition in the ground state of the one-dimensional quantum Potts model, we shall use the powerful tool of quantum-to-classical mapping. This mapping connects certain thermodynamical quantities in $d+1$-dimensional classical models and corresponding d-dimensional quantum systems. For the Potts model, this mapping was first developed by Mittag and Stephen [Mit71]. Since the critical field theory of the $d = 2$ dimensional, $Q = 3$ state classical Potts model is known, the quantum-to classical mapping shall enable us to construct time-dependent correlation functions analytically in the quantum critical region of the $d = 1$ quantum Potts model. In this subsection, the analysis follows the lines of Ref. [Sac99].

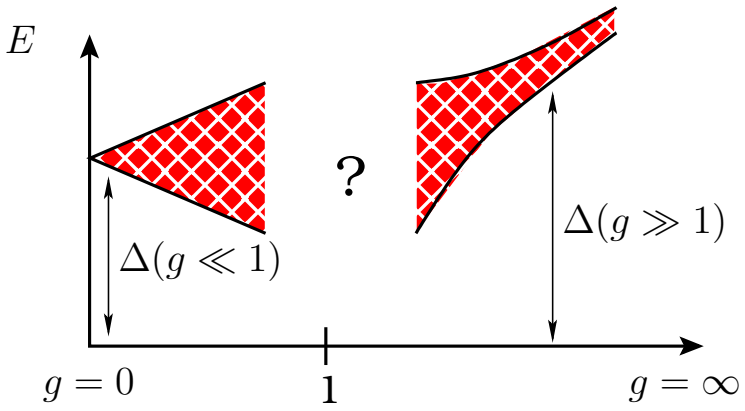

Figure 2.1: Sketch of the quasiparticle band (red region) of the quantum Potts model obtained by perturbation theory. According to perturbation theory, there is a level crossing with the ground state in the region $g \approx 1$. This is a signature of a quantum phase transition at $g_c \approx 1$.

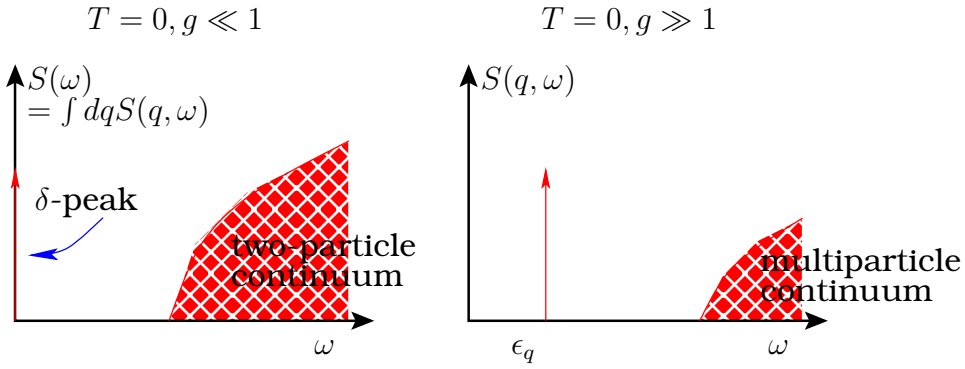

Figure 2.2: The $T = 0$ dynamic structure factors of the quantum Potts model. For $g \ll 1$, the ground state is ferromagnetic with long-range order. This is represented by the δ-peak at $\omega = 0$ in the dynamic structure factor. For $g \gg 1$, on the other hand, a quantum paramagnet had been found with local spin-flips as excitations.

The classical Potts model in one dimension and the quantum Potts spin

Before discussing the $d = 1$ dimensional quantum Potts model, let us consider first the simpler case of a one-dimensional classical system. We define the classical Potts model by the dimensionless Hamiltonian

$$\mathcal{H}_P^{d=1} = -J_\tau \sum_i \delta_{\mu(i),\mu(i+1)} \ . \tag{2.28}$$

Here Potts spins can have the values $\mu(i) = 1, \ldots, Q$. The inverse temperature is absorbed in the dimensionless coupling $J_\tau \sim 1/T_{\rm class}$, and we use the notation $T_{\rm class}$ to emphasize that the temperature of the classical system is not equivalent to the temperature of the quantum system. Let us consider the classical Potts chain with N_τ sites.

The partition function of the Hamiltonian in Eq. (2.28) can be written in the transfer matrix representation as

$$Z = \sum_{\{\mu(i)\}} e^{-\mathcal{H}_P^{d=1}} = {\rm Tr}(\hat{T}^{N_\tau}) \ , \tag{2.29}$$

where the transfer matrix $\hat{T}$ is given by $[\hat{T}]_{\mu\mu'} = e^{J_\tau}\delta_{\mu,\mu'} + (1 - \delta_{\mu,\mu'})$, or using the notation of the previous subsections,

$$\hat{T} = e^{J_\tau} + Q\tilde{P} \ . \tag{2.30}$$

The eigenvalues of the transfer matrix are $e^{J_\tau} + Q - 1$, which is non-degenerate, and $e^{J_\tau} - 1$, which is $Q - 1$-fold degenerate. Hence the partition function in Eq. (2.29) can be simply evaluated as

$$Z = (e^{J_\tau} + Q - 1)^{N_\tau} + (Q - 1)(e^{J_\tau} - 1)^{N_\tau} \ . \tag{2.31}$$

It is also instructive to study the classical correlation function, defined by

$$C^{\mu_1\mu_2}(j) = \langle \delta_{\mu(j)\mu_1}\delta_{\mu(0)\mu_2}\rangle = \frac{1}{Z}\sum_{\{\mu(i)\}} e^{-\mathcal{H}_P^{d=1}}\delta_{\mu(j)\mu_1}\delta_{\mu(0)\mu_2} \ . \tag{2.32}$$

Rewriting the correlation function in the transfer matrix formalism gives the expression

$$C^{\mu_1\mu_2}(j) = \frac{1}{Z}{\rm Tr}\left\{\hat{T}^{N_\tau - j}\hat{P}^{\mu_1}\hat{T}^j\hat{P}^{\mu_2}\right\} \ , \tag{2.33}$$

and by inserting the eigenvectors of the transfer matrix, this can be evaluated analytically as

$$C^{\mu_1\mu_2}(j) = \frac{\frac{1}{Q^2} + \epsilon^{N_\tau}(\delta_{\mu_1\mu_2} - \frac{1}{Q})^2}{1 + \epsilon^{N_\tau}(Q-1)} + \frac{\frac{1}{Q}(\epsilon^{N_\tau - j} + \epsilon^j)(\delta_{\mu_1\mu_2} - \frac{1}{Q})}{1 + \epsilon^{N_\tau}(Q-1)} \ , \tag{2.34}$$

where $\epsilon = (e^{J_\tau} - 1)/(e^{J_\tau} + Q - 1)$. The above expression defines the correlation length through the limiting behavior $j \to \infty$, when

$$\xi = \frac{a_\tau}{|\ln \epsilon|} \ , \tag{2.35}$$

where a_τ is the lattice spacing in the classical chain. For $T_{\text{class}} \to 0$, thus $J_\tau \to \infty$, the correlation length becomes much larger than the lattice spacing. In this limit, the coupling can be approximated as

$$e^{-J_\tau} \approx \frac{1}{Q}\frac{a_\tau}{\xi}(J_\tau \gg 1) \,. \tag{2.36}$$

Using this formula, we can express the partition function in a form suitable for the τ-continuum limit, where $a_\tau \to 0$ is taken while keeping the lengths $N_\tau a_\tau$ and ξ fixed. In this strong coupling limit, the partition function becomes

$$Z \sim \text{Tr}\; e^{-\beta \hat{H}_Q} + \mathcal{O}\left(\frac{a_\tau^2}{\xi^2}\right) \,. \tag{2.37}$$

This is the partition function of a zero-dimensional quantum system with the Hamilton operator

$$\hat{H}_Q = -Jg\tilde{P} \,. \tag{2.38}$$

Eq. (2.37) hence describes a single Potts spin in a "transverse field" $Jg = \frac{1}{\xi}$, in a thermal bath with temperature $T = \beta^{-1} = (N_\tau a_\tau)^{-1}$. We observe that the energy gap for the excited states of the quantum system is the inverse of the correlation length of the classical system.

We also observe that the size of the classical system is equivalent to the inverse temperature of the quantum system, i.e., the "size" of the quantum system in imaginary time. A further connection can be made by defining the imaginary time correlation function

$$C^{\mu_1\mu_2}(\tau) = \langle \mathbf{T}_\tau \hat{P}^{\mu_1}(\tau)\hat{P}^{\mu_2}(0)\rangle \,, \tag{2.39}$$

which can be written by definition as

$$C^{\mu_1\mu_2}(\tau) = \frac{1}{Z}\text{Tr}(e^{-(\beta-\tau)\hat{H}_Q}\,\hat{P}^{\mu_1}e^{-\tau\hat{H}_Q}\,\hat{P}^{\mu_2}) \,, \tag{2.40}$$

where $\mathbf{T}_\tau$ is the imaginary time ordering operator. This expression is equivalent to Eq. (2.33) when taking the τ-continuum limit: $a_\tau \to 0$, while keeping $\xi = a_\tau e^J/Q$, $\tau = ja_\tau$ and $\beta = N_\tau a_\tau$ fixed. We thus conclude that in this limit, spatial correlations of the $d = 1$ dimensional classical Potts model are identical to the correlations of a single quantum-Potts spin in imaginary time. To summarize, a finite temperature in the quantum system corresponds to a finite system size for the classical system, and the correlation length is equivalent to the gap of the quantum system. These conclusions are rather general and can be extended to many other models, see Ref. [Sac99].

The classical Potts model in two dimensions and the quantum Potts chain

The considerations for the one dimensional classical system can be generalized to higher dimensional models. We define the anisotropic classical two-dimensional Potts model with the dimensionless Hamiltonian

$$\mathcal{H}_P^{d=2} = -\sum_{ij}\left[J_x\delta_{\mu(i,j)\mu(i+1,j)} + J_\tau\delta_{\mu(i,j)\mu(i,j+1)}\right] \,, \tag{2.41}$$

where J_x and J_τ are dimensionless couplings, and the indeces i and j take values $1,\ldots,N$ and $1,\ldots,N_\tau$, respectively. Each Potts spin can have values $\mu(ij) \in \{1,\ldots,Q\}$. The lattice spacing is a in the x direction, while a_τ in the τ direction.

By introducing the $Q^N \times Q^N$ transfer matrices,

$$\hat{T}_1 = \otimes_{i=1}^{N} \left(e^{J_x \sum_\mu \hat{P}_i^\mu \hat{P}_{i+1}^\mu} \right) = e^{J_x \sum_i \sum_\mu \hat{P}_i^\mu \hat{P}_{i+1}^\mu} \ , \tag{2.42}$$

and

$$\hat{T}_2 = \otimes_{i=1}^{N} \left(e^{J_\tau} \hat{1}_i + Q \hat{P}_i - \hat{1}_i \right) \ , \tag{2.43}$$

we can rewrite the partition function as

$$Z = \mathrm{Tr} \left[(\hat{T}_1 \hat{T}_2)^{N_\tau} \right] \ . \tag{2.44}$$

Note that the matrix $\hat{T}_1$ is diagonal in the second site index and acts within a chain, while $\hat{T}_2$ is the generalization of the matrix $\hat{T}$ acting between chains j and $j+1$. Now we perform the τ-continuum limit by taking

$$a_\tau \to 0, J_x \to 0, J_\tau \to \infty, N_\tau \to \infty \ , \tag{2.45}$$

while keeping

$$J = J_x / a_\tau, \ 1/\xi = e^{-J_\tau} Q / a_\tau \text{ and } \beta = a_\tau N_\tau \tag{2.46}$$

fixed. We can take similar steps as in the case of the one-dimensional classical Potts model to express the partition function of the $d = 2$ classical model in the τ-continuum limit by the partition function of a quantum system in $d = 1$ dimension, namely

$$Z \sim \mathrm{Tr}\ e^{-\beta \hat{H}_P} \ , \tag{2.47}$$

where the Hamilton operator appearing in the exponent defines the Q-state Potts model in Eq. (2.1).

Although quantum-to-classical mapping is a very powerful theoretical tool, as emphasized in Ref. [Voj03], it might not be allways used. The direct interpretation of the classical dynamics for the quantum system often requires careful considerations as an approximation done on the imaginary time axis is generally not appropriate for real times. The topological Berry phase in certain quantum spin models also makes a qualitative difference to the classical counterparts.

2.3.2 The order of the ground state phase transition

In the previous subsection we mapped the two dimensional classical Potts model on the one-dimensional quantum Potts model. We found three important relations, namely

(A) the finite temperature quantum system is mapped on a classical system where one extension is equivalent to the inverse temperature;

(B) the inverse of the correlation length gives the energy gap between the ground state and the excited states;

(C) the control parameter g is a strictly monotonous function of the classical temperature T_{class}.

These relations can be used to construct the phase diagram of the quantum Potts model, since the thermodynamic behavior of the two dimensional classical system has been studied extensively [DiF99, Jos77, Mit71, Potts52, Sol81a, Sol81b, Wu82].

The $T = 0$ behavior of the quantum Potts model in $d = 1$ dimension is equivalent to the behavior of the infinite two-dimensional classical Potts model in the thermodynamic limit, which has a paramagnetic - ferromagnetic phase transition at a temperature $T^C_{\rm class}$. The $Q = 2$ classical model – which is equivalent to the Ising model – has a continuous transition corresponding to a quantum critical phase transition at $g_c = 1$. The correlation length diverges in the classical Ising model as $\xi \sim |T_{\rm class} - T^C_{\rm class}|^{-\nu}$, with an exponent $\nu = 1$. Thus the gap scales to zero linearly, in agreement with what we found by the exact diagonalization of the Hamiltonian [Sac99]. Interestingly, from the quantum-to-classical mapping one concludes that the quantum phase transition is also continuous in the $Q = 3$ case. However, this belongs to an other universality class with $\nu = 5/6$ [DiF99]. Although the transition for $Q = 4$ is continuous, the critical behavior is dominated by a marginal operator [Car80, Sal97, Swe81]. We shall not discuss the dynamical correlation functions of the $Q = 4$ Potts model in this thesis. For $Q > 4$, the transition is of first order [Jos77, Wu82].

At finite temperatures $T > 0$, there is no phase transition and only a crossover occurs since a stripe of the classical Potts model behaves as if it was effectively one-dimensional. However, we can understand the emergence of the quantum critical region by the concept of finite-size scaling. For $\xi(T_{\rm class}) \geq N_\tau a_\tau$, i.e. $\Delta(g) \leq T$, the fluctuations dominate the behavior in the classical model, leading to the anomalous scaling behavior. We discuss the corresponding quantum critical behavior in the $Q = 3$ quantum Potts model in the next subsection. We shall also discuss the finite temperature dynamics in the gapped (non-universal) phases within semiclassical approximation in a general framework in Section 2.4.

The mapping to the two dimensional classical Potts model also allows us to generalize some of the results obtained by perturbation theory. The ground state exhibits ferromagnetism and is oriented in a given direction μ for $g < g_c$, therefore we expect that the ground state expectation value of the order parameter $\tilde{P}^{\mu'}$ gets renormalized for finite g, and is given by

$$\langle \tilde{P}^{\mu'} \rangle_{T=0} = m(g) \left(\delta_{\mu\mu'} - \frac{1}{Q} \right) , \tag{2.48}$$

where the magnetization $m(g) \leq 1$ is reduced by the quantum fluctuations. Hence the dynamic correlation function on the ferromagnetic side is expected to be in leading order

$$C^{\mu_1\mu_2}(x,t)_{T=0} = m^2(g) \left(\delta_{\mu\mu_1} - \frac{1}{Q} \right) \left(\delta_{\mu\mu_2} - \frac{1}{Q} \right) + \ldots (g < g_c) . \tag{2.49}$$

Quantum fluctuations shall not destroy the quasiparticle pole of the correlation function on the paramagnetic side, $g > g_c$, due to the finite gap. They will, however, reduce the quasiparticle residue $A(g)$ in the dynamic susceptibility, defined by the Kubo formula

$$\chi^{\mu_1\mu_2}(q,\omega) = \int dx \int dt \; e^{-iqx_i + i\omega t} (-i)\Theta(t) \langle \left[\tilde{P}^{\mu_1}_i(t), \tilde{P}^{\mu_2}_0(0) \right] \rangle , \tag{2.50}$$

so that on the quantum paramagnetic side at zero temperature it becomes

$$\chi^{\mu_1\mu_2}(q,\omega)_{T=0} = \left(\delta_{\mu_1\mu_2} - \frac{1}{Q}\right) \frac{A(g)}{\omega - \epsilon_q + i\eta} + \ldots (g > g_c) \ , \tag{2.51}$$

where the infinitesimal constant η ensures analyticity in the upper half plane. The magnetization $m(g)$ and the quasiparticle residue $A(g)$ scale to zero at $g = g_c$ where the gap $\Delta(g)$ vanishes and the quasiparticle description breaks down.

2.3.3 Quantum criticality in the $Q = 3$ quantum Potts model

In this subsection we shall calculate the dynamic susceptibility of the $Q = 3$ quantum Potts model for finite temperature and $\Delta = 0$, in analogy with the $Q = 2$, Ising case. Let us start by reviewing some basic facts in the quantum critical region. The singular part of the free energy density is given by a scaling function

$$f(g - g_c, h, T) = b^{-2} f(b^{y_t}(g - g_c), b^{y_h} h, Tb) \ , \tag{2.52}$$

where $y_t = 2 - x_t$ and $y_h = 2 - x_h$ are the scaling dimensions of the temperature and magnetic field in the classical Potts model, and $x_t = 4/5$ and $x_h = 2/15$ denote the dimensions of the corresponding primary fields that are identified in conformal field theory [DiF99, Dot84]. These exponents determine the correlation length exponent $\nu = 1/y_t = 5/6$ for the classical Potts model in $d = 2$ dimensions, therefore the gap vanishes as

$$\Delta \sim \xi^{-1} \sim |g - g_c|^{5/6} \tag{2.53}$$

at the quantum critical point at $T = 0$. The functional form in Eq. (2.52) of the free energy implies that the susceptibility

$$\chi = \left.\frac{\partial^2 f}{\partial h^2}\right|_{h=0} = b^{2y_h - 2} f(b^{y_t}(g - g_c), 0, Tb) \tag{2.54}$$

diverges at $T = 0$ (by setting $b = |g - g_c|^{-1/y_t}$) as

$$\chi(T = 0, g \to g_c) \sim \frac{1}{|g - g_c|^{13/9}} \ , \tag{2.55}$$

while approaching the critical point at $g = g_c$ by decreasing the temperature leads to the expression

$$\chi(T \to 0, g = g_c) \sim \frac{1}{T^{26/15}} \ . \tag{2.56}$$

After discussing the static properties of the quantum Potts model in the quantum critical region, we shall use the conformal invariance of the critical theory to derive dynamic correlation functions at finite temperatures. At the quantum critical point, the *imaginary time* correlation function is scale invariant and has the form

$$C^{\mu\mu'}(x,\tau)_{T=0,g=g_c} = \left(\delta_{\mu\mu'} - \frac{1}{Q}\right) C(x,\tau)_{T=0,g=g_c} \ , \tag{2.57}$$

where the reduced correlation function is proportional to the scaling function

$$C(x,\tau)_{T=0,g=g_c} \sim \frac{1}{(\tau^2 + x^2)^{x_h}} \ . \tag{2.58}$$

In this expression, we assumed that the lattice anisotropy is an irrelevant perturbation at the transition and we set the velocity of light to $c = 1$.

The finite temperature, $T > 0$, imaginary time correlation function at $g = g_c$ can be computed similar to in the Ising case. We use the conformal mapping in Eq. (1.23) to obtain the following expression:

$$C(x,\tau)_{T>0,g=g_c} \sim \frac{T^{2x_h}}{\{\sin[\pi T(\tau+ix)]\}^{x_h}\{\sin[\pi T(\tau-ix)]\}^{x_h}} . \tag{2.59}$$

The derivation of this formula can be found in Appendix A.1.1. The correlation function in Eq. (2.59) is, however, defined for imaginary time, and any direct conclusion on the real time dynamics would be misleading. To compute the retarded correlation function, we need to use the analytical properties of Eq. (2.59), and we shall first calculate the Fourier transform

$$C(k,i\omega_n)_{T>0,g=g_c} = \int_{-\infty}^{\infty} dx \int_0^{\beta} d\tau \; e^{i\omega_n\tau - ikx} C(x,\tau)_{T>0,g=g_c} , \tag{2.60}$$

where $\omega_n = 2n\pi T$ are the even Matsubara frequencies. The actual calculation of this expression is rather technical and we present the details in Appendix A.1.2. Some guidelines for the calculation can be found in Ref. [Sac94]. The final result is shown below:

$$C(k,i\omega_n)_{T>0,g=g_c} \sim T^{-\frac{26}{15}} \frac{\Gamma(13/15)}{\Gamma(2/15)} \frac{\Gamma\left(\frac{1}{15} - i\frac{i|\omega_n|+k}{4\pi T}\right)\Gamma\left(\frac{1}{15} - i\frac{i|\omega_n|-k}{4\pi T}\right)}{\Gamma\left(\frac{14}{15} - i\frac{i|\omega_n|+k}{4\pi T}\right)\Gamma\left(\frac{14}{15} - i\frac{i|\omega_n|-k}{4\pi T}\right)} . \tag{2.61}$$

The next difficulty we face is that due to the finite temperature, $C(k,i\omega_n)$ is defined at the Matsubara frequencies. A continuation which is analytic on the upper half plane for all k and T is

$$C^{\mathrm{UHP}}(k,\omega) \sim T^{-\frac{26}{15}} \frac{\Gamma(13/15)}{\Gamma(2/15)} \frac{\Gamma\left(\frac{1}{15} - i\frac{\omega+k}{4\pi T}\right)\Gamma\left(\frac{1}{15} - i\frac{\omega-k}{4\pi T}\right)}{\Gamma\left(\frac{14}{15} - i\frac{\omega+k}{4\pi T}\right)\Gamma\left(\frac{14}{15} - i\frac{\omega-k}{4\pi T}\right)} . \tag{2.62}$$

This expression can now be identified with the dynamical linear response in the quantum critical region, which is related to the reduced response function in Eq. (2.62) by the expression

$$\chi^{\mu_1\mu_2}(k,\omega)_{T>0,g=g_c} = \left(\delta_{\mu_1\mu_2} - \frac{1}{Q}\right) C^{\mathrm{UHP}}(k,\omega) . \tag{2.63}$$

From this result we conclude that the homogeneous dynamical susceptibility has the scaling form

$$\chi(\omega) = \chi(k=0,\omega) \sim T^{-26/15} F_1(T/\omega) , \tag{2.64}$$

where we can identify the scaling function F_1 from Eq. (2.62) as

$$F_1(y) = \frac{\Gamma^2\left(\frac{1}{15} - i\frac{y}{4\pi}\right)}{\Gamma^2\left(\frac{14}{15} - i\frac{y}{4\pi}\right)} . \tag{2.65}$$

The function $F_1(y)$ has the following asymptotic behavior [Abr65]:

$$F_1(y) \approx \begin{cases} \Gamma^2(\frac{1}{15})/\Gamma^2(\frac{14}{15}) & \text{for } y \to 0 ; \\ \left(\frac{y}{4\pi}\right)^{-26/15} e^{i\pi 13/15} & \text{for } y \to \infty . \end{cases} \tag{2.66}$$

In contrast to the homogeneous susceptibility, the local dynamical susceptibility is dominated by short wavelength, non-universal modes. The computation of the local susceptibility is a subtle issue and not presented here.

2.4 Dynamical correlations in the gapped phases

To complete our analysis of the finite temperature dynamics of the quantum Potts model in $d = 1$ dimension, we shall also compute the dynamical correlation functions in the gapped phases. We shall use a semiclassical approximation similar to the methods of Refs. [Dam98, Jep65, Leb69, Sac97b], and derive an analytical expression for the relaxation.

2.4.1 Semiclassical dynamics

In the perturbative discussions, presented in Subsection 2.2.2 and Subsection 2.2.3 we have calculated the quasiparticles' approximate dispersion relations. We found gapped excitations and that the energy has minimum at zero momentum $k = 0$. Converging perturbation theories and the quantum-to-classical mapping imply that these results should also hold qualitatively for all $g \neq g_c$. In our approach we therefore assume that the quasiparticles form a $(Q-1)$-multiplet with the dispersion relation

$$\epsilon_k = \Delta(g) + \frac{c^2(g)}{\Delta(g)} \frac{k^2}{2} + \mathcal{O}(k^4) \; , \tag{2.67}$$

where the gap can be approximated as

$$\Delta(g) \approx \begin{cases} J - J\frac{2}{Q}g & \text{for } g \ll g_c \; ; \\ Jg - J\frac{2}{Q} & \text{for } g \gg g_c \; , \end{cases} \tag{2.68}$$

while the "velocity of light" is asymptotically given by $c(g) \approx Ja\sqrt{\frac{2}{Q}g}$ for both $g \ll g_c$ and $g \gg g_c$, which seems to be a mathematical coincidence. The quasiparticles carry internal quantum numbers $\theta = 1, \ldots, (Q-1)$ and $\lambda = 1, \ldots, (Q-1)$ for the ferromagnetic and quantum parametric side of the phase diagram, respectively.

The finite gap offers the possibility to apply a semiclassical approach at low temperatures, $T \ll \Delta$. In this temperature region, the momentum distribution of the quasiparticles is approximately

$$n(k) \approx e^{-\beta\Delta} e^{-\frac{c^2}{T\Delta}\frac{k^2}{2}} \; . \tag{2.69}$$

We can calculate the quasiparticle density, given by the Boltzmann distribution in Eq. (2.69), from the momentum integral

$$\rho = (Q-1) \int_{-\infty}^{\infty} dk \; n(k) = (Q-1)\sqrt{\frac{T\Delta}{2\pi c^2}} e^{-\Delta/T} \; , \tag{2.70}$$

and find that the average separation of the quasiparticles, $\xi_c \equiv \rho^{-1}$ is exponentially large in the low T limit. The quantummechanical extension of the excitations' wave functions, on the other hand, is given by the thermal de Broglie wavelength,

$\lambda_T \sim \frac{c}{\sqrt{T\Delta}}$. Combining these characteristic lengthscales in the definition of the phase space density Λ, we find that it is exponentially suppressed:

$$\Lambda \equiv \rho\lambda_T \sim e^{-\Delta/T} \ll 1 \text{ for } T \ll \Delta. \tag{2.71}$$

The low phase space density makes the semiclassical approximation valid in the gapped phases at low temperatures. Therefore the phase space can be parameterized by the positions, velocities and quantum indeces of the quasiparticles. The dynamics, however, requires a more subtle discussion. Due to the one-dimensional geometry, quasiparticles cannot avoid each other. As a consequence, neighboring quasiparticles will eventually have a separation $|x_1 - x_2| \leq \lambda_T$. In this region, the semiclassical description breaks down, therefore we need to analyze the collisions quantummechanically. In the temperature region under investigation, the probability that a further particle is also in the vicinity, $|x_3 - x_1|, |x_3 - x_2| \leq \lambda_T$, is exponentially small, and shall be neglected. We shall therefore restrict our considerations to two-body collissions only.

2.4.2 The two-particle $\mathcal{S}$-matrix

Scattering of quasiparticles with well-defined asymptotic states can be characterized by the $\mathcal{S}$ -matrix, which is generally a complicated function of the momenta and the quantum numbers of the scattering particles for general interaction potentials. In $d = 1$ dimension, however, certain simplifications arise. As we discussed earlier, energy and momentum conservation ($k_1 + k_2 = k_1' + k_2'$; $\epsilon_{k_1} + \epsilon_{k_2} = \epsilon_{k_1'} + \epsilon_{k_2'}$) implies for pairs $k_2 < k_1$ and $k_2' < k_1'$ that the incoming and outgoing momenta are pairwise conserved in $d = 1$ dimension: $k_1 = k_1' = k$ and $k_2 = k_2' = k'$. As a consequence, the quasiparticles have straight space-time trajectories. However, there is no conservation rule for the internal quantum numbers, leading to nontrivial and interesting dynamics for $Q > 2$. The asymptotic two-particle wave function for $|x_1 - x_2| \gg \lambda_T$ is a superposition of plain waves:

$$\begin{aligned} |\Psi\rangle \quad = \quad & \sum_{\kappa,\kappa'} \Big(A_{\kappa\kappa'} \sum_{j<j'} e^{i(kx_j + k'x_{j'})} |j, \kappa; j', \kappa'\rangle \\ & + B_{\kappa\kappa'} \sum_{j>j'} e^{i(kx_j + k'x_{j'})} |j, \kappa; j', \kappa'\rangle \Big) , \end{aligned} \tag{2.72}$$

where κ and κ' are the quantum numbers of the quasiparticles, and the state $|j, \kappa; j', \kappa'\rangle$ is constructed by *independent* excitations at site j and j'. The two-particle scattering matrix is then defined by the following matrix equation:

$$B_{\kappa_1,\kappa_2} = \sum_{\kappa_1',\kappa_2'} \mathcal{S}^{\kappa_1',\kappa_2'}_{\kappa_1,\kappa_2} A_{\kappa_1',\kappa_2'} \, . \tag{2.73}$$

For independent/non-interacting particles, the S-matrix is diagonal or "transmissive", $\mathcal{S}^{\kappa_1',\kappa_2'}_{\kappa_1,\kappa_2} = \delta^{\kappa_2'}_{\kappa_2} \delta^{\kappa_1'}_{\kappa_1}$. Now we shall supply two arguments that the long-wavelength limit of the scattering matrix for the $Q = 3$ Potts model (and very likely also for $Q > 4$) for any $g \neq g_c$ takes the universal *reflective* form

$$\mathcal{S}^{\kappa_1',\kappa_2'}_{\kappa_1,\kappa_2} = (-1)\delta^{\kappa_1'}_{\kappa_2} \delta^{\kappa_2'}_{\kappa_1} \, , \tag{2.74}$$

shown in Fig. 2.3. The physical interpretation of this scattering matrix is that at low momenta the quasiparticles are purely reflected at collisions.

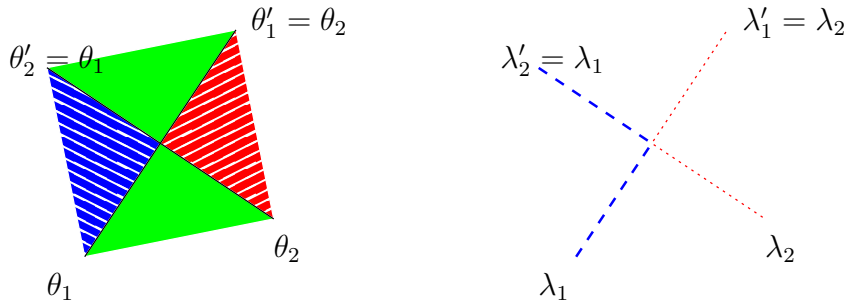

Figure 2.3: The reflective structure of the $\mathcal{S}$-matrix in the long wavelength limit for the $Q = 3$ quantum Potts model. On the left, we can see the graphical interpretation of the $\mathcal{S}$ -matrix in Eq. (2.74) for the ferromagnetic side, while on the right, for the paramagnetic side.

Argument (A)

From the renormalization analysis of the classical problem, we know that the RG flow has two fixpoints at $T = 0$, namely $g = 0$ and $g = \infty$, corresponding to the ferromagnetic and quantum paramagnetic phases. The long-wavelength dynamical behavior remains invariant under the renormalization group transformation. Thus for $g < g_c$, the asymptotic form of the scattering matrix must be the same as for $g = 0$, while for $g > g_c$ it is the same as for $g = \infty$, therefore the $\mathcal{S}$ -matrix can be obtained by perturbation theory in the $g \ll 1$ and $g \gg 1$ limits. These calculations can be found in Appendix A.2.1 and Appendix A.2.2, and the result is already displayed as Eq. (2.74). We note that this approach is not adequate for the case $Q = 4$, where the perturbative calculations provide a singular $\mathcal{S}$ -matrix.

Argument (B)

In the low momentum limit, an effective Hamiltonian to the quantum Potts model defined by Eq. (2.1) can be constructed based on general symmetry arguments. Without affecting the low temperature physics on a lattice, let us suppose that there is a high energy cutoff $\Gamma > \Delta$. Then for any $g \neq g_c$, a renormalization group transformation down to a lengthscale $b \gg \Delta^{-1}$ produces the effective Hamiltonian

$$\hat{H}_{\text{eff}} = -\sum_i \frac{c^2}{2\Delta} \frac{\partial^2}{\partial x_i^2} + \sum_{i<j} \mathbf{u}\delta(x_i - x_j) + \dots \,, \tag{2.75}$$

where x_i denotes the position of the i'th quasiparticle and the dots stand for irrelevant terms. The interaction term is local in the long-wavelength description, as no decimation transformation introduces long-range interaction terms [Sol81a, Sol81b]. The interaction matrix $\mathbf{u}$ acts on the internal degrees of freedom, and must be compatible with the permutation symmetry of the Hamiltonian, therefore the interaction amplitudes must satisfy the constraint

$$u_{\kappa_1\kappa_2}^{\kappa_1'\kappa_2'} = u_{(P\kappa_1)(P\kappa_2)}^{(P\kappa_1')(P\kappa_2')} \,, \forall P \in S_{Q-1} \,. \tag{2.76}$$

Now we shall restrict ourselves to the most simple nontrivial case of $Q = 3$. The quantum numbers κ are then chirality indeces $+$ or $-$, and the interaction matrix

can be characterized by three independent parameters, namely

$$u_1 \equiv u^{++}_{++} = u^{--}_{--} \tag{2.77}$$
$$u_2 \equiv u^{+-}_{+-} = u^{-+}_{-+} \tag{2.78}$$
$$u_3 \equiv u^{+-}_{-+} = u^{-+}_{+-} \, . \tag{2.79}$$

These parameters are functions of the dimensionless variables Δb and Δ/Γ: $u_\alpha = u_\alpha(\Delta b, \Delta/\Gamma)$, $\alpha = 1,2,3$. In the long-wavelength limit $b \to \infty$, these parameters still depend on the ratio Δ/Γ, and in general $u_1 \neq u_2 \neq u_3$.

Let us focus on the properties of the Hamiltonian given by Eq (2.75). The single particle spectrum gives the familiar quadratic dispersion relation $\epsilon^\kappa_k = \frac{c^2k^2}{2\Delta}$, and the eigenfunctions are simply plane waves $\Psi_{k\kappa}(x_1, \kappa_1) \sim e^{ikx_1}\delta_{\kappa,\kappa_1}$.

The effective Schrödinger-equation for two quasiparticles reads

$$\left\{ \left[-\frac{c^2}{2\Delta}\frac{\partial^2}{\partial x_1^2} - \frac{c^2}{2\Delta}\frac{\partial^2}{\partial x_2^2} \right] + \mathbf{u}\delta(x_1 - x_2) \right\} \Psi(x_1, x_2, \kappa_1, \kappa_2) = E\Psi(x_1, x_2, \kappa_1, \kappa_2) \, . \tag{2.80}$$

We can construct the two-particle eigenfunction using the singleparticle solution, and in the regions $x_1 < x_2$ and $x_1 > x_2$ this wave function is simply given by

$$\Psi^<_{k_1k_2\Lambda}(x_1, x_2, \kappa_1, \kappa_2) = (Ae^{ik_1x_1 + ik_2x_2} + Be^{ik_2x_1 + ik_1x_2})\chi^\Lambda_{\kappa_1\kappa_2} \tag{2.81}$$

and

$$\Psi^>_{k_1k_2\Lambda}(x_1, x_2, \kappa_1, \kappa_2) = (Ce^{ik_1x_1 + ik_2x_2} + De^{ik_2x_1 + ik_1x_2})\chi^\Lambda_{\kappa_1\kappa_2} \, , \tag{2.82}$$

respectively, where χ^Λ are the eigenvectors of $\mathbf{u}$. The full solution takes the form

$$\begin{aligned} \Psi_{k_1k_2\Lambda}(x_1, x_2, \kappa_1, \kappa_2) &= \Psi^<_{k_1k_2\Lambda}(x_1, x_2, \kappa_1, \kappa_2)\Theta(x_2 - x_1) \\ &+ \Psi^>_{k_1k_2\Lambda}(x_1, x_2, \kappa_1, \kappa_2)\Theta(x_1 - x_2) \, , \end{aligned} \tag{2.83}$$

where the coefficients A, B, C and D have to be determined from smoothness conditions at $x_1 = x_2$. Continuity requires

$$A + B = C + D \, . \tag{2.84}$$

To obtain the other boundary condition, we rewrite the two-particle problem in center-of-mass coordinates:

$$\Psi(x_1, x_2, \kappa_1, \kappa_2)) = \Phi(Y = (x_1 + x_2)/2, y = (x_1 - x_2)/2, \kappa_1, \kappa_2) \, . \tag{2.85}$$

Then the "cusp condition", obtained by integrating the Schrödinger equation in Eq. (2.80) over $y \in [0^-, 0^+]$, can be written as

$$0 = \Phi'_y(y = 0^+) - \Phi'_y(y = 0^-) + \frac{4\Delta}{c^2}\frac{1}{2}\mathbf{u}[\Phi(y = 0^+) + \Phi(y = 0^-)] \, . \tag{2.86}$$

Substituting the state corresponding to Eq. (2.83) gives the condition

$$i(k_1 - k_2)[B + C - A - D] = \frac{2\Delta}{c^2}u^\Lambda[A + B + C + D] \, , \tag{2.87}$$

where u^Λ is an eigenvalue of $\mathbf{u}$. Note that as long as $u_2 \neq u_3 \neq 0$, the interaction matrix is regular and $u^\Lambda \neq 0$ for all Λ.

Based on these general observations, we construct the solution in the scattering channel Λ given by the following expression:

$$\Psi^{\Lambda}_{k_1 k_2} = \hat{P}_{\Lambda} \left\{ \left[e^{ik_1 x_1 + ik_2 x_2} + r_{\Lambda}(k_1, k_2) e^{ik_1 x_2 + ik_2 x_1} \right] \right\} \chi^{\Lambda}_{\kappa_1 \kappa_2} \ , \tag{2.88}$$

where $\hat{P}_{\Lambda}$ is the (anti)symmetrizer operator acting on the spatial wavefunction with a determinant $P_{\Lambda} = \pm 1$, and r_{Λ} is the reflection coefficient that completely specifies the scattering properties of the quasiparticles [Dam98]. Substituting $A = 1$, $B = r_{\Lambda}$, $C = P_{\Lambda} r_{\Lambda}$, $D = P_{\Lambda}$ into the conditions given by Eqs. (2.84) and (2.87), we get a set of equations that the reflection coefficient has to satisfy:

$$1 + r_{\Lambda} = P_{\Lambda}(1 + r_{\Lambda}) \ ; \tag{2.89}$$

$$\left[i(k_1 - k_2) - \frac{2\Delta}{c^2} u^{\Lambda} \right] (1 + P_{\Lambda}) r_{\Lambda} = \left[i(k_1 - k_2) + \frac{2\Delta}{c^2} u^{\Lambda} \right] (1 + P_{\Lambda}) \ . \tag{2.90}$$

If $P_{\Lambda} = 1$, then the first equation is satisfied trivially. However, in the low momentum limit, $k_1 \to 0$ and $k_2 \to 0$, and assuming $u^{\Lambda} \neq 0$, the second condition holds only if $r_{\Lambda} = -1$. If $P_{\Lambda} = -1$, then the second condition becomes trivial. However, the first requires $r_{\Lambda} = -1$. We therefore conclude that the reflection coefficients have to be $r_{\Lambda} = -1$ for all scattering channels. According to Ref. [Dam98], the $\mathcal{S}$ -matrix is then *reflective*, and is given by the expression in Eq. (2.74).

We note that based on the assumption of integrability, Koberle [Kob79, Kob87] derived a transmissive/diagonal $\mathcal{S}$-matrix. However, we think that the assumption of integrability to derive their result is invalid in the region $\Delta \gg T$ under discussion. In fact, one can show that to satisfy integrability, i.e., the Yang – Baxter relations, one must have $u_2 = u_3$, which condition is usually not fulfilled for a general finite ratio Γ/Δ.

2.4.3 Ferromagnetic side

We collected all important ingredients needed to discuss dynamical correlation functions in the gapped phases. In this subsection, we shall calculate the finite temperature correlation function

$$C^{\mu\mu'}(x,t) = \langle e^{it\hat{H}_P} \tilde{P}^{\mu_1}(x) e^{-it\hat{H}_P} \tilde{P}^{\mu_2} \rangle \tag{2.91}$$

at low temperatures, $T \ll \Delta$, on the ferromagnetic side $g < g_c$.

By definition the thermal average of an operator $\hat{O}$ can be written using the Lehmann – representation as

$$\langle \hat{O} \rangle = \sum_n \langle n | \hat{O} | n \rangle \frac{e^{-\beta E_n}}{Z} \ , \tag{2.92}$$

where n denotes the exact many-body eigenstates of the Hamiltonian and E_n is their energy and Z is the canonical partition function. Within the semiclassical approximation, the quantum number n is replaced by the set $\{x_\nu, v_\nu, \theta_\nu\}$, $1 \leq \nu \leq M$. In this configuration, the ν'th quasiparticle is found at $t = 0$ at position x_ν with velocity v_ν and quantum number θ_ν. In the semiclassical limit, the dynamics is deterministic, and the thermal average can be replaced by an average over the initial conditions, therefore we use the approximation

$$\langle \hat{O} \rangle \approx \sum_{\{\theta_\nu\}} \prod_\nu \int dx_\nu \int dv_\nu P(\{x_\nu, v_\nu, \theta_\nu\}) \langle \{x_\nu, v_\nu, \theta_\nu\} | \hat{O} | \{x_\nu, v_\nu, \theta_\nu\} \rangle, \tag{2.93}$$

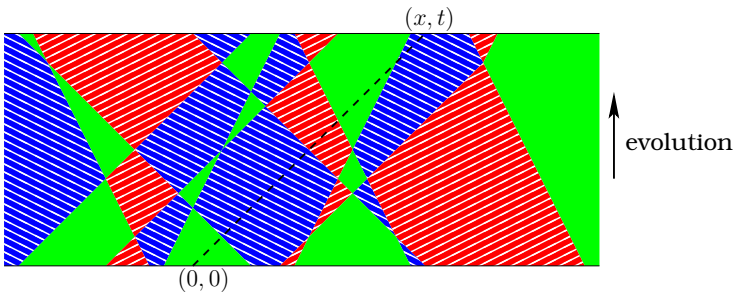

Figure 2.4: Semiclassical dynamics on the ferromagnetic side of the Potts model. Due to the reflective structure of the $\mathcal{S}$ -matrix at low momenta, the orientations of the "middle" domains are conserved in collisions.

where the function $P(\{x_\nu, v_\nu, \theta_\nu\})$ factorizes as

$$P(\{x_\nu, v_\nu, \theta_\nu\}) = \frac{1}{L^M} \frac{1}{(Q-1)^M} \prod_\nu P(v_\nu) \; , \tag{2.94}$$

with the distribution of the velocities given by the Maxwell-Boltzmann statistics,

$$P(v) = \sqrt{\frac{\Delta}{2\pi c^2 T}} \exp\left(-\frac{\Delta v^2}{2c^2 T}\right) \; . \tag{2.95}$$

In the thermodynamic limit, the relative deviations from the average particle number $M = \rho L$ become negligible. We shall not carry out the averaging over the particle number explicitly but restrict ourselves to a fixed number of quasiparticles, and take the limit $M \to \infty$ while keeping the density ρ fixed.

We can calculate the dynamical correlation function defined by Eq. (2.91) within the semiclassical approximation Eq. (2.93), using the methods of Ref. [Dam98] and Refs. [Jep65, Leb69]. As we discussed earlier, energy and momentum conservation implies that the space-time trajectories in one dimension are lying on the straight lines

$$x_\nu(t) := x_\nu + v_\nu t \; . \tag{2.96}$$

We observe that as a given configuration $\{x_\nu, v_\nu, \theta_\nu\}$ evolves, the sequence of the quasiparticles does not change, because of the special exchange form of the $\mathcal{S}$-matrix, see Fig. 2.4. Let's define the function $p_\nu(t)$, which returns the "sequence" number of the particle on the line ν at time t. Initially, $p_\nu(t=0) = \nu$ by definition, and in general we have to keep track of the collisions along the line $x_\nu(t)$:

$$p_\nu(t) = \nu + \sum_{\nu'} [\Theta(x_\nu(t) - x_{\nu'}(t)) - \Theta(x_\nu - x_{\nu'})] \; . \tag{2.97}$$

Note that the first term in the brackets counts the number of particles at time t to the left of the point $x_\nu(t)$, while the second counts them at time $t = 0$. The difference is thus the net number of trajectories the line $x_\nu(t)$ crosses from the right. The position of the νth particle at time t is given by

$$X_\nu(t) = \sum_{\nu'} x_{\nu'}(t) \delta_{\nu, p_{\nu'}(t)} \; . \tag{2.98}$$

After these definitions, let us now focus on a general term in Eq. (2.93), and evaluate the quantummechanical expectation value

$$\langle\{x_\nu, v_\nu, \theta_\nu\}|e^{it\hat{H}_P}\tilde{P}^{\mu_1}(x)e^{-it\hat{H}_P}\tilde{P}^{\mu_2}(0)|\{x_\nu, v_\nu, \theta_\nu\}\rangle \ . \tag{2.99}$$

We split the above expression in the middle, and calculate the resulting "bra" and "ket" parts separately. The operator $P^{\mu_2}(0)$ simply "reads" the orientation of the domain at $x = 0$. At $t = 0$, the positions x_ν define the sequence of domains, where the lth domain starts at x_{l-1} and ends at x_l. Hence the "ket" part can be written as

$$\begin{aligned} &e^{-it\hat{H}_P}\tilde{P}^{\mu_2}(0)|\{x_\nu, v_\nu, \theta_\nu\}\rangle \\ &= \sum_{l,\mu'} \chi(x_{l-1} \le 0 \le x_l)\chi(l\text{th} : \mu')\left(\delta_{\mu_2\mu'} - \frac{1}{Q}\right)e^{-it\hat{H}_P}|\{x_\nu, v_\nu, \theta_\nu\}\rangle \ , \end{aligned} \tag{2.100}$$

where we introduced the indicator function $\chi(A) = 1$ if A is true, else $\chi(A) = 0$. Acting with $\tilde{P}^{\mu_1}$ gives a similar expression, however, the boundaries of the domains are now rather given by $X_\nu(t)$:

$$\begin{aligned} &\tilde{P}^{\mu_1}(x)e^{-it\hat{H}_P}|\{x_\nu, v_\nu, \theta_\nu\}\rangle \\ &= \sum_{m,\mu} \chi(X_{m-1}(t) \le x \le X_m(t))\chi(m\text{th} : \mu) \\ &\qquad \left(\delta_{\mu_1\mu} - \frac{1}{Q}\right)e^{-it\hat{H}_P}|\{x_\nu, v_\nu, \theta_\nu\}\rangle \ . \end{aligned} \tag{2.101}$$

We can take the overlap of Eq. (2.100) and Eq. (2.101) to find

$$\begin{aligned} &\langle\{x_\nu, v_\nu, \theta_\nu\}|e^{it\hat{H}_P}\tilde{P}^{\mu_1}(x)e^{-it\hat{H}_P}\tilde{P}^{\mu_2}(0)|\{x_\nu, v_\nu, \theta_\nu\}\rangle \\ &= \sum_{m,l} \chi(x_{l-1} \le 0 \le x_l)\chi(X_{m-1}(t) \le x \le X_m(t)) \\ &\quad \sum_{\mu\mu'} (\delta_{\mu_1\mu} - \frac{1}{Q})\chi(m\text{th} : \mu)(\delta_{\mu_2\mu'} - \frac{1}{Q})\chi(l\text{th} : \mu') \ , \end{aligned} \tag{2.102}$$

since the phase factors coming from the evolution are equivalent and the configuration was considered to be normalized.

Taking the thermal average of Eq. (2.102) over the configurations $\{x_\nu, v_\nu, \theta_\nu\}$ is a purely mathematical problem, and its details are given in Appendix A.3.1. The conclusion is that the correlation function in the semiclassical approximation can be written in the form

$$C^{\mu_1\mu_2}(x,t) = \left(\delta_{\mu_1\mu_2} - \frac{1}{Q}\right)R_Q(\bar{x},\bar{t}) \ , \tag{2.103}$$

where the relaxation function is defined by

$$\begin{aligned} R_Q(\bar{x},\bar{t}) \ &= \ \int_0^{2\pi} \frac{d\phi}{2\pi} \frac{(Q-1)^2 - 1}{(Q-1)^2 + 2(Q-1)\cos(\phi) + 1} \\ &\qquad e^{-|\bar{t}|(1-\cos\phi)F(\bar{x}/\bar{t})}\cos(\bar{x}\sin\phi) \ , \end{aligned} \tag{2.104}$$

where $\bar{x} = x/\xi_c, \bar{t} = t/\tau_c$ are dimensionless lengths and times with the characteristic length

$$\xi_c \equiv \frac{1}{\rho} = \frac{1}{Q-1}\sqrt{\frac{2\pi c^2}{T\Delta}} e^{\Delta/T} \,, \tag{2.105}$$

and characteristic time

$$\tau_c = \frac{1}{Q-1}\frac{\sqrt{\pi}}{T} e^{\Delta/T} \,. \tag{2.106}$$

The function $F(u)$ is related to the error function by $F(u) = \frac{1}{\sqrt{\pi}} e^{-u^2} + u \, \mathrm{erf}(u)$, and $u = \bar{x}/\bar{t}$ is the dimensionless velocity. As we shall see in the following subsection, the same relaxation function emerges on the paramagnetic side as well. Let us therefore continue with the study of the paramagnetic phase, and postpone the analysis of $R_Q(\bar{x}, \bar{t})$ to Section 2.4.5.

2.4.4 Paramagnetic side

Let us now focus on the calculation of the dynamical correlation function at low temperatures, $T \ll \Delta$, on the paramagnetic side $g > g_c$. We can apply identical arguments as on the ferromagnetic side in the semiclassical limit to approximate the correlation function as

$$\begin{aligned} C^{\mu\mu'}_{\mathrm{para}}(x,t) \;\approx\; & \sum_{\{\lambda_\nu\}} \prod_\nu \int dx_\nu \int dv_\nu \big[P(\{x_\nu, v_\nu, \lambda_\nu\}) \\ & \langle \{x_\nu, v_\nu, \lambda_\nu\} | \tilde{P}^{\mu_1}(x,t) \tilde{P}^{\mu_2}(0,0) | \{x_\nu, v_\nu, \lambda_\nu\} \rangle \big] \,, \end{aligned} \tag{2.107}$$

where the distribution function is analogous to the one on the ferromagnetic side. We again start by examining a term with a given configuration $\{x_\nu, v_\nu, \lambda_\nu\}$.

In contrast to the ferromagnetic side, the operator $\tilde{P}^{\mu_2}(0)$ connects the M-particle eigenstate with the sectors with $M-1$ and $M+1$ quasiparticles. We shall neglect the contribution of the first case, since the probability that a thermally excited particle can be found at $(0,0)$ is negligible. To proceed, we expand the wave function $\tilde{P}^{\mu_2}(0)|\{x_\nu, v_\nu, \lambda_\nu\}\rangle$ in the $M+1$ particle subspace, and find that after evolution, the state can be written as

$$\begin{aligned} & e^{-it\hat{H}_P} \tilde{P}^{\mu_2}(0) |\{x_\nu, v_\nu, \lambda_\nu\}\rangle \\ & = e^{-it\hat{H}_P} \sum_l \chi(x_{l-1} < 0 < x_l) \sum_{\lambda'} \langle \lambda' | \tilde{P}^{\mu_2} | C \rangle \int dv' f(v') \\ & \qquad |\{x_\nu, v_\nu, \lambda_\nu\} \ll (0, v', \lambda')\rangle \,, \end{aligned} \tag{2.108}$$

where the sign "$\ll$" corresponds to the insertion of the extra quasiparticle in the sequence, and $f(v)$ is a currently unknown probability amplitude for the velocity of the quasiparticle inserted by the operator $\tilde{P}^{\mu_2}$. We shall rewrite the wave functions using a notation where the actual sequence of the quasiparticles appears more transparently:

$$|\{x_\nu, v_\nu, \lambda_\nu\} \ll (0, v', \lambda')\rangle \equiv \left| \ldots, \binom{\lambda_{l-1}}{x_{l-1}}, \binom{\lambda'}{0}, \binom{\lambda_l}{x_l}, \ldots \right\rangle \,. \tag{2.109}$$

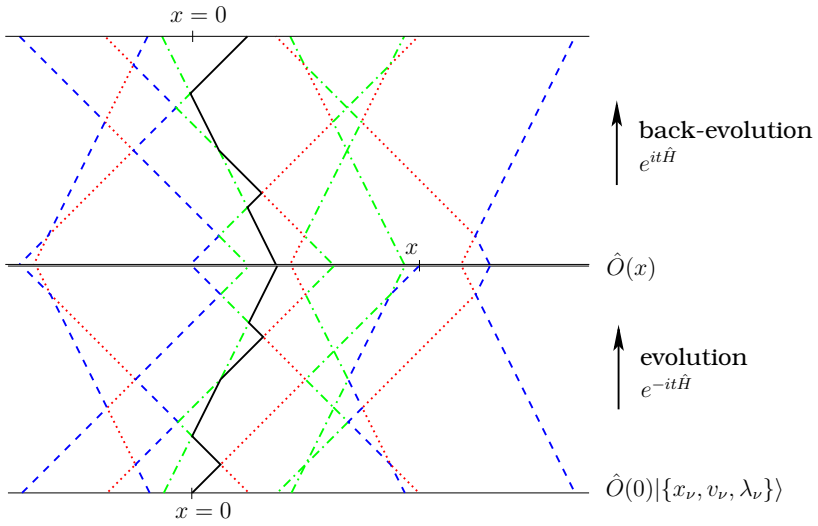

Figure 2.5: Semiclassical dynamics on the paramagnetic side of the quantum Potts model. The operator $\hat{O} = \tilde{P}^{\mu}$ creates an extra quasiparticle in addition to the thermally excited ones. Due to the reflective structure of the $\mathcal{S}$ -matrix at low momenta, the sequence of the quasiparticles does not change during the evolution.

Time evolution, due to the reflective $\mathcal{S}$ -matrix, does not change the sequence of the quantum numbers λ, however, after time t elapses, the wavefunction is given by

$$
\begin{aligned}
e^{-it\hat{H}_P}\left|\ldots,\begin{pmatrix}\lambda_{l-1}\\ x_{l-1}\end{pmatrix},\begin{pmatrix}\lambda'\\ 0\end{pmatrix},\begin{pmatrix}\lambda_{l}\\ x_{l}\end{pmatrix},\ldots\right\rangle = & \sum_{m>l}\chi(X_{m-1}(t)<v't<X_m(t))e^{-i\phi_{\rm ket}(t;m,l)} \\
&\left|\ldots,\begin{pmatrix}\lambda_{l-1}\\ X_{l-1}(t)\end{pmatrix},\begin{pmatrix}\lambda'\\ X_{l}(t)\end{pmatrix},\begin{pmatrix}\lambda_{l}\\ X_{l+1}(t)\end{pmatrix},\ldots,\begin{pmatrix}\lambda_{m-2}\\ X_{m-1}(t)\end{pmatrix},\begin{pmatrix}\lambda_{m-1}\\ v't\end{pmatrix},\begin{pmatrix}\lambda_{m}\\ X_{m}(t)\end{pmatrix},\ldots\right\rangle \\
&+\sum_{m<l}\chi(X_{m-1}(t)<v't<X_m(t))e^{-i\phi_{\rm ket}(t;m,l)} \\
&\left|\ldots,\begin{pmatrix}\lambda_{m-1}\\ X_{m-1}(t)\end{pmatrix},\begin{pmatrix}\lambda_{m}\\ v't\end{pmatrix},\begin{pmatrix}\lambda_{m+1}\\ X_{m}(t)\end{pmatrix},\ldots,\begin{pmatrix}\lambda_{l-1}\\ X_{l-2}(t)\end{pmatrix},\begin{pmatrix}\lambda'\\ X_{l-1}(t)\end{pmatrix},\begin{pmatrix}\lambda_{l}\\ X_{l}(t)\end{pmatrix},\ldots\right\rangle ,
\end{aligned}
\tag{2.110}
$$

where the phase factor $\phi_{\rm ket}(t;m,l)$ is the sum of phases of the individual evolutions of each quasiparticle and of the phases coming from the collisions between them. Note that for any configuration, only a single term has a contribution in the complicated-looking expression, Eq. (2.110). We can expand the "bra" part similarly, and the result is given by the following expression:

$$
\begin{aligned}
\tilde{P}^{\mu_1}(x)e^{-it\hat{H}_P}|\{x_\nu,v_\nu,\lambda_\nu\}\rangle \quad = \quad & \sum_{n,\lambda}\int dv\langle\lambda|\tilde{P}^{\mu_1}|C\rangle e^{-i\phi_{\rm bra}(t;n)} \\
& \chi(X_{n-1}(t)<x<X_n(t))f(v) \\
& \left|\ldots,\begin{pmatrix}\lambda_{n-1}\\ X_{n-1}(t)\end{pmatrix},\begin{pmatrix}\lambda\\ x\end{pmatrix},\begin{pmatrix}\lambda_{n}\\ X_{n}(t)\end{pmatrix},\ldots\right\rangle .
\end{aligned}
\tag{2.111}
$$

The quantummechanical overlap of the states in Eq. (2.110) and Eq. (2.111) is nonzero only if all quantum numbers are the same, therefore such configurations need to satisfy the following conditions:

$$x = v't \, , v' = v \, , m = n \, , \tag{2.112}$$

and for $m > l$

$$\lambda' = \lambda_l, \ \lambda_l = \lambda_{l+1}, \ldots, \ \lambda_{m-2} = \lambda_{m-1}, \ \lambda_{m-1} = \lambda \tag{2.113}$$

while for $m < l$:

$$\lambda_m = \lambda, \ \lambda_{m+1} = \lambda_m, \ldots, \ \lambda_{l-1} = \lambda_{l-2}, \ \lambda' = \lambda_{l-1} \, . \tag{2.114}$$

Note that the last two sets of equations can be written in a simpler form

$$\lambda' = \lambda, \ \lambda_{\min\{l,m\}} = \lambda_{\min\{l,m\}+1} = \ldots = \lambda_{\min\{l,m\}+|m-l|} = \lambda \, . \tag{2.115}$$

To conclude, a term in Eq. (2.107) can be written as

$$\begin{aligned}
&\langle \{x_\nu, v_\nu, \lambda_\nu\} | e^{it\hat{H}_P} \tilde{P}^{\mu_1}(x) e^{-it\hat{H}_P} \tilde{P}^{\mu_2}(0) | \{x_\nu, v_\nu, \lambda_\nu\} \rangle \\
&= \sum_\lambda \sum_{l,m} \int dv \ \langle C | \tilde{P}^{\mu_1} | \lambda \rangle \langle \lambda | \tilde{P}^{\mu_2} | C \rangle f^2(v) e^{-i(\phi_{\rm ket}(t;m,l) - \phi_{\rm bra}(t;m))} \\
&\qquad \chi(x_{l-1} < 0 < x_l) \chi(X_{m-1} < vt < X_m) \\
&\qquad \delta_{\lambda\lambda_{\min\{l,m\}}} \delta_{\lambda\lambda_{\min\{l,m\}+1}} \cdots \delta_{\lambda\lambda_{\min\{l,m\}+|m-l|}} .
\end{aligned} \tag{2.116}$$

We can carry out the average over the quantum numbers λ_ν explicitly, yielding a factor of

$$\langle \delta_{\lambda\lambda_{\min\{l,m\}}} \delta_{\lambda\lambda_{\min\{l,m\}+1}} \cdots \delta_{\lambda\lambda_{\min\{l,m\}+|m-l|}} \rangle_{\{\lambda_\nu\}} = \left(\frac{1}{Q-1} \right)^{|l-m|} \, , \tag{2.117}$$

which is independent of λ, and thus we can perform the summation in Eq. (2.116), giving the result

$$\sum_\lambda \langle C | \tilde{P}^{\mu_1} | \lambda \rangle \langle \lambda | \tilde{P}^{\mu_2} | C \rangle = \frac{1}{Q} \left(\delta_{\mu_1\mu_2} - \frac{1}{Q} \right) \, . \tag{2.118}$$

The phase difference between the "ket" and the "bra" states comes from the propagation of the extra quasiparticle and from the collisions it causes, and we can write

$$e^{-i(\phi_{\rm ket}(t;m,l) - \phi_{\rm bra}(t;m))} = (-1)^{|l-m|} e^{-i\epsilon_{k(v)}t} \, . \tag{2.119}$$

After inspecting the remaining terms in Eq. (2.116), we can factorize the correlation function in the following way:

$$C^{\mu_1\mu_2}_{\rm para}(x,t) = C^{\mu_1\mu_2}_{\rm para}(x,t)_{T=0} \ R_Q(x/\xi_c, t/\tau_c) \, , \tag{2.120}$$

where $C^{\mu_1\mu_2}_{\rm para}(x,t)_{T=0}$ is given in the limit $g \to \infty$ by Eq. (2.26), while the relaxation function is given by the same expression as for the ferromagnetic side in Eq. (2.104).

2.4.5 The universal relaxation function

We have found that the correlations of the quantum Potts model decay with the same universal function $R_Q(\bar{x},\bar{t})$ both on the ferromagnetic and on the paramagnetic side in the semiclassical limit. This is probably related to the self-duality of the quantum Potts model [Sol81a, Sol81b]. Now we shall discuss the properties of this relaxation function in detail, starting by showing plots for various values of its arguments for the cases $Q = 3$ and $Q = 4$ in Figs. 2.6, 2.8 and Figs. 2.7, 2.9, respectively.

Remarkably, as $Q \to 2$, the main contribution in the integral in Eq. (2.104) is coming from the pole of the prefactor at $\phi = \pi$. Evaluating the integral gives

$$R_{Q=2}(\bar{x},\bar{t}) = \exp\left(-2\bar{t}F(\bar{x}/\bar{t})\right), \tag{2.121}$$

which coincides with the result for the Ising model in Ref. [Sac99]. The exponential decay is a result of a destructive "quantum interference": The quasiparticles carry no inner quantum numbers, hence the domains on the ferromagnetic side are alternating, leading to a long-lasting oscillation in time with a characteristic time $\sim \tau_c$.

We find a qualitatively different behavior in the long-time limit in the $Q > 2$ case, which can be extracted from Eq. (2.104) as follows. In the $\bar{t} \gg 1$ limit, the main contribution in the integral comes from the neighborhood of $\phi \approx 0$, and thus one can make a Gaussian approximation to find that

$$R_{Q>2}(\bar{x},\bar{t} \gg 1) \approx \frac{1}{2\pi}\frac{Q-2}{Q}\int_{-\infty}^{\infty} d\phi \cos(\bar{x}\phi) e^{-|\bar{t}|\phi^2/(2\sqrt{\pi})} . \tag{2.122}$$

We can perform the integration to find the diffusive form

$$R_{Q>2}(\bar{x},\bar{t} \gg 1) \approx \frac{Q-2}{Q}\frac{1}{\sqrt{4\pi\bar{D}\bar{t}}} e^{-\frac{\bar{x}^2}{4\bar{D}\bar{t}}} , \tag{2.123}$$

where the diffusion constant is given by $\bar{D} = 1/2\sqrt{\pi}$. This diffusive behavior comes from the approximate conservation of the quantum numbers, which is a consequence of the reflective structure of the $\mathcal{S}$ -matrix.

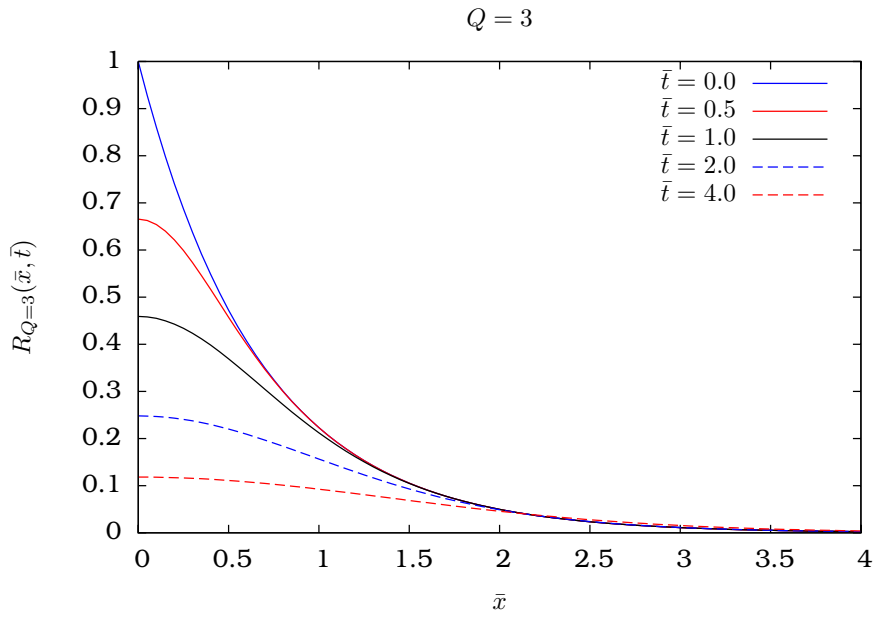

Figure 2.6: The relaxation function $R_{Q=3}(\bar{x}, \bar{t})$ for different values of $\bar{t}$.

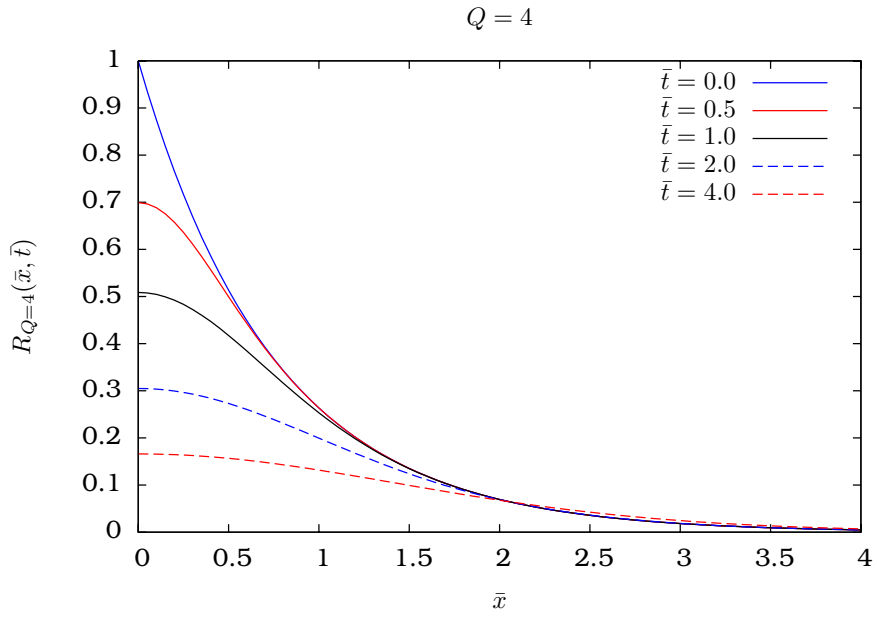

Figure 2.7: The relaxation function $R_{Q=4}(\bar{x}, \bar{t})$ for different values of $\bar{t}$.

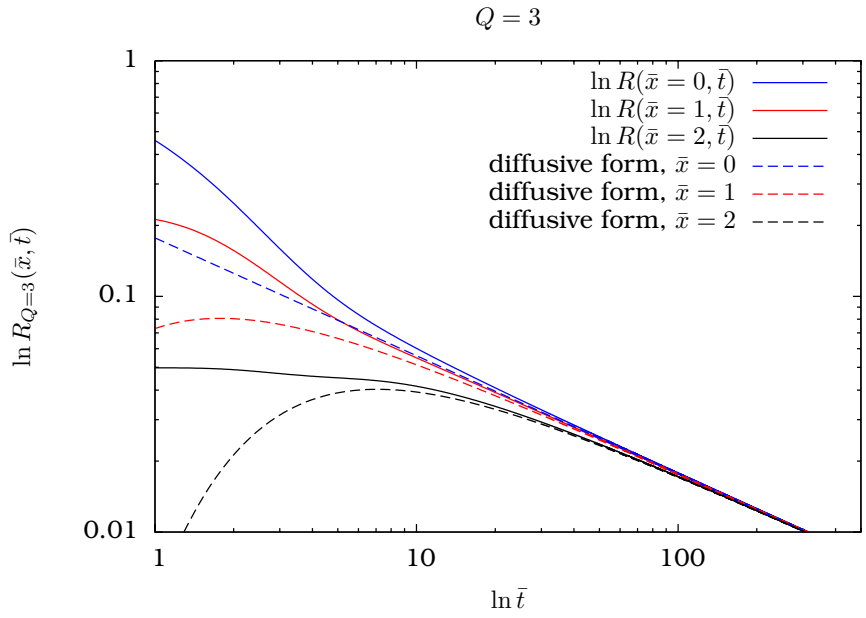

Figure 2.8: Asymptotic long-time behavior of $R_{Q=3}(\bar{x}, \bar{t})$ for different values of $\bar{x}$ (solid lines). We also show the values for the diffusive form of Eq. (2.123) (dashed lines).

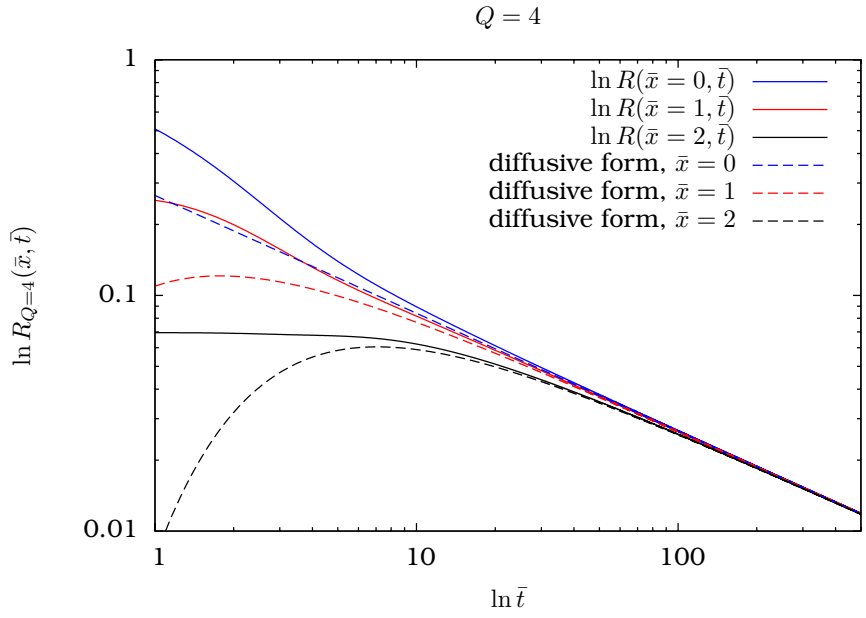

Figure 2.9: Asymptotic long-time behavior of $R_{Q=4}(\bar{x}, \bar{t})$ for different values of $\bar{x}$ (solid lines). We also show the values for the diffusive form of Eq. (2.123) (dashed lines).

2.5 Universal relaxation in gapped models

2.5.1 Introduction

In the previous sections, we calculated dynamical correlation functions of the quantum Potts model in $d = 1$ dimension. In the gapped phases, we applied a semiclassical approximation and derived an analytical expression for the relaxation function. The result was a universal function describing both the ferromagnetic and the quantum paramagnetic sides. Basically, there are two ingredients which we used in the method developed for the quantum Potts model: (A) the gap Δ in the quasiparticle spectrum at zero momentum $k = 0$ and (B) the reflective nature of the $\mathcal{S}$ -matrix. In this section we shall extend our analysis and consider one-dimensional models that possess these two properties. We shall also confirm that, indeed, a relaxation function equivalent to that in Eq. (2.104) governs the finite temperature dynamics in all models considered.

More than 20 years ago, Haldane pointed out that quantum Heisenberg chains with an integer spin S=1,2,... have a gap in the excitation spectrum [Hal83]. The astonishing difference between the gapless spin-half chains and the spin-integer case has been accepted and well understood analytically [Aff89] and numerically [Dei93], furthermore, the existence of the gap was confirmed experimentally [Mora88, Mut89, Mut91, Regn94, Sol03, Tak96, Xu96]. Although zero temperature integer-spin chains and their static properties at finite temperatures have been studied extensively, understanding the finite temperature dynamical behavior still poses a major theoretical challenge. Not even the dynamics of the S=1 Heisenberg antiferromagnet has been fully understood so far. Understanding these dynamical properties in detail would be, however, crucial in order to interpret inelastic neutron scattering [Mora88, Mut89, Mut91, Regn94, Xu96] or nuclear magnetic resonance [Cha97, Tak96] experiments. One of our goals shall be to approximate the dynamical correlations of the $S = 1$ antiferromagnetic Heisenberg chain, which is closely related to the inelastic lineshape measured directly via neutron scattering.

2.5.2 The AF Heisenberg chain and the quantum rotor model

The $S = 1$ Heisenberg chain is described by the Hamiltonian

$$\hat{H}^{\mathrm{Heis}} = J \sum_i \hat{\mathbf{S}}_i \hat{\mathbf{S}}_{i+1} \ , \tag{2.124}$$

where $\hat{\mathbf{S}}_i$ is an $S = 1$ spin on site i, and $J > 0$ is the antiferromagnetic coupling. As first proved by Haldane, antiferromagnetic spin waves have a gap, if S is an integer [Hal83]. Haldane's prediction is in good agreement with many experiments on different quasi-1D materials [Mora88, Mut89, Mut91, Regn94, Sol03, Tak96, Xu96], although perturbations like magnetic anisotropy, lattice distortions, disorder, etc., are allways present in physical systems.

Low-energy excitations of the Heisenberg model in Eq. (2.124) can be mapped onto the $O(3)$ rotor chain [Aff89, Hal83], defined by the following Hamiltonian:

$$\hat{H}^{\mathrm{rotor}} = \frac{\tilde{J}g}{2} \sum_i \hat{\mathbf{L}}_i^2 - \tilde{J} \sum_i \hat{\mathbf{n}}_i \hat{\mathbf{n}}_{i+1} \ . \tag{2.125}$$

Here $\hat{\mathbf{n}}_i$ is the position operator of the rotor on site i with the constraint $\hat{\mathbf{n}}_i^2 = 1$, and $\hat{\mathbf{L}}_i = \hat{\mathbf{n}}_i \times \hat{\mathbf{p}}_i$ is its angular momentum operator:

$$[\hat{L}_i^\alpha, \hat{L}_i^\beta] = i\epsilon_{\alpha\beta\gamma}\hat{L}_i^\gamma \ , \ [\hat{L}_i^\alpha, \hat{n}_i^\beta] = i\epsilon_{\alpha\beta\gamma}\hat{n}_i^\gamma \ . \tag{2.126}$$

The mapping can be done most straightforwardly in the path integral formalism by representing spins in terms of coherent states $\mathbf{N}_i(\tau) \Leftrightarrow \hat{\mathbf{S}}_i(\tau)$. The unit modulus field $\mathbf{N}_i(\tau)$ can be parameterized [Aff89, Hal83, Sac99] by slowly varying fields as

$$\mathbf{N}_i(\tau) = (-1)^i \mathbf{n}_i(\tau)\sqrt{1 - a^2\mathbf{L}_i^2(\tau)} + a\mathbf{L}_i(\tau) \ , \tag{2.127}$$

where $\mathbf{n}$ describes the staggered and $\mathbf{L}$ the uniform component of the Heisenberg spins, and a is the lattice spacing. In the $S = 1$ case, the excitations corresponding to both fields $\mathbf{n}(\tau)$ and $\mathbf{L}(\tau)$ are massive [Hal83]. Integration over $\mathbf{L}$ leads to the non-linear σ-model, defined by the action

$$\mathcal{A}^{\mathrm{nl}\sigma\mathrm{m}} = \frac{3}{2\tilde{c}\tilde{g}} \int_0^\beta d\tau \int dx [(\partial_\tau \tilde{\mathbf{n}}(x,\tau))^2 + \tilde{c}^2 (\partial_x \tilde{\mathbf{n}}(x,\tau))^2] \ , \tag{2.128}$$

where $\tilde{g}$ is a coupling constant, $\tilde{c}$ has a dimension of velocity, and the field $\mathbf{n}(x,\tau)$ satisfies the constraint $\tilde{\mathbf{n}}^2(x,\tau) = 1$. The non-linear σ-model is the continuum theory of the rotor chain [Sac99] .

2.5.3 Dynamical correlations in the $O(3)$ rotor model

Let us now discuss the properties of the rotor model. For $g \gg 1$, in the ground state, all rotors need to be in the $L = 0$ state to minimize kinetic energy. The lowest energy excitations form a triplet with a quantum number $L^z \equiv \lambda = -1, 0, 1$. In $d = 1$, the qualitative structure of the low-energy spectrum is the same for any $g > 0$ and the excitations have a gap $\Delta(g)$ [Dam98, Sac99]. The gap Δ allows us to apply a semiclassical approximation at temperatures low enough $T \ll \Delta$, similar to the transverse field Ising model [Sac97b], the quantum Potts model [Rap06], the $O(3)$ nonlinear σ-model [Dam98, Sac97a] and the sine-Gordon model [Dam05].

Let us focus on the dynamical correlation function of the rotor model, and follow the same steps as for the quantum Potts model [Rap06]. In the semiclassical limit, the correlation function can be approximated as:

$$\begin{aligned} C^{\mathrm{rotor}}(x,t) &= \langle \hat{n}^z(x,t)\hat{n}^z(0,0)\rangle_{\hat{H}^{\mathrm{rotor}}} \\ &\approx \sum_{\{\lambda_\nu\}} \int \prod_\nu dx_\nu \prod_\nu dv_\nu \Big[P(\{x_\nu, v_\nu, \lambda_\nu\}) \\ &\quad \langle \{x_\nu, v_\nu, \lambda_\nu\}|\hat{n}^z(x,t)\hat{n}^z(0,0)|\{x_\nu, v_\nu, \lambda_\nu\}\rangle \Big] \ , \end{aligned} \tag{2.129}$$

where $P(\{x_\nu, v_\nu, \lambda_\nu\})$ is a distribution analogous to Eq. (2.94). By calculating the matrix elements for $\hat{n}^z (\Leftrightarrow \cos\theta)$ with the first few spherical harmonics, one can find that $\hat{n}^z$ either creates a quasiparticle ($L = 1$) with $L^z = 0$ at $x = 0$ with some velocity v or destroys one created thermally in the configuration $\{x_\nu, v_\nu, \lambda_\nu\}$.[1] The probability

[1] There are also multiparticle contributions which are important at higher temperatures $T > \Delta$, however, we can neglect them in the semiclassical limit $T \ll \Delta$.

of latter is exponentially small since at $T \ll \Delta$ the quasiparticle density ρ is low, so we will neglect this. Due to the collisions with the thermally excited particles, there are only certain configurations where the quantummechanical overlap in Eq. (2.129) will be nonzero. Similar to the Potts model discussed in Section 2.4, the $O(3)$ rotor model has a pure reflective scattering matrix [Dam98, Zam78]:

$$\mathcal{S}_{\lambda_1\lambda_2}^{\lambda_1'\lambda_2'} = (-1)\delta_{\lambda_1}^{\lambda_2'}\,\delta_{\lambda_2}^{\lambda_1'}\,. \tag{2.130}$$

This structure implies that the *sequence* of the quantum numbers λ_ν does not change with time. Thus if the extra particle collides with N_+ particles from the right and N_- particles from the left, then to have a non-vanishing overlap, the first $n = N_+ - N_-$ particles to the right must also have $L_\nu^z = 0$ and $L_\nu = 1$. At time t a quasiparticle must be destroyed by $\hat{n}^z(x,t)$ such that the overlap does not vanish. These observations are analogous to the arguments given for the paramagnetic side of the quantum Potts model [Rap06]. Taking also the phase factors into account, we get an expression similar to that obtained for the paramagnetic side of the quantum Potts model:

$$C^{\rm rotor}(x,t) = C_{T=0}^{\rm rotor}(x,t)\tilde{R}(x,t)\,, \tag{2.131}$$

where the first term is the average of a phase factor coming from the propagation of a single particle from $(0,0)$ to (x,t) [Dam98]:

$$C_{T=0}^{\rm rotor}(x,t) = \frac{\mathcal{Z}}{2\pi}K_0(\Delta\sqrt{x^2/c^2 - t^2})\,, \tag{2.132}$$

where K_0 is the modified Bessel function of the second kind and $\mathcal{Z}$ is a nonuniversal quasiparticle residue. Well within the light cone, $x \ll ct$, one can recover the Feynman propagator of a particle with a mass of Δ:

$$C_{T=0}^{\rm rotor}(x \ll ct,t) \sim e^{-i\Delta t}\sqrt{\frac{\Delta}{2\pi i t}}\exp\left(i\frac{\Delta x^2}{2c^2 t}\right)\,. \tag{2.133}$$

The second term is given by

$$\tilde{R}(x,t) = \sum_{n=-\infty}^{\infty}\frac{(-1)^n}{3^{|n|}}\left\langle \delta_{n,\sum_\nu[\Theta(x-x_\nu-v_\nu t)-\Theta(-x_\nu)]}\right\rangle_{\{v_\nu,x_\nu\}} = R_{Q=4}(x/\xi_c, t/\tau_c). \tag{2.134}$$

In the middle expression, we already took the average over the angular momentum components $\{\lambda_\nu\}$, leading to the term $1/3^{|n|}$. The expression in the average indicates that the excited particle drifts to the right by n. The factor of $(-1)^n$ corresponds to the net phase accumulated in course of the scattering with the quasiparticles. The average over the velocities and coordinates can be carried out analytically to obtain the result on the right hand side of Eq. (2.134) [Rap06].

The correlation function of the antiferromagnetic Heisenberg chain

$$C^{zz}(x,t) \equiv \langle \hat{S}^z(x,t)\hat{S}^z(0,0)\rangle\,, \tag{2.135}$$

can thus be obtained at low temperatures as follows. As it can be seen from Eq. (2.127), and proved more rigorously in Ref. [Sac99], while the fluctuations around $q = 0$ in the Heisenberg chain are described by the $L^z - L^z$ correlation function of the $O(3)$ quantum rotor chain, the dynamics at $q = \pi/a$ is related to the $n^z - n^z$ correlation function. As a consequence, in the low temperature limit, the

dynamic structure factors of the Heisenberg and rotor models are simply related as

$$S^{zz}(q = \pi/a + k, \omega) \sim S^{\mathrm{rotor}}(k, \omega) \ . \tag{2.136}$$

The correlation function that we calculated for the rotor model analytically, has been obtained by Damle and Sachdev numerically using a stochastic sampling. The $L^z - L^z$ correlation function has been evaluated analytically in Ref. [Dam98].

2.5.4 The $O(N)$ rotor chain

As a generalization of the $O(3)$ quantum rotor chain, let us now investigate the correlations of rotor models with $O(N)$ symmetry, defined by the Hamiltonian

$$\hat{H}^{\mathrm{O(N)}} = \frac{Jg}{2} \sum_i \hat{\mathbf{L}}_i^2 - J \sum_i \hat{\mathbf{n}}_i \hat{\mathbf{n}}_{i+1} \ , \tag{2.137}$$

where $\hat{\mathbf{n}}_i$ is the $N \geq 3$-dimensional position operator of the rotor on site i with the constraint $\hat{\mathbf{n}}^2 = 1$. The angular momentum operator components are given by $\hat{L}_{\alpha\beta} = \hat{n}^\alpha \hat{p}_\beta - \hat{n}^\beta \hat{p}_\alpha$, where $[\hat{n}^\alpha, \hat{p}_\beta] = i\delta_{\alpha\beta}$. The square of the angular momentum operator is defined by

$$\hat{\mathbf{L}}^2 = \frac{1}{2} \sum_{\alpha \neq \beta} \hat{L}_{\alpha\beta}^2 \ . \tag{2.138}$$

We can find the low energy structure of the operator $\hat{\mathbf{L}}^2$ in a number of ways, we shall proceed according to Ref. [Ave89]. Let $h_\lambda(n_1, \ldots, n_N)$ be a harmonic homogeneous polynomial of order λ, so that it satisfies the N-dimensional Laplace equation: $\sum_\alpha \partial_\alpha^2 h_\lambda = 0$ and $h_\lambda(yn_1, \ldots, yn_N) = y^\lambda h_\lambda(n_1, \ldots, n_N)$. Then it can be shown that the hyperspherical function $Y_\lambda(\Omega) = r^{-\lambda} h_\lambda$, with $r = \sqrt{\sum_\alpha (n^\alpha)^2}$ is the hyperradius and Ω denotes the hyperspherical coordinates, satisfies the partial differential equation

$$\left(\hat{\mathbf{L}}^2 - \lambda(\lambda + N - 1) \right) Y_\lambda(\Omega) = 0 \ , \tag{2.139}$$

so that it is an eigenfunction of the generalized angular momentum [Ave89]. We can see that $\lambda = 0, 1, \ldots$ corresponds to the increasing energy levels of a single $O(N)$ rotor. The ground state wave function $Y_0(\Omega) \equiv |0\rangle \sim 1$ is a singlet. However, there is a number of linearly independent functions with $\lambda = 1$, namely

$$|\alpha\rangle \sim n_\alpha \ , \tag{2.140}$$

which are degenerate [Ave89]. Note that this observation is in agreement with the transformation property $[\hat{L}_{\alpha\beta}, \hat{n}^\gamma] = i \sum_\delta f_{\alpha\beta\gamma\delta} \hat{n}^\delta$, which suggests that $\hat{n}^\alpha$ transforms as a vector with respect to the $O(N)$ rotations. Note, however, that this latter, group theoretical argument is not capable of determining the position of the excited level with respect to the ground state and the other levels. Symmetry ensures that

$$\langle 0 | \hat{n}^\alpha | 0 \rangle = 0 \ , \ \langle 0 | \hat{n}^\alpha | \beta \rangle \sim \delta_{\alpha\beta} \ . \tag{2.141}$$

Strong coupling analysis [Ham79] and large-N expansion [Sac99] suggest that in $d = 1$ dimension, the ground state is $\prod_i |0\rangle_i$, while excitations are gapped with the quantum number $\alpha = 1, \ldots, N$. The $\mathcal{S}$ -matrix of the continuum $O(N)$ non-linear σ-model is purely reflective, and here we shall assume that this holds also for the lattice-regularized Hamiltonian [Zam78].

These arguments imply that the finite temperature dynamical correlations of the $O(N)$ rotor chains can also be factorized:

$$\begin{aligned} C^{O(N)}(x,t) &= \langle \hat{n}^N(x,t)\hat{n}^N(0,0)\rangle \\ &= C^{O(N)}_{T=0}(x,t)\; R_{Q=N+1}(\bar{x},\bar{t}), \end{aligned} \tag{2.142}$$

where $C^{O(N)}_{T=0}(x,t)$ corresponds to the $T=0$ temperature propagation of a quasiparticle. Hence the universal relaxation function $R_Q(\bar{x},\bar{t})$ indeed describes the decay of correlations in a number of gapped one-dimensional spin models at low temperatures, even in the limiting case of the Ising model in a transverse magnetic field, i.e., the $Q=2$ quantum Potts model which can be also identified with the "$O(1)$" quantum rotor model.

2.5.5 The sine-Gordon model

Diffusive behavior of the semiclassical correlation function of the sine-Gordon model, defined by the action

$$\mathcal{A}^{\rm sG} = \frac{c}{16\pi}\int_0^{1/T} d\tau \int dx \left[(\partial_x\Phi)^2 + \frac{1}{c^2}(\partial_\tau\Phi)^2 - g^2\cos(\gamma'\Phi)\right] , \tag{2.143}$$

was found first by Damle and Sachdev [Dam05]. In this model the correlation function is defined by

$$C_\Phi(x,t) = \langle e^{i\eta\Phi(x,t)}e^{-i\eta\Phi(0,0)}\rangle_{\mathcal{A}^{\rm sG}} . \tag{2.144}$$

Now we shall prove that the relaxation of correlations is described by Eq. (2.104), with the parameters set to

$$\frac{1}{Q-1} = -\cos\left(\frac{2\pi\eta}{\gamma'}\right) = -\mathbf{\Theta} . \tag{2.145}$$

Within the semiclassical approximation and using the results of the previous subsections, it is easy to show the equivalency of the correlators of the sine-Gordon model and the Potts model. We follow a somewhat different way to derive the results of Ref. [Dam05]. It is known that the sine-Gordon field can be described in terms of "domains" which are separated by soliton and anti-soliton trajectories. These domains can be labeled by integers so that the field is approximately

$$\Phi(x,t) = \frac{2\pi}{\gamma'}\sum_\nu m_\nu \Theta(x - x_\nu(t)) , \tag{2.146}$$

where $x_\nu(t)$ are the trajectories of the solitons and $m_\nu = \pm 1$ are the charges of the solitons (see Fig. 2.10 for a given configuration). The collision of the solitons is described by a reflective $\mathcal{S}$ -matrix [Dam05].

Within the semiclassical approximation, we find that the average over the kinetic variables and soliton charges factorizes as

$$\begin{aligned} C_\Phi(x,t) = \sum_n \quad & \left\langle \delta_{n,\sum_\nu[\Theta(x-x_\nu-v_\nu t)-\Theta(0-x_\nu)]}\right\rangle_{\{x_\nu,v_\nu\}} \\ (-1)^n \quad & \left\langle \sum_k P_k(n) e^{i\eta\frac{2\pi}{\gamma'}(2k-|n|)}\right\rangle_{\{m_\nu\}} . \end{aligned} \tag{2.147}$$

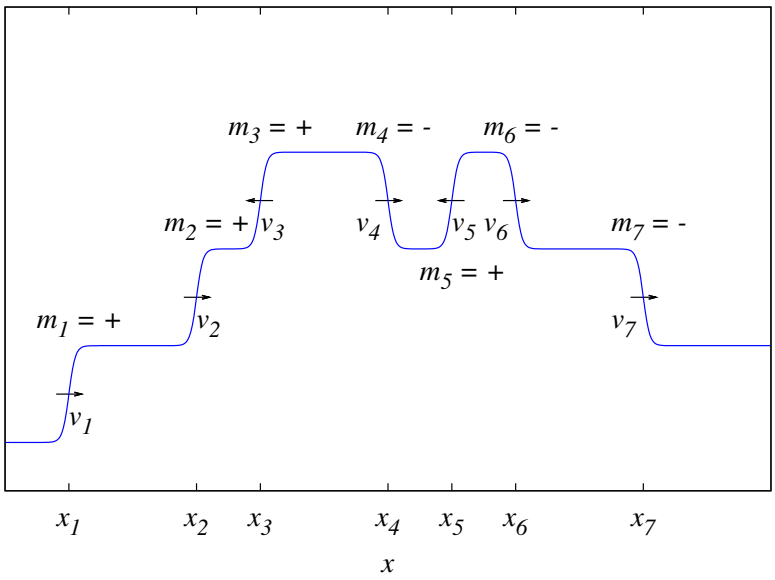

Figure 2.10: A configuration of kinks and antikinks in the sine-Gordon model at $t = 0$.

Here $P_k(n)$ is the probability that the number of $m_\nu = +1$-charge soliton lines crossing the section $(0,0) \to (x,t)$ is k, where the total number of collisions along the section is n. The second term in Eq. (2.147) can be simplified as follows. The probabilities that a soliton or an anti-soliton is associated with a given trajectory are equal in a configuration. Therefore the probability for intersecting k soliton lines has a binomial distribution

$$\langle P_k(n) \rangle_{\{m_\nu\}} = \binom{|n|}{k} \frac{1}{2^{|n|}} \,, \tag{2.148}$$

since every sequence of a given number of solitons and anti-solitons has equal probability. Using Eq. (2.148), we can compute the sum over k in Eq. (2.147) to obtain the result

$$\left\langle \sum_k P_k(n) e^{i\eta \frac{2\pi}{\gamma'}(2k-|n|)} \right\rangle_{\{m_\nu\}} = \cos\left(\eta \frac{2\pi}{\gamma'}\right)^{|n|} . \tag{2.149}$$

Comparing this expression with the relaxation function found for the Potts model one finds Eq. (2.145).

2.6 Summary

In this chapter, we investigated the dynamical correlations of the $Q = 3$ quantum Potts chain in three regions. One can identify two gapped phases which are separated by an anomalous region originating from the quantum critical point. In the quantum critical regime, we calculated the dynamic susceptibility at $g = g_c$ and $T > 0$ by using a conformal mapping from the expression of the $T = 0$ temperature critical correlation function. On the other hand, we obtained the dynamical correlation functions in the gapped phases at finite, low temperatures $T \ll \Delta$ in a semiclassical approximation. The calculation was based on the universal form of the $\mathcal{S}$ -matrix of the quasiparticles, which was found to be purely reflective in the long wavelength limit. We concluded that the correlation function can be generally factorized as

$$C(x,t) = C_{T=0}(x,t)\ R_Q(\bar{x},\bar{t})\ , \tag{2.150}$$

where the universal relaxation function $R_Q(\bar{x},\bar{t})$ applies both to the ferromagnetic and to the paramagnetic side. This discovery is probably a manifestation of the self-duality of the quantum Potts model [Wu82]. In the case $Q = 3$, the relaxation function was shown to have diffusive decay for long timescales.

Although the precise structure of the $\mathcal{S}$ -matrix for $Q \geq 4$ is unknown, we found that calculations carried out for $Q \neq 3$ are relevant for other one-dimensional spin systems. The $Q = 2$ case reproduces the results found for the transverse field Ising model, where the relaxation is exponential for long times rather than diffusive [Sac99]. We have also been able to calculate the $n_z - n_z$ correlation function of the $O(3)$ quantum rotor model analytically, and have shown that there the relaxation function is characterized by the parameter $Q = 4$ in Eq. (2.150). Furthermore, this correlation function is also related to the dynamical structure factor of the $S = 1$ antiferromagnetic Heisenberg model at the wavevector $q \approx \pi/a$. We also applied the semiclassical method to rotor chains with general $O(N)$ symmetry. Finally, we demonstrated that correlations in the sine-Gordon model are also characterized by the same relaxation function.

Our computations thus show that Eq. (2.150) applies to a variety of different models. This universality relies on the universality of the scattering matrix, i.e., that for most models, the $\mathcal{S}$ -matrix of gapped systems becomes purely reflective in the long wavelength limit. In this sense, the main result of Ref. [Rap06], the universal relaxation function defined by Eq. (2.104), is a crucial result in order to understand the finite temperature dynamics of gapped one-dimensional systems.

Chapter 3

The three-component Hubbard model

3.1 Introduction

In a pioneering experiment thirteen years ago, Anderson and collaborators [And95] succeeded in cooling a vapor of ^{87}Rb atoms to approximately $T \approx 170$ nK, and observed the Bose-Einstein condensation of the atoms. Since then, a large number of studies on manipulating ultracold atomic systems appeared. Achieving quantum degeneracy in atomic vapors offers new possibilities to realize novel states of matter and to compare with theoretical predictions coming from various branches of physics, ranging from atomic and condensed matter physics to quantum information theory. We shall first give a brief introduction to this extended field to serve as a motivation for our study of the three-component Hubbard model.

Noble gases, due to their closed shells, have the simplest electronic structure. However, the high-energy electronic transitions and the lack of electronic spin makes them unsuitable for manipulation with (electro)magnetic fields. Alkali metal atoms, on the other hand, have one s-electron in addition to the noble gas structure, and still have a simple electronic structure and spin momentum. Probably this is why experimentalists favor alkali metals over other elements of the periodic table.

Whether or not an ideal gas is in the quantum degenerate limit, is determined by two microscopic lengthscales: the thermal de Broglie-wavelength, given by

$$\lambda_T = \frac{2\pi\hbar}{\sqrt{k_{\mathrm{B}} T m}} \,, \tag{3.1}$$

where m is the mass of the particles, and the average spatial separation, which we define by

$$\xi = 1/\rho^{1/d} \,, \tag{3.2}$$

where ρ is the number density of the particles. These length scales can be combined to define the phase space density,

$$\Lambda \equiv \left(\lambda_T/\xi\right)^d = \rho \lambda_T^d \,. \tag{3.3}$$

Classical behavior is expected for $\Lambda \ll 1$, when the de Broglie-wavelength is much smaller than the average separation of the particles.

It is worth estimating the phase space density for a few systems at room temperature, $T \approx 300$K. In noble gases at atmospheric pressure with a typical density $\rho \approx 2.7 \cdot 10^{19}$ cm^{-3} and atomic mass $m \approx Am_p$, we get

$$\Lambda^{\mathrm{NG}} \approx \frac{0.00043}{A^{3/2}} , \tag{3.4}$$

where A is the mass number of the given element. In intrinsic Ge semiconductors with a conduction electron density of $\rho \approx 10^{14}$ cm^{-3} and effective mass $m \approx 0.04m_e$ [Kit96], the corresponding phase space density is

$$\Lambda^{\mathrm{e-Ge}} \approx 0.016 . \tag{3.5}$$

These two systems are therefore classical, and the momentum distribution of the particles is well described by the Maxwell-Boltzmann statistics.

For the (free) electron gas in sodium, on the other hand, one has $\rho = 2.5 \cdot 10^{22}$ cm^{-3}, and $m \approx m_e$ [Kit96], and we get

$$\Lambda^{\mathrm{e-Na}} \approx 31381 , \tag{3.6}$$

which is consistent with the existence of the sharp Fermi surface ($T \ll T_F$).

Alkali metals at atmospheric pressure and room temperature are found in a solid phase, while the gas is stable only at very low pressures. The ^{87}Rb vapor for the first BEC was produced at 300 K in a high-vacuum chamber with pressure $p \approx 1.33 \times 10^{-9}$ Pa [And95]. This corresponds to a very low phase space density

$$\Lambda^{\mathrm{Rb-vapor}} \approx 10^{-20} . \tag{3.7}$$

To achieve quantum degeneracy in a vapor of alkali atoms, the density has to be increased and the temperature has to be decreased by several orders of magnitude. In the next subsections we shall briefly discuss how these ultrasmall temperatures can be reached experimentally.

3.1.1 Doppler cooling

Atomic gases can be cooled efficiently by laser beams. The principle behind the process is the Doppler effect: Let's assume that the atoms are in their atomic ground states and the velocities are distributed according to the Maxwell-Boltzmann statistics. Let us furthermore assume that they have a certain excited state with a transition energy Δ_D and lifetime τ_D and that a laser light propagates in the $+\hat{x}$ direction with a frequency $\omega_D = \Delta_D - \delta_D$, where $\delta_D > \tau_D^{-1}$ is the detuning. For atoms at rest, the resonance condition is not fulfilled, so no absorption takes place. Atoms moving towards the laser source, however, experience a blue shift in the frequency due to the Doppler effect. For a given detuning, atoms within a narrow range of velocities will absorb photons and therefore also momentum $\Delta k = -\omega_D/c$. These excited atoms will eventually emit the absorbed photons again isotropically. Taking the average of the $\hat{x}$ components of the velocities over a timescale larger than the absorbtions-emission cycles, one can see that atoms are slowed down by the light "pressure".

It is possible to decrease the average of all three components of the velocities using three pairs of laser beams in perpendicular directions, resulting in optical

isotope	I	F	$E_{F+1} - E_F = a_{hf}2(F+1)$
^{6}Li	1	1/2	11 mK
^{7}Li	3/2	1	39 mK
^{23}Na	3/2	1	85 mK
^{40}K	4	7/2	62 mK
^{87}Rb	3/2	1	328 mK

Table 3.1: Hyperfine ground states of selected alkali metal isotopes [Ari77, Mac50].

molasses of reduced temperature. Since the detuning has to be adjusted to an optimal value at any given temperature, one has to tune smoothly the laser frequency as the gas is cooled.

A different approach is to create a collimated beam of the vapor by a slit, with atoms moving opposite to the single laser beam. An inhomogeneous magnetic field $\mathbf{B}(x) = (0, 0, B_z(x))$ is applied perpendicular to this axis. The function $B_z(x)$ is chosen such that the transition energy $\Delta_D(x)$ decreases as the atoms get closer to the laser source. The atoms' average kinetic energy and thus the temperature decreases along the x-axis, while - for a carefully designed $B_z(x)$ - the optimum detuning is maintained. This method is called the Zeeman-slower technique [Fir90].

The final temperature range reached via Doppler cooling is limited by the linewidth τ_D^{-1} of the excited state used for cooling, and it is typically of the order of $T_{\text{Doppler}} \approx 100\mu$K.

3.1.2 Bosons and fermions

The hyperfine magnetic Hamiltonian of an alkali atom in an external magnetic field B is given by

$$\hat{H}_{hf} = a_{hf}\hat{\mathbf{I}}\hat{\mathbf{S}} + (g_e\mu_B\hat{\mathbf{S}} - g_N\mu_N\hat{\mathbf{I}})\mathbf{B} \,, \tag{3.8}$$

where $\hat{\mathbf{I}}$ and $\hat{\mathbf{S}}$ (in units of $\hbar$) are the nuclear and the electronic spin momentum, respectively. In this Hamiltonian, a_{hf} is the hyperfine coupling, g_e and g_N are the electronic and nuclear gyromagnetic ratios, and μ_B and μ_N are the Bohr and nuclear magnetons. In the absence of a magnetic field, the lowest eigenstates of the atom can be characterized by the hyperfine quantum numbers $\mathbf{F}^2$ and F_z, where $\hat{\mathbf{F}} = \hat{\mathbf{I}} + \hat{\mathbf{S}}$ is the hyperfine angular momentum of the atom. The ground state nuclear moments and hyperfine constants of selected isotopes are listed in the Table 3.1 [Ari77, Mac50]. The hyperfine splitting is typically by a factor of 100-1000 larger at $T \approx T_{\text{Doppler}}$, than the temperature itself. Therefore, atomic transitions take place between hyperfine states at these small temperatures, and atoms must be described in terms of the hyperfine quantum numbers.

Let us make a few observations, which will play some role in later discussions. (A) For large magnetic fields, the electron spin is essentially aligned opposite to the direction of the magnetic field. (B) We define the low- or high-field seeker states at a given magnetic field strength B_0 whether or not the energy of the level decreases or increases with the magnetic field:

$$\left.\frac{\partial E_i}{\partial B}\right|_{B_0} \begin{cases} > 0 \rightarrow \text{low field seeker} \\ < 0 \rightarrow \text{high field seeker} \end{cases} \tag{3.9}$$

For large magnetic fields, however, the low-field seeking states correspond to $S_z \approx 1/2$. (C) Alkali atoms with an odd mass number – ^{7}Li, ^{23}Na, ^{87}Rb –, have necessarily an integer hyperfine momentum F: these isotopes are *bosons*. Atoms with an even mass number – ^{6}Li and ^{40}K–, however, behave like *fermions*. The difference in the statistics can be observed once the gas is in the quantum degenerate regime.

3.1.3 Confinement

Quantum degeneracy is typically not achieved by Doppler cooling. Furthermore, the laser beams used for Doppler cooling do not create sufficient confining potentials for the vapor, and the atoms can drift away from the optical "molass", getting lost for the experiment. To prevent these atomic losses, magnetic and optical trapping techniques are used.

We shall start by shortly discussing *magnetic traps*. Let us assume that we apply a static, but inhomogeneous magnetic field $\mathbf{B}(\mathbf{r})$ to trap the atoms. We can see that

$$\mathrm{Tr}\ \nabla \circ \nabla \mathbf{B}^2 = 2\mathrm{Tr}\ (\nabla \circ \mathbf{B})^2 + 2\mathrm{Tr}\ \mathbf{B}\nabla^2\mathbf{B} = 2\mathrm{Tr}\ (\nabla \circ \mathbf{B})^2 \geq 0, \tag{3.10}$$

where ∇ is the gradient operator and $\circ$ means the dyadic product of the corresponding vectors. In the last equation we exploited that, for free space and static fields, $\nabla^2\mathbf{B} = 0$. Eq. (3.10) means that the eigenvalues of the second derivative matrix $\nabla \circ \nabla \mathbf{B}^2$ cannot be all negative. As a consequence, it is impossible to create a (local) maximum with a static magnetic field in free space, and only a local minimum of the field can be produced. Therefore, only the low-field seeker states can be trapped using a magnetic trap. The simplest scenario (and basically, all advanced magnetic traps are somehow related to this geometry) is to use inverted Helmholtz rings to create the trap. However, in an inverted Helmholtz trap the magnetic field disappears at the origin, and the low- and high-field seeking states become degenerate. At this point, transition to a high-field seeking state is possible, and atoms can get lost from the trap. This process is called the Majorana spin-flip, and to avoid it, different methods were invented. In the time orbiting potential trap, e. g., a small uniform transverse field is applied to shift the minimum and its direction is rotated [And95].

A different approach is to use a laser to produce an *optical dipole trap*. The electric field component of a laser wave detuned from a dipole-active transition (which can be different from the one used for the Doppler cooling) induces a dipole moment on the atom. On the other hand, the dipole moment created by the electric field interacts with the laser field, and as a consequence, in a standing wave, the atoms feel a time averaged effective potential proportional to the local intensity. For red- and blue-detuning, the atoms gather at the maximum and minimum of the laser field, respectively. Sometimes this phenomenon is referred to as the AC Stark effect. The optical dipole trap is created usually by focusing a red detuned laser. The advantage of optical dipole traps is that one can trap any hyperfine state. Using only optical techniques for trapping requires, however, high-power laser fields even around the temperature range T_{Doppler} to produce deep enough traps.

Therefore, many experimental groups use a combined method: they confine a single hyperfine level in a magnetic trap, and after achieving low enough temperatures, they turn on the optical dipole field. Then it is possible to populate the desired hyperfine levels by radiofrequency pulses [Sta98].

3.1.4 Sub-Doppler cooling

As we mentioned earlier, Doppler-cooling down to a few hundred μK usually still corresponds to phase space densities of $\Lambda < 1$ in alkali metal vapors. Further reduction of the temperature requires new methods, which we shall discuss shortly now.

The first BEC [And95] was achieved by *forced evaporation*, which is still broadly applied. The temperature can be decreased below $T_{\rm Doppler}$ by selectively removing the atoms with the highest energies, provided that the remaining atoms can rethermalize. In harmonic traps, the highest energy atoms are also located at the edge of the trap. A radiofrequency "scalpel" can then be used to flip these atoms to an untrapped spin state. The maximal value of this frequency determines the number of the remaining particles and the final temperature of the vapor. After the Doppler cooling, $10^9 - 10^{12}$ atoms are usually trapped, which number is reduced down to $10^4 - 10^8$ after forced evaporation. This process can provide temperatures of the order of $T_{\rm evap} \approx 100$nK. To achieve the phase space density required for Bose-Einstein condensation, the trapping potential is also usually ramped up adiabatically to increase the density.

While this technique works well for bosons, cooling of fermions becomes problematic at lower temperatures. As the occupation of singleparticle states becomes $n_F \approx \mathcal{O}(1)$, scattering processes among fermions become more and more suppressed due to the Pauli principle. Thus the rethermalization time increases and finally exceeds the lifetime of the vapor in the trap. This discrepancy can be avoided by *sympathetic cooling*, i.e., cooling of different hyperfine states or isotopes together. In Ref. [DeM99], two hyperfine states of ^{40}K were trapped, and the rethermalization during the forced evaporation was based on the scattering between different hyperfine states. In Ref. [Tru01], bosonic ^{7}Li atoms were evaporated, and ^{6}Li atoms were cooled sympathetically. It is also possible to use an isotope of a different bosonic element, as was done in Ref. [Had02], where ^{6}Li atoms were cooled by ^{23}Na. Sodium atoms were then selectively evaporated by radiofrequency fields.

3.1.5 Optical lattices

Making use of the previously mentioned AC Stark-effect, it is possible to superimpose periodic amplitude modulations over the trap potential. A pair of phase-locked laser beams can be used to produce a standing wave. Using more pairs, it is possible to create even two- and three-dimensional lattice structures. To produce a simple cubic lattice, one can use three pairs of identical laser beams (produced usually by beam splitters) arranged orthogonally. The resulting effective potential is approximately

$$V(\mathbf{x}) = V_0 \sum_{i=x,y,z} \cos^2(2\pi x_i/\lambda_L) \ , \tag{3.11}$$

where λ_L is the wavelength of the laser and the amplitude of the potential V_0 is proportional to the laser intensity. For red detuned lasers, the atoms go to the intensity maxima, while for blue detuning, they go to the minima. The lattice depth V_0 is usually measured in units of the recoil energy E_R, given by

$$E_R = \frac{(2\pi\hbar)^2}{2m\lambda_L^2}, \tag{3.12}$$

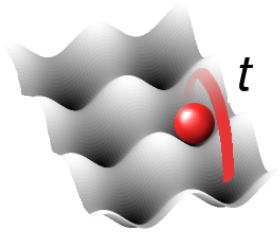

Figure 3.1: Tunneling from a site of an optical lattice to the next with an amplitude t.

where m is the mass of the atoms. This is the energy an atom at rest would have after absorbing a photon from the laser beam. It is possible to create lattice depths up to $V_0/E_R \approx 10$.

A one - dimensional lattice for $\approx 5 \times 10^4$ ^{40}K atoms was created at a laser wavelength $\lambda_L = 754$nm in Ref. [Mod03]. The sample was cooled sympathetically to 129 nK using ^{87}Rb. A three-dimensional optical lattice at a wavelength $\lambda_L = 826$nm was also created for ^{40}K [Koh05]. The filling factor of the lattice was successfully controlled and the Fermi surface was also observed. As a final example, let us mention that in the experiment of Ref. [Chi06], ^{6}Li atoms were loaded in a sheared cubic lattice, with all light produced by a $\lambda_L = 1064$ nm laser, and the pairs were detuned by tens of MHz to avoid interference.

Taking only the lattice potential into account, and neglecting the slowly varying confining potential, one can choose the lowest lying Wannier states $w(\mathbf{x})$ as a singleparticle basis of an effective Hamiltonian describing the atoms in the lattice. Neglecting the other Wannier orbitals is justified at the typical fillings and lattice temperatures, since then the bands with higher energies are essentially empty. Within this basis, the second quantized non-interacting Hamiltonian for a single hyperfine component in a $d = 3$ dimensional cubic lattice is given by [Jak98]

$$\hat{H}_{\rm latt} = \epsilon_0 \sum_i \hat{c}_i^+ \hat{c}_i - t \sum_{\langle i,j \rangle} [\hat{c}_i^+ \hat{c}_j + h.c.] + \dots \ , \tag{3.13}$$

where

$$\epsilon_0 = \int d^3\mathbf{x}\ V(\mathbf{x}) |w(\mathbf{x})|^2 \ , \tag{3.14}$$

is the on-site energy, and

$$t = \int d^3\mathbf{x}\ w^*(\mathbf{x} - \mathbf{x}_i) \left[-\frac{1}{2m} \hat{\mathbf{p}}^2 + V(\mathbf{x}) \right] w(\mathbf{x} - \mathbf{x}_j) \ , \tag{3.15}$$

is the nearest-neighbor hopping amplitude between adjacent sites i and j (see Fig. 3.1). The dots in Eq. (3.13) stand for terms with longer range hoppings, which shall be neglected from now on. For deep lattices, one can approximate a minimum of the lattice potential by a harmonic function. Within this approximation,

the hopping amplitude can be evaluated analytically [Hof02]

$$t = E_R \frac{2}{\sqrt{\pi}} \left(\frac{V_0}{E_R}\right)^{3/4} e^{-2\left(\frac{V_0}{E_R}\right)^{1/2}} . \tag{3.16}$$

The consistency of this approximation requires the size of the oscillator ground state wave function to be much smaller than the lattice constant:

$$a_{\mathrm{HO}} \equiv \frac{\hbar}{\sqrt{2mE_R}} \left(\frac{V_0}{E_R}\right)^{-1/4} \ll \lambda_L/2 . \tag{3.17}$$

3.1.6 Detection

A direct visualization of the momentum distribution of the atoms is possible in *time-of-flight measurements*. This approach is certainly not possible for traditional solid state systems, and benefits from the high level of control of ultracold atomic systems.

In the detection stage of an experiment, the trap potential is instantly switched off. At this moment, the cloud is usually too small for direct imaging techniques,[1] and the atoms are allowed to expand freely typically for a few tens of milliseconds. Originating from a pointlike object, the spatial distribution of the atoms after the expansion is in one-to-one correspondence with the momentum distribution before the expansion: faster atoms fly farther. The expansion rate, however, can be anisotropic due to many-body correlations. An absorption image of the cloud is taken using a resonant pulse detected by a CCD camera. Although the system is destroyed when using this method, the cooling-trapping-preparation process can be repeated at wish. The images taken are usually stored and analyzed digitally.

The normal-BEC transition on time-of-flight images can be seen as an emergence of a sharp peak on the top of a broad momentum distribution, indicating the macroscopic degeneracy of the lowest quantum level [And95]. Bose and Fermi systems exhibit strikingly different properties, as demonstrated in Ref. [Tru01]: the Fermi pressure kept the diameter of the ^{6}Li cloud approximately constant with decreasing temperature, while ^{7}Li atoms were contracted to the growing BEC-peak. This peak was used as a sensitive thermometer to determine the common temperature of the isotopes, and to fit the Fermi-distribution to the shape of the Fermi cloud. Using this fit, one can make a precise estimate on the number of the fermionic atoms.

With optical lattices, one can strongly influence the momentum distribution of the confined atoms. In Ref. [Gre02], ^{87}Rb atoms were cooled to the BEC regime in a periodic potential. The height of the optical lattice was varied. For a shallow lattice, in addition to the BEC peak, an interference pattern corresponding to the reciprocal lattice was observed. For a deep lattice, however, this pattern completely disappeared and a broad incoherent background was visible. The destruction of the Bragg peaks was actually a consequence of the strong interactions between trapped atoms, which we neglected so far. As we shall discuss in the next subsections, these interactions become stronger and stronger in deeper and deeper optical lattices, and may lead to the appearance of strongly correlated states.

[1] We note that direct imaging techniques are not impossible, however, this rather technical discussion is beyond the scope of this introduction, see Ref. [Shi06].

3.1.7 Interaction

Although they are seemingly not very strong, interactions play an essential role for trapped ultracold atoms. Neutral atoms interact through van der Waals forces, and their interaction potential can be well approximated by the Lennard-Jones potential [Len31]

$$V_{\mathrm{LJ}}(\mathbf{x}) = -4\epsilon\left[\left(\frac{\sigma}{x}\right)^6 - \left(\frac{\sigma}{x}\right)^{12}\right] . \tag{3.18}$$

The attractive part of the interaction comes from dipolar forces [Eis30], while the second term is responsible for the repulsion at short distances. The parameter determining the range of the interaction is of the order of $\sigma \approx 4$Å [Rei98]. We note that the non-additive three-body interaction potential [Axi43, Bel66] may be relevant for strong interactions, however, such term has not been analyzed in this context.

In the ultracold environments with temperatures $T_{\mathrm{evap}} \approx 100$nK, the typical momentum of the atoms is

$$\langle p\rangle/\hbar \approx \hbar^{-1}\sqrt{A m_p k_{\mathrm{B}} T_{\mathrm{evap}}} \leq 4.3\mu\mathrm{m}^{-1} , \tag{3.19}$$

where we have substituted $A = 87$ for the heaviest isotope we have encountered. As the range of the dipolar forces is of the order of σ, the typical relative angular momentum of two atoms is

$$\langle p\rangle\sigma \ll \hbar , \tag{3.20}$$

therefore, scattering in other than the s-wave channel is suppressed. Scattering for these very small momenta, however, is solely determined by the scattering length a_s. The Lennard-Jones potential can be replaced by an effective delta-potential [Jak98]

$$V_{\mathrm{LJ}}(\mathbf{x}) \to \tilde{U}\delta(\mathbf{x}) , \tag{3.21}$$

where the strength of the potential is proportional to the s-wave scattering length,

$$\tilde{U} = \frac{4\pi a_s \hbar^2}{m} . \tag{3.22}$$

For an optical lattice with only the lowest Wannier orbital taken into account, this description leads to an on-site (Hubbard) interaction term with the interaction strength (see Fig. 3.2)

$$U = \tilde{U}\int d^3\mathbf{x}\, |w(\mathbf{x})|^4 . \tag{3.23}$$

If $a_s \ll a_{\mathrm{HO}} \ll \lambda_L/2$ (see also Eq. (3.17)), then the lattice potential minima can be approximated by harmonic functions, and one finds [Hof02, Jak98]

$$U = (2\pi a_s/\lambda_L)E_R\sqrt{8}\pi\left(\frac{V_0}{E_R}\right)^{3/4} . \tag{3.24}$$

Comparing this expression with the hopping amplitude in Eq. (3.16), we can see that one can change the ratio U/t by simply tuning the laser intensity $\sim V_0$.

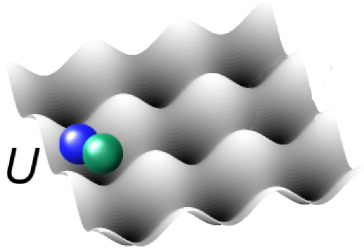

Figure 3.2: On-site interaction of the atoms in an optical lattice: the strength of the interaction U is proportional to the s-wave scattering length.

Feshbach resonances

In fact, it is also possible to change both the amplitude and the sign of the effective interaction by exploiting Feshbach resonances that appear as the magnetic field is changed. The vicinity of a molecular (quasi - bound) level induces changes in the s-wave scattering length. The energy of the bound state depends on the external magnetic field, and can be tuned to zero. At this point, the scattering length diverges, and a resonance appears. The positions of the resonances and the magnetic field-dependence of the s-wave scattering lengths have been determined both numerically [Moe95, Tie91, Vog97] and experimentally [Abr97, Bar05, Ino98, Mar02] for the alkali metal isotopes of our interest. In the vicinity of the Feshbach resonance, the scattering length is well approximated by the form

$$a_s(B) \approx a_{bg}\left(1 + \frac{\Delta}{B - B_0}\right) , \tag{3.25}$$

where a_{bg} is the background s-wave scattering length, B_0 is the position of the resonance, and Δ is the width of the resonance. Let us take here as an example the Feshbach resonance between the hyperfine states $|S_z = -1/2, I_z = 1\rangle$ and $|S_z = -1/2, I_z = 0\rangle$ of ^{6}Li [Bar05]. In this channel, the Feshbach resonance is located at $B_0 = 83.4149$mT and has a width $\Delta = 30.0$ mT. The background scattering length is large and negative, $a_{bg} = -1405a_0 = -74$nm. For $B > B_0$, an attractive system of particles can be realized, while for $B_0 - \Delta < B < B_0$, the bound state is below the scattering threshold, and a gas of weakly bound molecules is formed. For a typical optical lattice used for ^{6}Li, the lattice constant is $\lambda_L/2 = 532$nm [Chi06], so that for magnetic fields $B \gg B_0$, neglecting nearest-neighbor contributions to the interaction is a good approximation.

3.2 Many-body phenomena in cold atomic systems

Let us briefly review some phenomena which are related to the strong correlations in ultracold atomic experiments. First we shall discuss two examples for purely bosonic, then another two for purely fermionic systems. We shall not discuss the case when both particle species are present.

3.2.1 Bosonic systems

Collapse of Bose-Einstein condensates

The description of the Bose condensate on the mean-field level in terms of the Gross-Pitaevski theory gives usually accurate results, provided that the s-wave scattering length is non-negative $a_s \geq 0$. For strong enough effective attraction, however, the zero-point kinetic energy in a trap cannot compete with the interaction energy: the BEC collapses and the mean field description fails. This robust phenomenon has been realized and observed in ultracold atomic systems of ^{7}Li [Ger00] and ^{85}Rb [Don01].

Bosonic Mott-insulator

Atoms of a single hyperfine component of a bosonic alkali atom in an optical lattice can be described by the bosonic Hubbard model [Jak98]:

$$\hat{H}^{\text{boson}} = -t \sum_{\langle i,j \rangle} [\hat{b}_i^+ \hat{b}_j + h.c.] + \frac{1}{2} U \sum_i \hat{n}_i (\hat{n}_i - 1) \; , \tag{3.26}$$

where t and U are given by Eq. (3.15) and Eq. (3.23), respectively, and $\hat{n}_i = \hat{b}_i^+ \hat{b}_i$ is the bosonic counting operator at site i. The bosonic creation and annihilation operators satisfy the usual commutation relations $[\hat{b}_i, \hat{b}_j^+] = \delta_{ij}$, $[\hat{b}_i^+, \hat{b}_j^+] = 0$. The ground state of the noninteracting system is simply a superfluid state when all atoms populate the lowest lying single particle level with zero momentum:

$$|SF\rangle = \left(\sum_{i=1}^{N} \hat{b}_i^+ \right)^M |0\rangle \; , \tag{3.27}$$

where M is the number of atoms and N is the number of lattice sites. For strong repulsive interactions, however, and at commensurate fillings, where $\rho = M/N$ is an integer, the lowest energy of the homogeneous system is achieved if precisely ρ atoms reside at each lattice site, forming a Mott insulator:

$$|MI\rangle = \prod_{i=1}^{N} (\hat{b}_i^+)^\rho |0\rangle \; . \tag{3.28}$$

Note that while the superfluid $|SF\rangle$ is described by a single macroscopic wavefunction and exhibits long-range phase coherence, there is no phase coherence in the Mott insulator $|MI\rangle$, where, on the other hand, the atom number of each site is the same. The transition from a superfluid to a Mott insulator in a bosonic system was first observed in Ref. [Gre02].

3.2.2 Pairing in fermionic systems

BEC-BCS crossover

On the repulsive side of a Feshbach resonance, in the open channel, a weakly bound molecular state appears. Therefore, on this side of the resonance, atoms are actually bound into dimers, which are, nevertheless, bosons, and at low enough

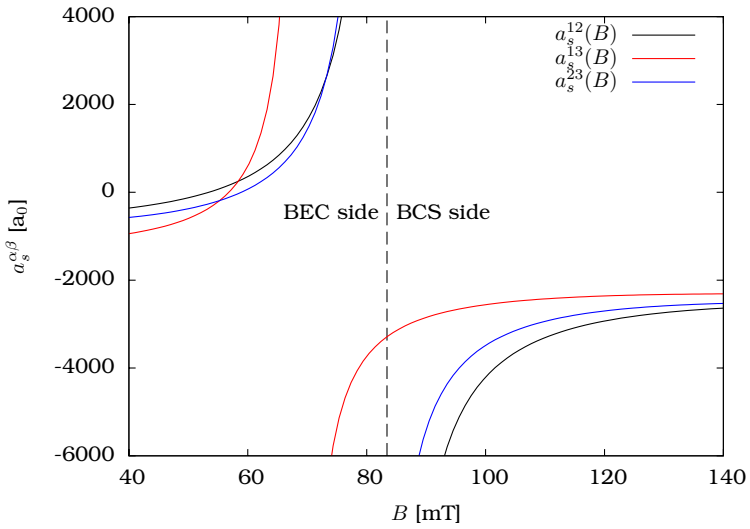

Figure 3.3: Feshbach resonances in ^{6}Li. The magnetic field dependence is approximated according to Ref. [Bar05]. The vertical dashed line corresponds to $B_0 = 83.4149$mT, the resonance point in the channel '12'. The labels "BEC side" and "BCS side" also refer to this channel.

temperatures, the subjects of Bose-Einstein condensation. The condensate of these molecules has been observed in harmonic traps (without an optical lattice) [Gre03, Joc03, Zwi03]. Therefore the $a_s > 0$ side of a Feshbach resonance is usually called the *BEC side*. For $a_s < 0$, the presence of the Fermi sea leads to a qualitatively different mechanism for pairing: this is the Bardeen-Cooper-Schieffer instability of the Fermi system. Observing the fermionic pairs on this *BCS side* of the Feshbach resonance was more challenging, but was successful just a year after the observation of the BEC of the molecular pairs, see Ref. [Zwi04] for ^{6}Li and Ref. [Rega04] for ^{40}K. Superfluidity of both dimers and BCS pairs of ^{6}Li atoms in an optical lattice was also demonstrated recently [Chi06]. Feshbach resonances between the lowest hyperfine states of ^{6}Li are shown in Fig. 3.3 [Bar05].

The transition between the two limits is not a phase transition, but a crossover. At the Feshbach resonance, the relevant microscopic lengthscale, the s-wave scattering length diverges, and there a universal behavior of the gas is expected [Nik07]. This resonance point is therefore usually referred to as the unitary limit.

Imbalanced superfluidity

The possibility of producing systems with different densities of hyperfine components leads to a field of research which is only hardly accessible in traditional solid state systems. In an electronic system, imbalanced spin populations could be created by applying a magnetic field. However, in a traditional BCS superconductor, the magnetic field couples strongly to orbital degrees of freedom. This effect is typically much stronger than the Zeeman splitting and the imbalance generated by the external field.

In atomic gases, however, the imbalance in the system can be described as

a pure "exchange field" acting on the two pseudospin states. A solution to the spatially homogeneous problem was discussed by Sarma [Sar63], who found that below a certain temperature, the magnetic field-induced transition between the BCS and the normal state becomes of first order. A proposal for pairing at a finite pair momentum (FFLO state) was given independently by Fulde and Ferrel [Ful64] and Larkin and Ovchinnikov [Lar64].

In ultracold atomic experiments, however, no sign of this rotational symmetry-breaking FFLO state has been seen [Par06a, Par06b, Shi06, Zwi06a, Zwi06b]. Rather, the large enough imbalance and the trapping potential lead to phase separation, with a BCS core in the middle surrounded by unpaired atoms of the majority component. A recent proposal on the phase diagram based on the experimental data can be found in Ref. [Shi08].

3.2.3 Outlook

As we have seen in this short introduction, purely bosonic and fermionic systems provide a number of new and interesting phenomena in ultracold atomic systems. The combinations of different hyperfine levels of these or even the behavior of mixed systems with bosonic and fermionic atoms offer further interesting possibilities. These are, however, beyond the scope of this thesis, and shall not be discussed here. A recent review on the topic by Bloch and Zwerger can be found in Ref. [Blo07].

Let us now discuss shortly how the seemingly remote quantum Potts model in one dimension is related to cold atomic systems. The quantum Potts model, in addition to having a quantum phase transition at zero temperature, also has discrete internal degrees of freedom. Since one has a number of variational possibilities when choosing the isotopes and the hyperfine components in experiments, we can address models where the internal quantum numbers are provided by the hyperfine quantum numbers. As we shall see, three-component systems exhibit a behavior qualitatively different from the two-(or one-) component case. Therefore these internal quantum numbers play a role as important as in the quantum Potts model. We also note that as the experimental techniques get more and more advanced, one day the quantum Potts model could also be realized in some ultracold atomic experiment.

3.3 The attractive SU(3) Hubbard model

3.3.1 Model

As proposed by Hofstetter and colleagues [Hof02], two-component fermionic atoms in an optical lattice can be described at low temperatures by the Hubbard model. In principle, the production of more than two hyperfine components is possible in ultracold atomic systems. The Hamiltonian describing these systems is a generalized, multiple component Hubbard model [Hon04a, Hon04b]

$$\hat{H} = -t \sum_{\langle i,j\rangle\alpha} [\hat{c}^+_{i\alpha}\hat{c}_{j\alpha} + \hat{c}^+_{j\alpha}\hat{c}_{i\alpha}] + \sum_{i,\alpha\neq\beta} \frac{U_{\alpha\beta}}{2}\hat{n}_{i\alpha}\hat{n}_{i\beta} \,. \tag{3.29}$$

Here $\hat{n}_{i\alpha} = \hat{c}^+_{i\alpha}\hat{c}_{i\alpha}$ is the number operator of the hyperfine component $\alpha = 1, 2, \ldots$ at site i. We shall call the hyperfine label as the *color* of the atoms henceforth. The

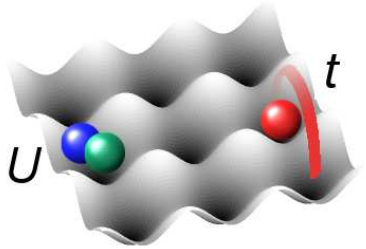

Figure 3.4: The Hubbard model is a good approximation to describe cold atoms in an optical lattice.

creation and annihilation operators obey the anticommutation relations $\{\hat{c}^+_{i\alpha}, \hat{c}_{j\beta}\} = \delta_{ij}\delta_{\alpha\beta}$, $\{\hat{c}_{i\alpha}, \hat{c}_{j\beta}\} = 0$. The hopping amplitude t and the local interactions $U_{\alpha\beta}$ between the different colors could be changed by tuning the optical lattice depth or the strength of an external magnetic field.

We made certain approximations using the form in Eq. (3.29) for the effective Hamiltonian. Most importantly, we neglected the confining trap potential. Second, we assume that the number of atoms of each color $\sum_i \langle \hat{n}_{i\alpha} \rangle \equiv N\rho_\alpha$ is conserved. Furthermore, we shall also neglect more complicated hopping and interaction terms. We remark that the inhomogeneity the trap produces is essential for certain phenomena, however, the latter two approximations are very well satisfied in many experiments.

The Hubbard model with multiple components and repulsive interactions has been discussed by Affleck and Marston [Aff88, Mar89], and with even number of components in the unitary regime by Nicolic and Sachdev [Nik07]. The general discussion of multi-component Hubbard models is a complicated theoretical problem. Therefore we shall consider a more specific model. We shall restrict ourselves to three colors: $\alpha = 1, 2, 3$. Furthermore, we shall assume that the interactions are uniform $U_{\alpha\beta} = U$ and attractive $U < 0$. We shall consider a simple (hyper)cubic lattice: $\mathbf{R}_i \in [\mathcal{Z}]^d$, therefore the lattice spacing shall be set to unity $a = 1$.

Due to the high level of control of ultracold atomic systems, such conditions can, in principle, be created experimentally: three hyperfine components of ^{6}Li in an optical lattice in strong external magnetic fields $B \gg 84$mT would be our primary candidate to produce such a system. Stability of the mixture can, however, be an important problem: in certain systems, three-body recombination rates can be so high that the mixture is simply not stable.

The conditions we specified define a model given by the following Hamiltonian:

$$\hat{H} = -t \sum_{\langle i,j \rangle \alpha} [\hat{c}^+_{i\alpha}\hat{c}_{j\alpha} + \hat{c}^+_{j\alpha}\hat{c}_{i\alpha}] + U \sum_i [\hat{n}_{i1}\hat{n}_{i2} + \hat{n}_{i1}\hat{n}_{i3} + \hat{n}_{i2}\hat{n}_{i3}] \,. \tag{3.30}$$

It is easy to see that global SU(3) transformations

$$\hat{b}_{j\alpha} = e^{\left(i\theta_a \lambda^a_{\alpha\beta}\right)} \hat{c}_{j\beta} \tag{3.31}$$

leave the Hamiltonian in Eq. (3.30) invariant, where $\lambda^a_{\alpha\beta}, a = 1, \ldots, 8$ are the Gell-Mann matrices, the generators of the SU(3) group.

In the rest of this section, we shall study the properties of this SU(3) Hubbard model. First, we shall study its properties in the weak and in the strong coupling limits. Then we shall present the Gutzwiller approximation to the ground state.

3.3.2 Weak coupling limit

At $U = 0$, the Hamiltonian (3.30) is quadratic and can be diagonalized by a Fourier transformation on the lattice. The ground state is the Fermi sea

$$|FS\rangle = \prod_{\alpha} \prod_{\mathbf{k}:\epsilon_{\mathbf{k}}<\epsilon_F} \hat{c}^+_{\mathbf{k}\alpha}|0\rangle \; . \tag{3.32}$$

Here the wave vector $\mathbf{k}$ is in the first Brillouin zone of the reciprocal lattice, and we introduced the Fourier transformed fermion operators by the relation

$$\hat{c}_{\mathbf{k}\alpha} = \frac{1}{\sqrt{N}} \sum_j e^{-i\mathbf{k}\mathbf{x}_j} \hat{c}_{j\alpha} \; . \tag{3.33}$$

These operators diagonalize the kinetic part of the Hamiltonian, and the single particle energies are given by

$$\epsilon_{\mathbf{k}} = -2t \sum_{\nu=1}^{d} \cos(k_\nu) \; , \tag{3.34}$$

where k_ν denote the components of the lattice momentum $\mathbf{k}$. The Fermi energy ϵ_F in Eq. (3.32) is fixed by the condition

$$\sum_i \langle FS|\hat{n}_{i\alpha}|FS\rangle = N\rho_\alpha \; . \tag{3.35}$$

On cubic lattices of any dimension d, the singleparticle spectrum has the nesting property $\epsilon_{\mathbf{k}+\mathbf{Q}} = -\epsilon_{\mathbf{k}}$, where we defined the nesting vector $\mathbf{Q} = (\pi, \pi, \ldots)$. At half filling, $\rho_\alpha = 1/2$, the nesting of the Fermi surfaces thus opens possibilities to density wave instabilities. We shall not discuss these in this thesis, and we shall restrict ourselves to fillings $\rho_\alpha \neq 1/2$. In two-component systems with an infinitesimally weak attraction, the Fermi sea becomes unstable with respect to BCS pairing. Therefore, away from half filling, BCS pairing is expected to be the most important instability also for the three-component case, which shall be discussed here on a mean-field level. The BCS superfluidity and other possible symmetry breaking instabilities for the weak coupling region in the three-component case were analyzed first by Honerkamp and Hofstetter [Hon04a, Hon04b].

The partition function of the Hamiltonian (3.30) can be written in a path integral representation [Neg98] as

$$Z = \int \mathcal{D}\bar{c}\mathcal{D}c \, \exp\left(-\int_0^\beta d\tau \sum_{i,\alpha} \bar{c}_{i\alpha}(\tau)(\partial_\tau - \mu)c_{i\alpha}(\tau) - \int_0^\beta d\tau H[\bar{c}(\tau), c(\tau)] \right) , \tag{3.36}$$

where the Hamilton function $H[\bar{c}(\tau), c(\tau)]$ is obtained from Eq. (3.30) by formally replacing the fermionic operators $\hat{c}$ by imaginary time-dependent Grassmann variables $c(\tau)$. We introduce complex pairing fields for each pair of colors $\alpha < \beta$, site i and time instant τ by a Hubbard-Stratonovich transformation [Hub59],

$$e^{-U_{\alpha\beta} n_\alpha n_\beta} \sim \int d\bar{\Delta} d\Delta \; e^{-\frac{1}{|U_{\beta\alpha}|}|\Delta_{\alpha\beta}|^2 + \bar{\Delta}_{\alpha\beta} c_\beta c_\alpha + \Delta_{\alpha\beta} \bar{c}_\alpha \bar{c}_\beta} \; . \tag{3.37}$$

Note that there are no convergence problems in the integral when the interactions are attractive, $U_{\alpha\beta} < 0$. Therefore the partition function can be written as

$$Z = \int \mathcal{D}\bar{\Delta}\mathcal{D}\Delta \int \mathcal{D}\bar{c}\mathcal{D}c \; e^{-S[\bar{c}, c, \bar{\Delta}, \Delta]} \; , \tag{3.38}$$

where the action $S[\bar{c}, c, \bar{\Delta}, \Delta]$ is given by

$$\begin{aligned} S[\bar{c}, c, \bar{\Delta}, \Delta] &= \int_0^\beta d\tau \sum_{i,j,\alpha} \bar{c}_{i\alpha}(\tau)[\delta_{ij}(\partial_\tau - \mu) + \delta_{|i-j|,1}(-t)] c_{j\alpha}(\tau) \\ &+ \int_0^\beta d\tau \sum_{i,\alpha<\beta} \left[\bar{\Delta}_{\alpha\beta}(i,\tau) c_{i\beta}(\tau) c_{i\alpha}(\tau) + \Delta_{\alpha\beta}(i,\tau) \bar{c}_{i\alpha}(\tau) \bar{c}_{i\beta}(\tau) \right] \\ &+ \int_0^\beta d\tau \sum_{i,\alpha<\beta} \frac{1}{|U|} |\Delta_{\alpha\beta}(i,\tau)|^2 \; . \end{aligned} \tag{3.39}$$

This action is quadratic in the Grassmann fields, which we shall integrate out eventually. Before we do that, it is worth to introduce Fourier transformed fields, defined through the relation

$$c_{i,\alpha}(\tau) = \frac{1}{\sqrt{N}} \sum_{\mathbf{k},n} e^{i\mathbf{k}\mathbf{x}_i - i\omega_n \tau} c_{\mathbf{k}\alpha}(n) \; , \tag{3.40}$$

where $\omega_n = \pi T(2n+1)$ stand for the odd Matsubara frequencies. For the pairing fields, the transformation reads

$$\Delta_{\alpha\beta}(i,\tau) = \frac{1}{\sqrt{N}} \sum_{\mathbf{q},m} e^{i\mathbf{q}\mathbf{x}_i - i\nu_m \tau} \Delta_{\alpha\beta}(\mathbf{q}, m) \; , \tag{3.41}$$

where $\nu_m = \pi T 2m$ are even Matsubara frequencies. With these definitions, we can recast the action in the form

$$\begin{aligned} S[\bar{c}, c, \bar{\Delta}, \Delta] &= \frac{\beta}{|U|} \sum_{\mathbf{q},m} \sum_{\alpha<\beta} |\Delta_{\alpha\beta}(\mathbf{q}, m)|^2 \\ &- \frac{\beta}{N} \sum_{\mathbf{k},\mathbf{k}',n,n'} \sum_{\alpha<\beta} \left[\bar{\Delta}_{\alpha\beta}(\mathbf{k}-\mathbf{k}', n-n') c_{\mathbf{k}'\beta}(n') c_{\mathbf{k}\alpha}(n) + h.c. \right] \\ &+ \beta \sum_{\mathbf{k},n,\alpha} \bar{c}_{\mathbf{k}\alpha}(n)(\epsilon_{\mathbf{k}} - \mu - i\omega_n) c_{\mathbf{k}\alpha}(n) \; . \end{aligned} \tag{3.42}$$

This expression contains all possible configurations and fluctuations for the pairing field: the general form in Eq. (3.42) allows for pair formation in an arbitrary

channel (s,p,d, etc.) and even at finite momenta (Fulde-Ferrel-Larkin-Ovchinnikov state). Whether there is a nontrivial static solution, which minimizes the thermodynamic potential, $\Omega = T \ln Z$, is a very complicated mathematical question. Since the interaction is local, we shall assume that the pairing takes place at momentum $\mathbf{q} = \mathbf{k} - \mathbf{k}' = 0$ and in the s-channel. The saddle point condition $\delta\Omega/\delta\bar{\Delta}_{\alpha\beta}(0,0) = 0$ then leads to the gap equation

$$\Delta_{\alpha\beta}(0,0) = \frac{|U|}{N} \sum_{\mathbf{k},n} \langle c_{\mathbf{k}\alpha}(n) c_{-\mathbf{k}\beta}(-n) \rangle \ . \tag{3.43}$$

As we can see, once the pairing field takes a nontrivial value $\Delta_{\alpha\beta}(0,0) \neq 0$, the global SU(3) symmetry is spontaneously broken.

To proceed, we revisit the effective action in Eq. (3.42), and group the terms containing the Grassmann variables to a compact Nambu form:

$$S_{\rm fermion} = \frac{\beta}{2} \bar{\Psi} \hat{G}^{-1} \Psi \ . \tag{3.44}$$

Here Ψ is a six-spinor $[\Psi]_{kn\alpha} = c_{k\alpha}(n)$; $[\Psi]_{N+k\ n\alpha} = \bar{c}_{-k\alpha}(-n)$ are the upper and lower blocks of a Nambu vector. We can read off the components of $\hat{G}^{-1}$ from Eq. (3.42). The diagonal blocks are associated with the non-interacting propagator, while the offdiagonal terms correspond to the pairing fields:

$$\hat{G}^{-1} = \begin{pmatrix} \hat{G}^{0-1} & \hat{\Delta}^{+} \\ \hat{\Delta} & -[\hat{G}^{0-1}]^{+} \end{pmatrix} \ , \tag{3.45}$$

where

$$[\hat{G}^{0-1}]_{\mathbf{k}\mathbf{k}'\alpha\beta} = \delta(\mathbf{k} - \mathbf{k}') \ \delta_{nn'} \ \delta_{\alpha\beta} \ (\epsilon_{\mathbf{k}} - \mu - i\omega_n) \ , \tag{3.46}$$

and

$$[\hat{\Delta}]_{\{\mathbf{k}n\alpha\} \ \{\mathbf{k}'n'\beta\}} = \bar{\Delta}_{\alpha\beta}(\mathbf{k} - \mathbf{k}', n - n') \ , \alpha < \beta \ , \tag{3.47}$$

and the lower triangular components are fixed by the antisymmetry $\Delta_{\beta\alpha} = -\Delta_{\alpha\beta}$.

With these definitions, the integration over the Grassmann fields leads to the following effective action:

$$S_{\rm eff}[\Delta] = \frac{\beta}{|U|} \sum_{\mathbf{q},m,\alpha<\beta} |\Delta_{\alpha\beta}(\mathbf{q},m)|^2 - \frac{1}{2} {\rm Tr} \ln(\beta \hat{G}^{-1}) \ . \tag{3.48}$$

Here the trace has to be taken over all the Nambu coordinates, the frequencies, and the color indeces. Although Eq. (3.48) is a compact expression, the second term is highly nonlinear in the pairing fields, and contains all information about the fluctuations. In the weak coupling limit, the pairing amplitudes are expected to be small. Therefore we can expand Eq. (3.48) in the amplitude of the pairing field, and up to fourth order we find

$$\begin{aligned} S_{\rm eff}[\Delta] \ &= \ \frac{\beta}{|U|} \frac{1}{N} \sum_{\mathbf{q},m,\alpha<\beta} |\Delta_{\alpha\beta}(\mathbf{q},m)|^2 - \frac{1}{2} {\rm Tr}(\hat{G}^0 \hat{\Delta}^{+} \hat{G}^{0+} \hat{\Delta}) \\ &\quad + \frac{1}{4} {\rm Tr}(\hat{G}^0 \hat{\Delta}^{+} \hat{G}^{0+} \hat{\Delta})^2 + \dots \ , \end{aligned} \tag{3.49}$$

and the trace is now taken over the wave vectors of the Brillouin zone, over the frequencies, and the color indeces.

Let us now restrict ourselves to a static s-wave pairing solution at $\mathbf{q} = 0$. This enables us to calculate the terms in the effective action as a function of $\Delta_{\alpha\beta}(0,0)$ explicitly. The second order term can be written as

$$\frac{1}{2}\mathrm{Tr}(\hat{G}^0\hat{\Delta}^+\hat{G}^{0+}\hat{\Delta}) = \frac{1}{2}\sum_{\alpha\beta}|\Delta_{\alpha\beta}(0,0)|^2\sum_{\mathbf{k},n}\frac{1}{\epsilon_\mathbf{k}-\mu-i\omega_n}\frac{1}{\epsilon_\mathbf{k}-\mu+i\omega_n}\ . \tag{3.50}$$

Note that the rightmost term is equivalent to the Cooperon diagram. From now on, we shall use the abbreviation $\Delta^0_{\alpha\beta} = \Delta_{\alpha\beta}(0,0)$. Using some standard approximations, we write

$$\begin{aligned}\sum_{\mathbf{k},n}\frac{1}{\epsilon_\mathbf{k}-\mu-i\omega_n}\frac{1}{\epsilon_\mathbf{k}-\mu+i\omega_n} &= \beta\sum_\mathbf{k}\frac{n_F(-(\epsilon_\mathbf{k}-\mu))-n_F(\epsilon_\mathbf{k}-\mu)}{2\epsilon_\mathbf{k}}\\ \approx \beta D(0)\int_{-W}^{W}d\xi\frac{1}{2\xi}\tanh(\beta\xi/2) &\approx \beta D(0)\ln\left(\frac{2e^\gamma}{\pi}\frac{W}{T}\right)\ ,\end{aligned} \tag{3.51}$$

where $n_F(x) = 1/(e^{\beta x}+1)$ is the Fermi function, and we assumed an isotropic band with a constant density of states $D(0)$, a bandwidth $W \gg T$, and $\gamma \approx 0.577$ is the Euler constant. The fourth order term is equivalent to

$$\begin{aligned}\frac{1}{4}\mathrm{Tr}(\hat{G}_0\hat{\Delta}^+\hat{G}_0^+\hat{\Delta})^2 &= \frac{1}{4}\sum_{\alpha\beta\gamma\delta}\Delta^{0+}_{\alpha\beta}\Delta^0_{\beta\gamma}\Delta^{0+}_{\gamma\delta}\Delta^0_{\delta\alpha}\\ &\quad\times\sum_{\mathbf{k},n}\frac{1}{(\epsilon_\mathbf{k}-\mu-i\omega_n)^2(\epsilon_\mathbf{k}-\mu+i\omega_n)^2}\ .\end{aligned} \tag{3.52}$$

The Fermionic part can be evaluated as

$$\begin{aligned}\sum_{\mathbf{k}n}\frac{1}{(i\omega_n-(\epsilon_\mathbf{k}-\mu))^2}\frac{1}{(-i\omega_n-(\epsilon_\mathbf{k}-\mu))^2} &\approx \sum_n\int_{-W}^{W}d\xi D(0)\frac{1}{(i\omega_n-\xi)^2(-i\omega_n-\xi)^2}\\ \approx D(0)\sum_n\int_{-\infty}^{\infty}d\xi\frac{1}{(\omega_n^2+\xi^2)^2} &\approx D(0)\sum_n|\omega_n|^{-3}\int_{-\infty}^{\infty}dy\frac{1}{(1+y^2)^2}\\ &= D(0)\frac{1}{2T^3\pi^2}\left[\frac{7}{4}\zeta(3)-1\right]\ .\end{aligned} \tag{3.53}$$

The more detailed derivation can be found in Appendix B.1. To simplify the expressions for the pairing fields in Eqs. (3.50) and (3.52), we observe that, by introducing the three-vector

$$\tilde{\Delta}^0_\alpha \equiv \frac{1}{2}\sum_{\beta\gamma}\epsilon_{\alpha\beta\gamma}\Delta^0_{\beta\gamma}\ , \tag{3.54}$$

we can write

$$\sum_\beta\Delta^{0+}_{\alpha\beta}\Delta^0_{\beta\gamma} = [\tilde{\Delta}^0\circ\tilde{\Delta}^{0+} - \tilde{\Delta}^{0+}\tilde{\Delta}^0]_{\alpha\gamma}\ . \tag{3.55}$$

Therefore, the fourth-order term is equivalent to the expression

$$\sum_{\alpha\beta\gamma\delta}\Delta^{0+}_{\alpha\beta}\Delta^0_{\beta\gamma}\Delta^{0+}_{\gamma\delta}\Delta^0_{\delta\alpha} = \mathrm{Tr}[\tilde{\Delta}^0\circ\tilde{\Delta}^{0+} - \tilde{\Delta}^{0+}\tilde{\Delta}^0]^2 = 2(\tilde{\Delta}^{0+}\tilde{\Delta}^0)^2\ , \tag{3.56}$$

where we used the properties $(u \circ v)^2 = (vu)(u \circ v)$ and $\mathrm{Tr}(u \circ v) = (vu)$ of the dyadic product.

Finally, the effective action for the BCS s-wave pairing in the weak coupling limit can be written as [Rap08c]

$$\begin{aligned} S_{\mathrm{BCS}}[\Delta^0] &= \beta \left[\frac{1}{|U|} - D(0) \ln \left(\frac{2e^\gamma}{\pi} \frac{W}{T} \right) \right] \sum_{\alpha<\beta} |\Delta^0_{\alpha\beta}|^2 \\ &+ \beta \frac{1}{T^2\pi^2} \left[\frac{7}{4}\zeta(3) - 1 \right] \left(\sum_{\alpha<\beta} |\Delta^0_{\alpha\beta}|^2 \right)^2 . \end{aligned} \tag{3.57}$$

At this mean field level, the critical temperature T_C is defined as the temperature where the coefficient of the quadratic term changes sign, given by

$$T_C = \frac{2e^\gamma}{\pi} W e^{-\frac{1}{|U|D(0)}} . \tag{3.58}$$

At high temperatures in the disordered phase, $T > T_C$, the action $S_{\mathrm{BCS}}[\Delta^0]$ has a minimum at $\Delta^0_{\alpha\beta} = 0$. However, below the critical temperature, this point becomes unstable, and finite values of $\Delta^0_{\alpha\beta}$ minimize the action. This leads to the spontaneous breaking of the SU(3) symmetry, according to Eq. (3.43). The basic difference with respect to the SU(2) case is that, while in this latter case the pairing field is scalar, in the SU(3) case every solution with $\sum_{\alpha<\beta} |\Delta^0_{\alpha\beta}|^2 = \Delta_0^2$ is equally minimizing the effective action in Eq. (3.57). Therefore we can conclude that the number of Goldstone modes is five, corresponding to the global phase, the two relative phases between the components and two modes modulating $|\tilde{\Delta}^0_1|$, $|\tilde{\Delta}^0_2|$ and $|\tilde{\Delta}^0_3|$ with a fixed amplitude Δ_0 [Hon04b].

Furthermore, this degeneracy also allows one to rotate to a global gauge, where only a single component differs from zero: $\tilde{\Delta}^0_3 \neq 0$, which corresponds to $\Delta^0_{12} \neq 0, \Delta^0_{13} = \Delta^0_{23} = 0$. Therefore the ground state is simply given by a BCS-like wave function

$$|BCS\rangle \equiv \prod_{\mathbf{k}:\epsilon_{\mathbf{k}}<\epsilon_F} \hat{c}^+_{\mathbf{k}3} \prod_{\mathbf{k}'} [u_{\mathbf{k}'} + v_{\mathbf{k}'} \hat{c}^+_{\mathbf{k}'1} \hat{c}^+_{-\mathbf{k}2}] |0\rangle , \tag{3.59}$$

where ϵ_F is determined from fixing the density of the third color, and $u_{\mathbf{k}}$ and $v_{\mathbf{k}}$ are the usual BCS coherence factors, satisfying

$$|u_{\mathbf{k}}|^2 = \frac{1}{2} \left[1 + \frac{\epsilon_{\mathbf{k}} - \mu_{12}}{\sqrt{(\epsilon_{\mathbf{k}} - \mu_{12})^2 + \Delta_0^2}} \right] , |v_{\mathbf{k}}|^2 = 1 - |u_{\mathbf{k}}|^2 , \tag{3.60}$$

and

$$u^*_{\mathbf{k}} v_{\mathbf{k}} = \frac{\Delta_0}{2\sqrt{(\epsilon_{\mathbf{k}} - \mu_{12})^2 + \Delta_0^2}} . \tag{3.61}$$

The chemical potential μ_{12} fixes the number of particles with colors 1 and 2. It is also instructive to calculate the expectation value

$$m_8 = \frac{1}{N} \sum_{\mathbf{k}} \langle BCS| \sum_{\alpha\beta} \hat{c}^+_{\mathbf{k}\alpha} \lambda^8_{\alpha\beta} \hat{c}_{\mathbf{k}\beta} |BCS\rangle , \tag{3.62}$$

which can be simply evaluated, yielding

$$m_8 \sim \rho_1 + \rho_2 - 2\rho_3 . \tag{3.63}$$

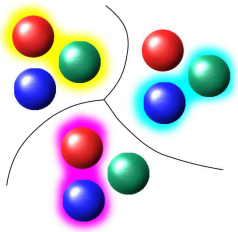

Figure 3.5: In the attractive SU(3) Hubbard model, color superfluid domains are formed. In each domain, the "orientation" of the superfluid order parameter $\tilde{\Delta}^0_\alpha$ determines the orientation of the ferromagnetic order parameter $\langle \hat{c}^+_\alpha \lambda^a_{\alpha\beta} \hat{c}_\beta \rangle$.

This quantity corresponds to the magnetization $m_z = \langle \sum_{\nu\nu'} \hat{c}_\nu \sigma^z_{\nu\nu'} \hat{c}_{\nu'} \rangle$ in the SU(2) case. In the phase with broken symmetry, the system gains condensation energy *locally* if, for a fixed filling, the unpaired color has a slightly smaller density: $n_1, n_2 > \rho > n_3$. This fact together with Eq. (3.63) implies that color superfluidity with broken SU(3) symmetry is accompanied by *ferromagnetic order*. This phenomenon has no analogy in the two component case. In a homogeneous phase with fixed and equal numbers of atoms for all colors, different superfluid domains will form, where the pairing order parameter points in different directions. This also determines the orientation of the ferromagnetic order parameter in the given domain. Similar results were obtained by Cherng, Refael and Demler [Che07]. To summarize, for weak attractive interactions, the ground state is a BCS state, where, in a particular global gauge, Cooper pairs are formed in the channel '12', while the third color forms a Fermi sea.

3.3.3 Strong coupling limit

For strong coupling $|U|/t \gg 1$, the structure of the ground state is qualitatively different. Without hopping, $t = 0$, the lowest energy states (for an equal number of atoms in each color) are those where sites are either empty or have one atom of each color. If we assume that the sites where these so-called trions sit are given by the subset Λ of the lattice points including $|\Lambda| = N\rho$ sites, then such a trionic state is given by

$$|T\rangle = \prod_{i\in\Lambda} \hat{c}^+_{i1} \hat{c}^+_{i2} \hat{c}^+_{i3} |0\rangle \; . \tag{3.64}$$

The energy of the trionic states for $t = 0$ is

$$E_T/N = 3U\rho \; . \tag{3.65}$$

The trionic subspace is highly degenerate, and trions will most likely form a band once the hopping t is turned on. Let us discuss the transformation properties of trions under global SU(3) rotations. Suppressing the site index and using Einstein's summation, by definition we have to consider the mapping

$$\hat{c}^+_1 \hat{c}^+_2 \hat{c}^+_3 \rightarrow \left(e^{-i\theta_a \lambda^a_{1\alpha}}\right) \left(e^{-i\theta_b \lambda^b_{2\beta}}\right) \left(e^{-i\theta_c \lambda^c_{3\gamma}}\right) \hat{c}^+_\alpha \hat{c}^+_\beta \hat{c}^+_\gamma \; . \tag{3.66}$$

Among the $3^3 = 27$ terms for the color indeces, only $3! = 6$ terms corresponding to $\alpha \neq \beta \neq \gamma$ give nonzero contributions. These terms can be written as

$$\sum_P \left[(-1)^{\mathrm{sgn}(P)} \left(e^{-i\theta_a \lambda^a_{1P(1)}} \right) \left(e^{-i\theta_b \lambda^b_{2P(2)}} \right) \left(e^{-i\theta_c \lambda^c_{3P(3)}} \right) \right] \hat{c}_1^+ \hat{c}_2^+ \hat{c}_3^+ \ , \tag{3.67}$$

where P denotes the permutations of the colors. The coefficients, however, simply give the determinant

$$\det e^{-i\theta_a \lambda^a} = e^{\ln \det e^{-i\theta_a \lambda^a}} = e^{\mathrm{tr} \ln e^{-i\theta_a \lambda^a}} = 1 \ , \tag{3.68}$$

where we used that the Gell-Mann matrices are traceless. As a consequence, trions are color-SU(3) singlets.

Let us now discuss the case of small, but non-zero hopping $t > 0$. We shall treat the hopping term perturbatively to derive the effective Hamiltonian within the trionic subspace. Let us use the notation

$$\hat{H}_0 = \frac{U}{2} \sum_i \sum_{\alpha \neq \beta} \hat{n}_{i\alpha} \hat{n}_{i\beta} \ , \tag{3.69}$$

and

$$\hat{H}_1 = -t \sum_{\langle ij \rangle \alpha} \hat{c}^+_{i\alpha} \hat{c}_{j\alpha} + \mathrm{h.c.} \ . \tag{3.70}$$

In third order perturbation theory, we have to evaluate the following terms according to Goldstone's perturbation series:

$$\begin{aligned} \langle f|\tilde{H}|i\rangle \ &= \ \langle f|\hat{H}_1|i\rangle \\ &+ \ \frac{1}{2} \sum_j{}' \ \langle f|\hat{H}_1|j\rangle\langle j|\hat{H}_1|i\rangle \left[\frac{1}{E_f - E_j} - \frac{1}{E_j - E_i} \right] \\ &+ \ \frac{1}{3} \sum_{jj'}{}' \ \langle f|\hat{H}_1|j\rangle\langle j|\hat{H}_1|j'\rangle\langle j'|\hat{H}_1|i\rangle \\ &\times \ \left[\frac{1}{E_f - E_j} \frac{1}{E_j - E_{j'}} + \frac{1}{E_j - E_{j'}} \frac{1}{E_{j'} - E_i} \right] + \dots \ , \end{aligned} \tag{3.71}$$

where we denote two *fixed* eigenstates of $\hat{H}_0$ lying in the trionic subspace by $|f\rangle$ and $|i\rangle$, a general eigenstate of $\hat{H}_0$ with energy E_j by $|j\rangle$, the primes are standing for the restrictions $i, f \neq j, j'$, and the ellipsis denote higher order hopping and interaction terms.

The first order term in Eq. (3.71) has no contribution. The second order term describes processes when an atom jumps out from a trion to a nearest neighbor site and back, provided there is no trion on that site. This process leads to a nearest neighbor interaction term. The third order term enables a trion to hop to an empty site. It is somewhat lengthy but straightforward to check [Rap08d] that the effective Hamiltonian of the trions can be written up to additive constants as

$$\tilde{H} = -\frac{3t^3}{2|U|^2} \sum_{<ij>} [\hat{F}_i^+ \hat{F}_j + \mathrm{h.c.}] + \frac{3t^2}{2|U|} \sum_{<ij>} \hat{F}_i^+ \hat{F}_i \hat{F}_j^+ \hat{F}_j + \dots \ , \tag{3.72}$$

where we introduced the *fermionic* trion annihilation operators, $\hat{F}_i = \hat{c}_{i1}\hat{c}_{i2}\hat{c}_{i3}$. This Hamiltonian describes a spinless fermion gas on a lattice with nearest-neighbor repulsion.

In one dimension, the model can be written as

$$\tilde{H} = -\frac{3t^3}{2|U|^2}\sum_i [\hat{F}_i^+\hat{F}_{i+1} + \hat{F}_{i+1}^+\hat{F}_i] + \frac{3t^2}{2|U|}\sum_i \hat{F}_i^+\hat{F}_i\hat{F}_{i+1}^+\hat{F}_{i+1} \ . \tag{3.73}$$

Now we can use the Jordan-Wigner relations

$$1 - 2\hat{F}_i^+\hat{F}_i = \hat{\sigma}_i^z \ ; \hat{F}_i = \left(\prod_{j<i}\hat{\sigma}_j^z\right)\hat{\sigma}_i^+ \ ; \hat{F}_i^+ = \left(\prod_{j<i}\hat{\sigma}_j^z\right)\hat{\sigma}_i^- \ , \tag{3.74}$$

where $\hat{\sigma}^z$ and $\hat{\sigma}^\pm = \frac{1}{2}(\hat{\sigma}^x \pm i\hat{\sigma}^y)$ are the usual Pauli matrices. With this mapping, we find that the lattice fermion model is equivalent to a spin model, defined by the Hamiltonian

$$\tilde{H}^{\text{spin}} = -\frac{3t^3}{4|U|^2}\sum_i [\hat{\sigma}_{i+1}^x\hat{\sigma}_i^x + \hat{\sigma}_{i+1}^y\hat{\sigma}_i^y] + \frac{3t^2}{2|U|}\sum_i \hat{\sigma}_{i+1}^z\hat{\sigma}_i^z \ , \tag{3.75}$$

which is the antiferromagnetic XXZ-chain. In the $|U|/t \to \infty$ strong coupling limit, this model becomes uniaxial (Ising), and prefers antiferromagnetic alignment of the neighboring spins. Note that this corresponds to a staggered distribution of the trions, i.e., a commensurate density wave. In $d > 1$ dimensions, there is no exact mapping to a spin model using a Jordan-Wigner transformation. Nevertheless, the tendency to form a commensurate density wave has been verified analytically and numerically in $d = 2$ dimensions [Gub85, Morg88]. In $d = \infty$ dimensions, incommensurate density wave order was also found [Uhr93].

To summarize, for strong attraction in the SU(3) Hubbard model, we found that the ground state is composed by trions, and has global SU(3) symmetry. At finite temperatures, these trions will have a finite lifetime. At half filling $\rho = 1/2$, a density wave of the trions is expected to emerge with a checkerboard pattern on a simple cubic lattice. At general fillings, the phase diagram could be decorated by different trionic phases at low temperatures, like a Fermi liquid or an incommensurate density wave of trions. Nevertheless, the discussion of these are beyond the scope of this thesis, and shall not be investigated here.

3.3.4 Phase transition

We summarize the results for the weak and strong coupling analysis in Fig. 3.6. As the two limiting phases have different symmetries, phase transitions must happen in the ground state. Away from half filling, we shall assume that there is only a single transition. To determine whether it is continuous or not, one has to apply non-perturbative methods, which are able to capture the physics even for intermediate couplings, $|U|/t \approx 1$.

In the hope of analytical results, one could take the $d = 1$ or $d = \infty$ dimensional limits, where powerful analytic techniques are available for this investigation. It is believed that the results of $d = \infty$ dimensional "mean - field" approximations describe better a $d = 3$ dimensional system, than the $d = 1$ dimensional results. Therefore, we shall study the ground state of the $d = \infty$ dimensional attractive

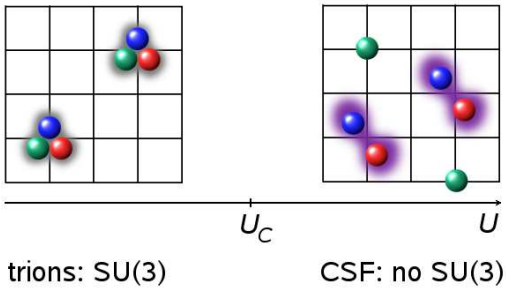

Figure 3.6: Summary of the weak and strong coupling analysis: in the strong coupling limit, trions are formed, while in the weak coupling limit, a BCS-like color superfluid (CSF) ground state breaks SU(3) symmetry.

SU(3) Hubbard model. In our analysis, we will strongly rely on the contributions of Metzner and Vollhardt [Met87, Met88, Met89].

However, some care must be taken while taking the $d = \infty$ dimensional limit. The single particle energy in Eq. (3.34) seems to diverge in this limit. Since the single particle energy is the sum of the energies associated with each spatial dimension, one can use the central limit theorem to evaluate the density of states,

$$D(\epsilon) = \sum_{\mathbf{k}} \delta(\epsilon - \epsilon_{\mathbf{k}}) \to \frac{1}{\sqrt{\pi 4dt^2}} e^{-x^2/(4dt^2)} , \tag{3.76}$$

which gives an infinite band in the limit t =const. and $d \to \infty$. The physical meaning of this expression is that the kinetic energy increases with the number of nearest neighbor sites and the average kinetic energy of an atom is $\sim \sqrt{2dt^2}$. We can see from Eq. (3.76) that in order to have a well-defined high-dimensional limit, the hopping amplitude has to be scaled as

$$t = \frac{t^*}{2\sqrt{d}} , \tag{3.77}$$

where t^* sets the scale of the average kinetic energy. Using any other scaling exponent would either lead to infinitely large or zero kinetic energies, which, compared to the dimension-independent average interaction energy, give trivial models in the limit $d \to \infty$. This scaling assures that the fragile balance between the kinetic and interaction energies results in a non-trivial transition point between the color superfluid and the trionic phases even in the limit of $d \to \infty$ dimensions.

As we shall see, the scaling form in Eq. (3.77) determines the structure of many-body correlations in infinite dimensions [Met87, Met88, Met89]. In fact, trions become localized as $d \to \infty$, since their hopping amplitude vanishes as

$$\frac{t^3}{|U|^2} \sim \frac{1}{d^{3/2}} . \tag{3.78}$$

Hence we are strongly motivated to approximate the ground state by the following Gutzwiller correlated wave function in $d = \infty$ dimensions:

$$|G\rangle = \prod_i (1 + (g-1)\hat{F}_i^+ \hat{F}_i \,)|BCS\rangle . \tag{3.79}$$

If the Gutzwiller parameter is set to unity, $g = 1$, the wave function trivially reproduces the ground state in the weak coupling limit. If $g < 1$, then the amplitude of terms containing trions is suppressed. For $g > 1$, on the other hand, the amplitude of terms with trions is increased, thus the trions are favored. In the limit, $g \to \infty$, only contributions with pure trionic occupancies survive, and one obtains a state like Eq. (3.64), with the lowest energy in the strong coupling limit. Thus, as $|U|/t^*$ changes from the small to large values, increasing three-body correlations are expected to manifest in increasing values of g.

To obtain the approximate ground state, one has to calculate the variational energy

$$E(g, \Delta_0) = \langle G|\hat{H}|G\rangle / \langle G|G\rangle \ , \tag{3.80}$$

where the Hamiltonian $\hat{H}$ is given by Eq. (3.30). The ground state is then approximated by a state with parameters g and Δ_0, which minimize the function $E(g, \Delta_0)$. In finite dimensions the evaluation of Eq. (3.80) is a complicated problem. In the $d = \infty$ limit, however, we shall be able to calculate the Gutzwiller expectation values without further approximations.

3.3.5 Gutzwiller calculation

In order to calculate the Gutzwiller expectation values, first we shall express them in terms of expectation values in a static effective field theory. We observe that we can write the norm of the Gutzwiller state as

$$\langle G|G\rangle = \langle BCS| \prod_l (1 + (g^2 - 1)\hat{F}_l^+ \hat{F}_l \ )|BCS\rangle \ , \tag{3.81}$$

which is a non-interacting ground state expectation value of a normal ordered product: all $\hat{c}_{i\alpha}^+$ operators are to the left of the corresponding $\hat{c}_{i\alpha}$ operators. Formally, this could be evaluated using Wick's theorem, however, the large number of terms makes this impractical. The key observation is that the very same terms are generated when one considers the functional integral

$$\langle G|G\rangle = \int \mathcal{D}\bar{\eta}\mathcal{D}\eta \ e^{-\mathcal{S}_0} \prod_l (1 + (g^2 - 1)t_l) \ , \tag{3.82}$$

where $\eta_{i\alpha}$ are Grassmann variables, $t_l \equiv n_{l1}n_{l2}n_{l3} = \bar{\eta}_{l1}\eta_{l1}\bar{\eta}_{l2}\eta_{l2}\bar{\eta}_{l3}\eta_{l3}$ corresponds to the trionic occupation at site l, and the non-interacting action is given by

$$\mathcal{S}_0 = \sum_{fh} \bar{\Psi}_f D_{fh}^{0-1} \Psi_h \ . \tag{3.83}$$

In Eq. (3.83), $\bar{\Psi}_f = (\bar{\eta}_{f1}, \bar{\eta}_{f2}, \bar{\eta}_{f3}, \eta_{f1}, \eta_{f2}, \eta_{f3})$ is a Nambu vector, and the kernel is the inverse of the bare propagator, given by the matrix

$$D^0 = \begin{pmatrix} G^0 & F^0 \\ F^{0+} & -G^{0+} \end{pmatrix} \ , \tag{3.84}$$

with

$$G^0_{fh\alpha\beta} = -\langle \eta_{f\alpha}\bar{\eta}_{h\beta}\rangle_{\mathcal{S}_0} = \langle BCS|\hat{c}^+_{h\beta}\hat{c}_{f\alpha}|BCS\rangle \ , \tag{3.85}$$

and

$$F^0_{fh\alpha\beta} = -\langle \eta_{f\alpha}\eta_{h\beta}\rangle_{\mathcal{S}_0} = \langle BCS|\hat{c}_{h\beta}\hat{c}_{f\alpha}|BCS\rangle \ . \tag{3.86}$$

In momentum space, the uncorrelated propagator can be evaluated to give

$$D^0(k) = \begin{pmatrix} |v_{\mathbf{k}}|^2 & 0 & 0 & 0 & u^*_{\mathbf{k}} v_{\mathbf{k}} & 0 \\ 0 & |v_{\mathbf{k}}|^2 & 0 & -u^*_{\mathbf{k}} v_{\mathbf{k}} & 0 & 0 \\ 0 & 0 & \Theta(\epsilon_F - \epsilon_{\mathbf{k}}) & 0 & 0 & 0 \\ 0 & -u_{\mathbf{k}} v^*_{\mathbf{k}} & 0 & -|v_{\mathbf{k}}|^2 & 0 & 0 \\ u_{\mathbf{k}} v^*_{\mathbf{k}} & 0 & 0 & 0 & -|v_{\mathbf{k}}|^2 & 0 \\ 0 & 0 & 0 & 0 & 0 & -\Theta(\epsilon_F - \epsilon_{\mathbf{k}}) \end{pmatrix} , \tag{3.87}$$

where the BCS coherence factors are given by Eqs. (3.60) and (3.61). If we now examine the functional integral in Eq. (3.82), we see that to complete the mapping, we can exponentiate the Gutzwiller factor using that $t_l^2 = 0$ for the Grassmann variables, to obtain the effective action:

$$\langle G|G\rangle = \int \mathcal{D}\bar{\eta}\mathcal{D}\eta \; e^{-\mathcal{S}} \; , \tag{3.88}$$

where the effective action is given by

$$\mathcal{S} = \mathcal{S}_0 - (g^2 - 1) \sum_l t_l \; . \tag{3.89}$$

This effective action at $g = 1$ correctly generates the expectation values with the uncorrelated $|BCS\rangle$ state, and thus describes the BCS pairing by the anomalous parts of the kernel D^0. On the other hand, an effective three-body interaction term appears in it, which is attractive if $g > 1$, and repulsive if $g < 1$. The third important property of this effective field theory is that it is entirely static by construction.

To proceed, let us rewrite the expectation value of the density as

$$\begin{aligned} \langle G|\hat{n}_{i\alpha}|G\rangle &= \langle BCS|\hat{n}_{i\alpha} \prod_{l\neq i} (1 + (g^2-1)\hat{F}_l^+ \hat{F}_l \;)|BCS\rangle \\ &+ (g^2-1)\langle BCS|\hat{F}_i^+ \hat{F}_i \prod_{l\neq i} (1 + (g^2-1)\hat{F}_l^+ \hat{F}_l \;)|BCS\rangle \; . \end{aligned} \tag{3.90}$$

Again, we can observe that all these terms are normal-ordered expectation values in a single particle product state. We can proceed just like in the previous discussion to find that, in the end, the Gutzwiller expectation value of the density is given by the expression

$$\langle \hat{n}_{i\alpha}\rangle_G \equiv \langle G|\hat{n}_{i\alpha}|G\rangle / \langle G|G\rangle = \langle n_{i\alpha}\rangle_{\mathcal{S}} + (g^2-1)\langle t_i\rangle_{\mathcal{S}} \; , \tag{3.91}$$

where $n_{i\alpha} \equiv \bar{\eta}_{i\alpha}\eta_{i\alpha}$. Similar steps can be used to map the Gutzwiller expectation values of different terms in the Hamiltonian to functional integrals with the same effective action $\mathcal{S}$. The double occupation, e.g., of colors "2" and "3" at site i, can be written as:

$$\langle \hat{n}_{i2}\hat{n}_{i3}\rangle_G = \langle d_{i1}\rangle_{\mathcal{S}} + (g^2-1)\langle t_i\rangle_{\mathcal{S}} \; , \tag{3.92}$$

where $d_{i1} \equiv n_{i2}n_{i3} = t_i/n_{i1}$. For $i \neq j$, the hopping term is given by

$$\begin{aligned} \langle \hat{c}^+_{i\alpha}\hat{c}_{j\alpha}\rangle_G &= \langle \bar{c}_{i\alpha}c_{j\alpha}\rangle_{\mathcal{S}} + (g-1)\langle \bar{c}_{i\alpha}\left[d_{i\alpha} + d_{j\alpha}\right]c_{j\alpha}\rangle_{\mathcal{S}} \\ &+ (g^2-1)\langle \bar{c}_{i\alpha}d_{i\alpha}d_{j\alpha}c_{j\alpha}\rangle_{\mathcal{S}} \; . \end{aligned} \tag{3.93}$$

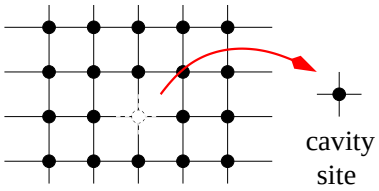

Figure 3.7: We use the cavity method to solve the effective field theory in $d = \infty$ dimensions.

Now we face the problem of evaluating expectation values in an interacting field theory. We shall be able to solve this static field theory in the limit of infinite dimensions. To this end, we shall first define certain quantities. We define the (dressed) propagator of the effective theory by

$$D_{ij} = -\langle \Psi_i \circ \bar{\Psi}_j \rangle_{\mathcal{S}} \; . \tag{3.94}$$

In the limit $g \to 1$, this reduces to the non-interacting propagator D^0. We also define the self-energy S and proper self-energy Σ:

$$D = D^0 + D^0 S D^0 \; , \tag{3.95}$$

and

$$D = D^0 + D^0 \Sigma D \; , \tag{3.96}$$

where all multiplications are matrix multiplications. The second relation is also known as Dyson's equation [Fet71]. In $d = \infty$ dimensions, the proper self-energy is local, as first pointed out for the Hubbard model by Metzner and Vollhardt [Met87, Met88, Met89]. The proper self-energy, in principle, could be evaluated by a series of one-particle irreducible diagrams, where the lines correspond to the components of the bare propagator D^0 while the vertices to the three-body local interaction $1-g^2$. In each order of the interaction, one can show that

$$\Sigma_{ij} \sim \frac{1}{d^{3||i-j||/2}} \; , \tag{3.97}$$

so that in infinite dimensions, all off-diagonal terms $i \neq j$ vanish: $\Sigma_{ij} = \delta_{ij}\Sigma_i$. Furthermore, we can use translation invariance to represent the proper self-energy by the 6×6 matrix $\Sigma_i \equiv \Sigma$.

Similar arguments can be used for deriving a cavity field theory in infinite dimensions, which enables us to calculate the *local* expectation values exactly in terms of the proper self-energy. This method is similar to the cavity method of dynamical mean field theory [Geo96], but leads to a simpler structure due to the static nature of the effective field theory.

The cavity action is defined by the following expression:

$$\frac{1}{Z_{\rm cav}} e^{-\mathcal{S}_{\rm cav}} = \frac{1}{Z} \int \mathcal{D}'\bar{\eta}\mathcal{D}'\eta \; e^{-\mathcal{S}} \; , \tag{3.98}$$

where the primes mean integrations over all Grassmann variables except for those defined at the origin, which shall be referred to as the "cavity" (see Fig. 3.7). We

shall derive the functional form of the cavity action in $d = \infty$ dimensions. It is useful to collect the terms in the action in three groups:

$$\mathcal{S} = \mathcal{S}_0 + \mathcal{S}' + \mathcal{S}^{(0)} \ , \tag{3.99}$$

where

$$\mathcal{S}_0 = \frac{1}{2}\bar{\Psi}_0[D^{0-1}]_{00}\Psi_0 - (g^2-1)t_0 \tag{3.100}$$

contains only terms at the cavity site,

$$\mathcal{S}^{(0)} = \frac{1}{2}\sum_{i,j\neq 0}\bar{\Psi}_i[D^{0-1}]_{ij}\Psi_j - (g^2-1)\sum_{i\neq 0}t_i \tag{3.101}$$

is the effective action on the lattice without the cavity, and

$$\mathcal{S}' = \frac{1}{2}\sum_{i\neq 0}\left[\bar{\Psi}_i[D^{0-1}]_{i0}\Psi_0 + \bar{\Psi}_0[D^{0-1}]_{0i}\Psi_i\right] \tag{3.102}$$

contains terms, which connect the lattice and the cavity. The action $\mathcal{S}'$ can be viewed as a generating functional term with the "currents" $\bar{h}_i \equiv \bar{\Psi}_0[D^{0-1}]_{0i}$ and their adjungates. Thus we can write

$$\begin{aligned}\ln\int \mathcal{D}'\bar{\eta}\mathcal{D}'\eta\, e^{-\mathcal{S}^{(0)}-\mathcal{S}'} \quad &= \quad \sum_n \sum_{i_1\ldots i_n, j_1\ldots j_n\neq 0} \bar{h}_{i_1}\ldots\bar{h}_{i_n}h_{j_1}\ldots h_{j_n} \\ &\quad \times\langle\Psi_{i_1}\ldots\Psi_{i_n}\bar{\Psi}_{j_1}\ldots\bar{\Psi}_{j_n}\rangle^{\rm conn}_{\mathcal{S}^{(0)}} ,\end{aligned} \tag{3.103}$$

since only connected graphs are generated this way. Let us first restrict ourselves to a set of sites $\{i_q\}$ and $\{j_q\}$ being only nearest neighbors, and consider terms of order n. If all site indices are different, then the sum over the sites gives a factor d^{2n}. Since D^{0-1} is proportional to $t \sim 1/\sqrt{d}$, the product of the "currents" gives a factor of the order of $\sim d^{-n}$. The correlation function is connected, and thus the distance between external sites is at least $||i-j|| \geq 2$, and the scaling of the hopping ensures that the correlation function is bounded,

$$\langle\Psi_{i_1}\ldots\Psi_{i_n}\bar{\Psi}_{j_1}\ldots\bar{\Psi}_{j_n}\rangle^{\rm conn}_{\mathcal{S}^{(0)}} \leq {\rm const}/d^{2n-1} \ . \tag{3.104}$$

Therefore these terms give a contribution of the order $1/d^{n-1}$. If two of the labels $\{i_q\}$ and $\{j_q\}$ are the same, then the sum over the sites gives a factor d^{2n-1}, however, connected diagrams scale at most as $\sim 1/d^{2n-2}$, and the final result is again of the order of $\sim 1/d^{n-1}$. This argument can be generalized to any combination of identical labels and it can be also extended to the case where i_q and j_q run over non-nearest neighbor sites. One only has to use the property that $(D^0)^{-1}_{ij}$ decays faster than $1/d^{||i-j||/2}$, with $||i-j||$ the number of steps needed to reach the lattice site j from site i. Hence only the quadratic term, $n = 1$, survives the limit $d \to \infty$, which can be added to $\mathcal{S}_0$, leading to the bare kernel of the cavity $\mathcal{D}_0^{-1} \neq D^{0-1}$. The direct evaluation of the bare cavity propagator $\mathcal{D}_0$ is a complicated problem, and we shall rather use a set of selfconsistency relations to determine it's value. We conclude that the cavity action can be written as

$$\mathcal{S}_{\rm cav}[\eta_i,\bar{\eta}_i] = \frac{1}{2}\bar{\psi}\mathcal{D}_0^{-1}\psi + (g^2-1)n_1n_2n_3 \ , \tag{3.105}$$

where the cavity bare propagator $\mathcal{D}_0$ has to be determined selfconsistently and $\bar{\psi} = (\bar{\eta}_1, \bar{\eta}_2, \bar{\eta}_3, \eta_1, \eta_2, \eta_3)$.

By construction, the expectation values of local variables in the effective field theory are the same as the expectation values of the corresponding quantities in the cavity theory:

$$\langle O_{\rm cav} \rangle_{\mathcal{S}} = \langle O \rangle_{\mathcal{S}_{\rm cav}} \ . \tag{3.106}$$

Therefore, the selfconsistency relation for the bare cavity propagator is based on the requirement that the local propagator has to coincide with the dressed propagator of the cavity:

$$D_{00} = -\langle \Psi_0 \bar{\Psi}_0 \rangle_{\mathcal{S}} = -\langle \psi \bar{\psi} \rangle_{\mathcal{S}_{\rm cav}} = \mathcal{D} \ . \tag{3.107}$$

The left hand side can be evaluated using the homogeneity of the system and Dyson's equation on the lattice as:

$$-\langle \Psi_0 \bar{\Psi}_0 \rangle_{\mathcal{S}} = \sum_k D(k) = \sum_k \left[D^{0-1}(k) - \Sigma \right]^{-1} \ . \tag{3.108}$$

The right hand side of Eq. (3.107) can be calculated exactly by evaluating the functional integral over the six independent Grassmann variables. We observe that by a transformation $\mathcal{U}$, the bare cavity propagator can be diagonalized (for details, see Appendix B.2):

$$\mathcal{U} \mathcal{D}_0^{-1} \mathcal{U}^+ = {\rm diag}({\rm d}^{-1}, -{\rm d}^{-1}) \tag{3.109}$$

where ${\rm d}$ is now a 3×3 diagonal matrix with real entries. Thus the "partition function" of the cavity is given by

$$Z_{\rm cav} = \int d\eta d\bar{\eta}\ e^{-\mathcal{S}_{\rm cav}} = \det {\rm d}^{-1} + (g^2 - 1) = \sqrt{-\det \mathcal{D}_0^{-1}} + (g^2 - 1) \ . \tag{3.110}$$

The dressed propagator can be then evaluated using the following identities

$$\begin{aligned} \mathcal{D} &= \frac{1}{Z_{\rm cav}} \int d\eta d\bar{\eta}\ e^{-\mathcal{S}_{\rm cav}} (-\psi \circ \bar{\psi}) \\ &= \frac{1}{Z_{\rm cav}} \int d\eta d\bar{\eta} e^{-\frac{1}{2} \bar{\psi} \mathcal{D}_0^{-1} \psi} (-\psi \circ \bar{\psi}) \\ &= \frac{1}{Z_{\rm cav}} \int d\eta d\bar{\eta} e^{-\frac{1}{2} (\bar{\psi} \mathcal{U}^+)(\mathcal{U} \mathcal{D}_0^{-1} \mathcal{U}^+)(\mathcal{U} \psi)} (-\psi \circ \bar{\psi}) \ . \end{aligned} \tag{3.111}$$

In the end, the cavity propagator can be expressed as a function of $\mathcal{D}_0$ as

$$-\langle \psi \circ \bar{\psi} \rangle_{\mathcal{S}_{\rm cav}} = \frac{\mathcal{D}_0}{1 + (g^2 - 1)\sqrt{-\det \mathcal{D}_0}} \ . \tag{3.112}$$

The selfconsistency requirement in Eq. (3.107) is therefore equivalent to the matrix equation

$$\sum_k \left[D^{0-1}(k) - \Sigma \right]^{-1} = \frac{\mathcal{D}_0}{1 + (g^2 - 1)\sqrt{-\det \mathcal{D}_0}} \ . \tag{3.113}$$

A second matrix equation for $\mathcal{D}_0$ and Σ has to be added to set the selfconsistency equations. This relation comes from the observation that the proper self-energy appearing in the Dyson's equation for the cavity is equivalent to the proper self-energy on the lattice. From Eq. (3.112) we can see

$$\Sigma = -(g^2 - 1)\sqrt{-\det \mathcal{D}_0}\ \ \mathcal{D}_0^{-1} \ . \tag{3.114}$$

For a given g and Δ_0, one can, in principle, solve Eqs. (3.113) and (3.114) for the proper self-energy matrix Σ or the cavity bare propagator $\mathcal{D}_0$. We emphasize that we have not evaluated any diagrams to calculate the proper self-energy. The diagrammatic approach is a very complicated task even without BCS pairing. The result of summing up the so-called "flower diagrams" in the SU(2) repulsive case [Met87, Met88, Met89] is simply reproduced by relations analogous to Eqs. (3.113) and (3.114).

Next we show that we can express the *local* quantities in terms of the bare cavity propagator. The density of the atoms with a given color is equivalent to the corresponding diagonal element of the dressed propagator: $\langle n_\alpha \rangle_{\mathcal{S}_{\rm cav}} = \mathcal{D}_{\alpha\alpha}$, $\alpha = 1, 2, 3$. The double occupancy can be evaluated as

$$\langle d_\alpha \rangle_{\mathcal{S}_{\rm cav}} = \frac{\sqrt{-\det \mathcal{D}_0}[\mathcal{D}_0^{-1}]_{\alpha\alpha}}{1 + (g^2 - 1)\sqrt{-\det \mathcal{D}_0}} \, . \tag{3.115}$$

The trion occupancy is simply given by

$$\langle t \rangle_{\mathcal{S}_{\rm cav}} = \frac{\sqrt{-\det \mathcal{D}_0}}{1 + (g^2 - 1)\sqrt{-\det \mathcal{D}_0}} \, . \tag{3.116}$$

The above derivations are also based on the exact evaluation of the Grassman integrals of the cavity field theory. We can now express all local Gutzwiller expectation values as a function of the bare cavity propagator $\mathcal{D}_0$. The filling factor can be written as

$$3\rho = \frac{1}{N} \sum_{i\alpha} \langle \hat{n}_{i\alpha} \rangle_G = \frac{\sum_{\alpha=1}^{3} [\mathcal{D}_0]_{\alpha\alpha} + 3(g^2 - 1)\sqrt{-\det \mathcal{D}_0}}{1 + (g^2 - 1)\sqrt{-\det \mathcal{D}_0}} \, , \tag{3.117}$$

while the full double occupancy is given by the expression

$$\begin{aligned} \frac{1}{N} \sum_i \langle \hat{n}_{i1}\hat{n}_{i2} + \hat{n}_{i1}\hat{n}_{i3} + \hat{n}_{i2}\hat{n}_{i3} \rangle_G = \\ = \frac{\sqrt{-\det \mathcal{D}_0} \sum_{\alpha=1}^{3} [\mathcal{D}_0^{-1}]_{\alpha\alpha} + 3(g^2 - 1)\sqrt{-\det \mathcal{D}_0}}{1 + (g^2 - 1)\sqrt{-\det \mathcal{D}_0}} \, . \end{aligned} \tag{3.118}$$

The last obstacle that we must overcome while expressing the variational energy in Eq. (3.80) in terms of the bare cavity propagator (or the proper self-energy) is that the hopping terms are not local. To handle these non-local expectation values, it is useful to define the generating functional

$$\Gamma \equiv \ln \int \mathcal{D}\bar{\eta}\mathcal{D}\eta \; e^{-\mathcal{S} + \sum_i \bar{I}_i \tau_3 \Psi_i} \, , \tag{3.119}$$

where $\tau_3 = \sigma_3 \otimes \delta_{\alpha\beta}$, and the "current" $\bar{I}_i$ is a six-component Grassmann vector,

$$\bar{I}_i = (\bar{J}_{i1}, \bar{J}_{i2}, \bar{J}_{i3}, J_{i1}, J_{i2}, J_{i3}) \, , \tag{3.120}$$

and make use of standard field theoretical methods [Neg98]. We shift the Grassmann fields $\bar{\eta}_i$ and η_i in the generating functional Γ as:

$$\Psi_i \to \Phi_i = \Psi_i + \lambda \sum_p D^0_{ip} \tau_3 I_p \, , \tag{3.121}$$

where λ is a real valued parameter. Note that this equation also determines how the field $\bar{\Psi}_i$ is changed, since the components of $\bar{\Psi}_i$ and Ψ_i are not independent. Proceeding with the functional derivation after this change of integration variables, leads to an expression of the dressed propagator, D, in terms of expectation values of Grassmann fields related to the terms in the expression Eq. (3.93) (for details see Appendix B.3.). Comparing these with the definition of the self-energy gives the following "Ward identities" ($i \neq j$),

$$
\begin{aligned}
-(g^2-1)^2\tau_3\langle\Psi_i d_i^F d_j^F \bar{\Psi}_j\rangle_{\mathcal{S}}\tau_3 &= S_{ij} \ , && (3.122)\\
(g^2-1)\langle\Psi_i d_j^F \bar{\Psi}_j\rangle_{\mathcal{S}}\tau_3 &= \sum_p D^0_{ip}S_{pj} \ , && (3.123)\\
(g^2-1)\tau_3\langle\Psi_i d_i^F \bar{\Psi}_j\rangle_{\mathcal{S}} &= \sum_p S_{ip}D^0_{pj} \ , && (3.124)
\end{aligned}
$$

where $d_i^F = d_{i1} + d_{i2} + d_{i3} = \frac{1}{8}(\bar{\Psi}_i\tau_3\Psi_i)^2$. Using these identities, it is possible to express in terms of the self-energy S the density supermatrix $\mathcal{P}_{ij}$. This is defined by

$$
\mathcal{P}_{ij} = \begin{pmatrix} P_{ij} & Q^+_{ij} \\ Q_{ij} & -P^+_{ij} \end{pmatrix} \ , \tag{3.125}
$$

with the 3×3 matrices P_{ij} and Q_{ij} defined as

$$
\begin{aligned}
P_{i\neq j,\alpha\beta} &= \langle \hat{c}^+_{i\alpha}\hat{c}_{j\beta}\rangle_G && (3.126)\\
&= \langle \bar{\eta}_{i\alpha}\eta_{j\beta}\rangle_{\mathcal{S}} + (g-1)\langle \bar{\eta}_{i\alpha}\eta_{j\beta}(d_{i\alpha}+d_{j\beta})\rangle_{\mathcal{S}}\\
&+ (1-g)^2\langle \bar{\eta}_{i\alpha}\eta_{j\beta}(d_{i\alpha}d_{j\beta}))\rangle_{\mathcal{S}}
\end{aligned}
$$

and

$$
\begin{aligned}
Q_{i\neq j,\alpha\beta} &= \langle \hat{c}_{i\alpha}\hat{c}_{j\beta}\rangle_G && (3.127)\\
&= \langle \eta_{i\alpha}\eta_{j\beta}\rangle_{\mathcal{S}} + (g-1)\langle \eta_{i\alpha}\eta_{j\beta}(d_{i\alpha}+d_{j\beta})\rangle_{\mathcal{S}}\\
&+ (1-g)^2\langle \eta_{i\alpha}\eta_{j\beta}d_{i\alpha}d_{j\beta}\rangle_{\mathcal{S}} \ .
\end{aligned}
$$

These formulas are valid for $i \neq j$. The relation between the self-energy and the density matrix is more transparent in Fourier space, where it reads

$$
\begin{aligned}
\mathcal{P}^t(\mathbf{k}) &= D^0(\mathbf{k}) + C && (3.128)\\
&+ \left[D^0(\mathbf{k}) - \frac{\tau_3}{g+1}\right] S(\mathbf{k}) \left[D^0(\mathbf{k}) - \frac{\tau_3}{g+1}\right] \ .
\end{aligned}
$$

The superscript t refers now to the transposed matrix in color space, and C is a k-independent 6×6 matrix related to the $i=j$ contributions. This term does not play a role in the evaluation of the kinetic energy,

$$
K = \sum_{\mathbf{k}} \epsilon_{\mathbf{k}} \sum_{\alpha} P_{\alpha\alpha}(\mathbf{k}) \ . \tag{3.129}
$$

since we assumed only nearest neighbor hopping, and therefore $\sum_{\mathbf{k},\alpha} C_{\alpha\alpha}\epsilon_{\mathbf{k}} = 0$.

Relations to the multiband Gutzwiller correlator method

Let us shortly discuss some differences between the multiband Gutzwiller correlator method of Bünemann, Gebhard and Weber [Bun97, Bun98, Bun05] and the functional integral method. The former technique applies multiple variational parameters, which might lead to a better approximation of the ground state. The Gutzwiller projector we introduced, however, can also describe both the weak and the strong coupling ground states, and we believe that the results would change only quantitatively by the application of a more complex variational ansatz.

There are also some differences regarding the evaluation of the Gutzwiller expectation values. As we mentioned, the diagrammatic calculation of the self-energy diagrams would be very difficult, if not impossible, for a general correlator, even in infinite dimensions. In the multiband method, it is possible to get rid of the proper self-energy in $d = \infty$ dimensions exactly by introducing certain single particle correlators (Hartree terms). On the other hand, we also avoided such complications using the cavity method, since the proper self-energy is determined by the set of selfconsistency equations.

The mapping to an effective field theory seems to have two advantages. First, it includes the three-body correlations in a transparent way. Second, it may serve as a better foundation for finite dimensional evaluation of the Gutzwiller expectation values, since the "Ward identities" used to connect the self-energy and the density matrix are valid in any dimension. Furthermore, the effective field-theoretical formulation provides an ideal framework to extend the Gutzwiller approximation using cluster-DMFT-type calculations.

Numerical solution of the selfconsistency relations

Let us now discuss the solution of selfconsistency equations. It seems to be impossible to solve the selfconsistency relations analytically as a function of g and Δ_0. We can, however, calculate the components of the proper self-energy matrix, or equivalently, the bare cavity propagator with arbitrary accuracy numerically. By analyzing the symmetries of the problem, we can parameterize the bare cavity propagator with three independent non-trivial entries,

$$[\mathcal{D}_0]_{11} = a, [\mathcal{D}_0]_{33} = b, [\mathcal{D}_0]_{15} = c \,, \tag{3.130}$$

in analogy to the structure of $D^0(k)$ in Eq. (3.87). Using Eq. (3.114), we can express the independent components of the proper self-energy,

$$\Sigma_1 \equiv [\Sigma]_{11} = -uab, \Sigma_2 \equiv [\Sigma]_{33} = -u(a^2 + c^2), \Sigma_3 \equiv [\Sigma]_{15} = -ubc \,, \tag{3.131}$$

where we introduced the abbreviation, $u = (g^2 - 1)$. After some matrix algebra, the selfconsistency equations involving the parameters a, b and c can be cast to the form

$$\begin{aligned} a &= h \sum_{\mathbf{k}} \frac{1}{1 + f_{\mathbf{k}}^2} \\ b &= \frac{\rho_3}{1 + u(a^2 + c^2)(1 - \rho_3)} \\ c &= h \sum_{\mathbf{k}} \frac{f_{\mathbf{k}}}{1 + f_{\mathbf{k}}^2} \end{aligned} \tag{3.132}$$

where the parameters are given by $h = \frac{1+u(a^2+c^2)b}{1+uab}$, $f_{\mathbf{k}} = \frac{\theta_{\mathbf{k}}+ubc}{1+uab}$ and the function $\theta_{\mathbf{k}} = \frac{1}{\Delta_0}\left(\epsilon_{\mathbf{k}} - \mu_{12} + \sqrt{(\epsilon_{\mathbf{k}} - \mu_{12})^2 + \Delta_0^2}\right)$. Since all quantities depend on the momentum through the single particle energy, we can replace the momentum sums by energy integrals using the density of states defined by Eq. (3.76).

The selfconsistency relations in Eq. (3.132) are solved for a given g and Δ_0 iteratively. For a given set of a, b and c, we first evaluate the new b parameter. The parameter b then defines the new values of a and c. The energy integrals involved in this calculation are evaluated by the trapezoidal method. The procedure is repeated until the required relative accuracy is achieved. The entries of the proper self-energy matrix can be evaluated using Eq. (3.131).

Evaluation of the variational energy

Let us focus on the evaluation of the variational energy as a function of the variational parameters, g and Δ_0. After some matrix algebra and using Eq. (3.129), one can see that the kinetic energy of the first two colors is

$$K_1 + K_2 = 2\sum_{\mathbf{k}} \epsilon_{\mathbf{k}} \frac{1}{1-\Sigma_1}\left[\frac{(1-\Sigma_1/(1+g) - \Sigma_3 f_{\mathbf{k}}/(1+g))^2}{1+f_{\mathbf{k}}^2}\right] . \tag{3.133}$$

The kinetic energy of the third color has a form similar to the kinetic energy in the Gutzwiller ansatz for the SU(2) repulsive Hubbard model,

$$K_3 = qK_3^0 , \tag{3.134}$$

where $K_3^0 = \sum_{\mathbf{k}} \epsilon_{\mathbf{k}} \Theta(\epsilon_F - \epsilon_{\mathbf{k}})$, is the kinetic energy of the Fermi sea and the renormalization factor

$$q = \frac{(1-\Sigma_2/(1+g))^2}{1-\Sigma_2} \tag{3.135}$$

gives the quasiparticle residue, or equivalently, the discontinuity in the Fermi function. In the expressions above, we can replace the momentum sums by energy integrals with an appropriate density of states $D(\epsilon)$. Finally, the kinetic energy of the Gutzwiller correlated BCS state can be written as

$$\begin{aligned} K(g,\Delta_0)/N &= \frac{2}{1+(g^2-1)ab}\int d\epsilon D(\epsilon)\,\epsilon\,\frac{[1+(g-1)ab+(g-1)bcf(\epsilon)]^2}{1+f(\epsilon)^2} \\ &+ \frac{[1+(g-1)(a^2+c^2)]^2}{1+(g^2-1)(a^2+c^2)}\int d\epsilon D(\epsilon)\,\epsilon\,\Theta(\epsilon_F-\epsilon) , \end{aligned} \tag{3.136}$$

where the g and Δ_0 dependence of a,b and c is not displayed explicitly. Some details on the derivation of these expressions can be found in Appendix B.4.

The interaction energy can be evaluated simply using the expression for the full double occupancy in Eq. (3.118):

$$H_{\rm int}/N = U\frac{2ab+a^2+c^2+3(g^2-1)(a^2+c^2)b}{1+(g^2-1)(a^2+c^2)b} . \tag{3.137}$$

The variational energy is then given by the expression

$$E(g,\Delta_0) = K(g,\Delta_0) + H_{\rm int}(g,\Delta_0) . \tag{3.138}$$

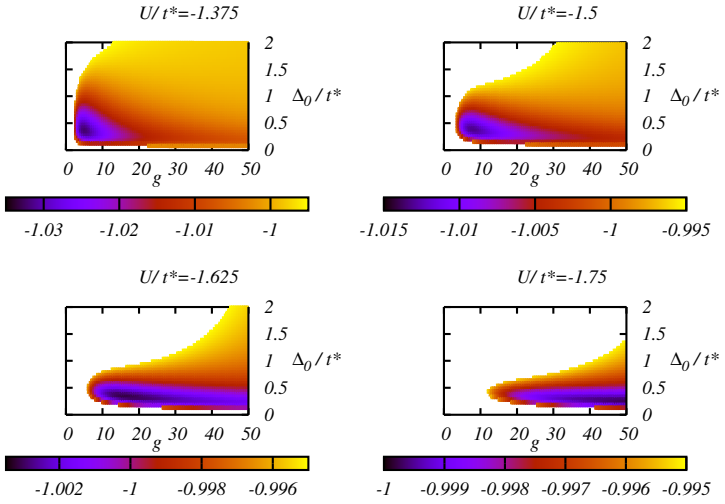

Figure 3.8: Contour plots of the variational energy $E(g, \Delta_0)$ at $\rho = \rho_\alpha = 1/3$. We show the variational energy surface for $E(g, \Delta_0) < 0.995 E_T$, where E_T is the energy of a trionic state corresponding to the filling ρ, given by Eq. (3.65).

Minimalization of the variational energy

For a fixed interaction strength U and filling $\rho = \rho_1 = \rho_2 = \rho_3$, we solve the selfconsistency relations numerically and calculate the variational energy as a function of g and Δ_0. For filling $\rho = 1/3$, we show these maps for different values of the interaction strength in Fig. 3.8. For weak interactions, the global minimum is found at $\Delta_0 > 0$ and $g > 1$. This is the color superfluid state with enhanced three-body correlations. Above a critical value $|U| > |U_C|$, however, the minimum can be found at $g = \infty$ and $\Delta_0 = 0$, which corresponds to the trionic phase. To see how the transition takes place, we minimized the variational energy numerically.

Before we proceed, let us discuss how we incorporated the "ferromagnetic tendency" in the calculations. To this end, we introduced the filling factor of the unpaired density, ρ_3 as a third variational parameter. The values of the "chemical potentials" μ_{12} and ϵ_F were then used to fix the filling factors of the different colors in the optimal ratio, for a given fixed overall filling $3\rho = \rho_1 + \rho_2 + \rho_3$. When solving the selfconsistency relations, we made use of the fact that the density of the third color is not renormalized:

$$\rho_3 = \langle \hat{n}_3 \rangle_G = \langle \hat{n}_3 \rangle_{BCS} \; . \tag{3.139}$$

The minimum of the variational energy $E(g, \Delta_0, \rho_3)$ for a fixed ρ and U is then approximated by a gradient method. Because of the shallow minimum, at each cycle of the minimalization, we approximate the energy function by a quadratic form

$$\begin{aligned} E(g, \Delta_0, \rho_3) \;&\approx\; E_0 + \nabla E \cdot (\delta g, \delta\Delta_0, \delta\rho_3) \\ &+\; \frac{1}{2} (\delta g, \delta\Delta_0, \delta\rho_3) \cdot [(\nabla \circ \nabla) E] \cdot (\delta g, \delta\Delta_0, \delta\rho_3) \; . \end{aligned} \tag{3.140}$$

The entries in the gradient vector and in the second derivative matrix are approxi-

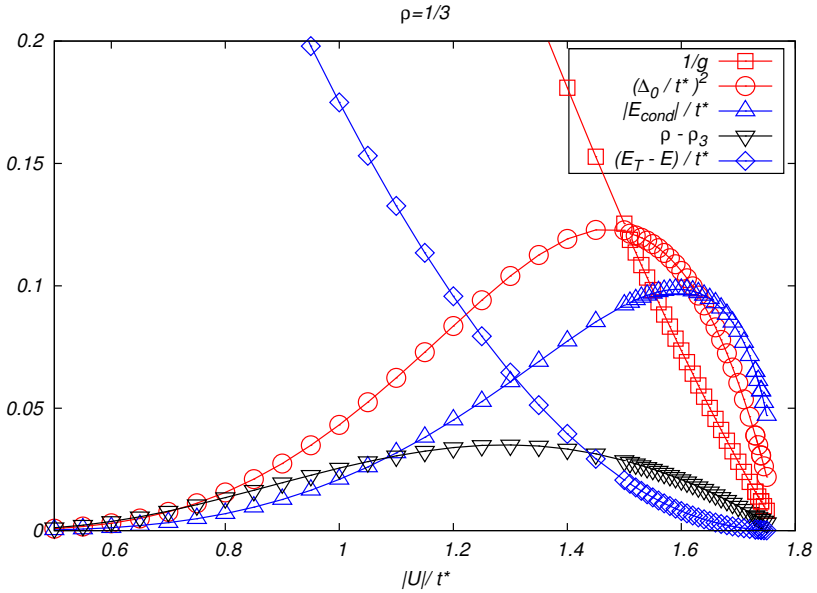

Figure 3.9: Optimal values of g, ρ_3 and Δ_0 for the filling $\rho = 1/3$ as a function of the interaction strength U. We also show the condensation energy, E_{cond}, and the energy difference with respect to the trionic state, $E_T - E$.

mated by finite differences. The optimal step size is then given by

$$(\delta g, \delta\Delta_0, \delta\rho_3)_{\mathrm{opt}} = -[(\nabla \circ \nabla)E]^{-1} \cdot \nabla E \,. \tag{3.141}$$

To avoid certain long-term diffusions around the minimum, a fraction $\approx 0.5..0.8$ of the optimal step size is taken. We repeat these steps until a given relative accuracy both in the energy and in the step size are achieved. Other numerical methods might have converged faster, however, we chose the more time-consuming technique explained above to have a more controlled convergence even for the shallow minimum of the energy and the divergence $g \to \infty$ at the transition point.

We shall now discuss the results of the minimalization. The optimal values of g, ρ_3 and Δ_0 as a function of the interaction strength U are shown in Fig. 3.9 for the filling $\rho = 1/3$. We also display the condensation energy E_{cond}, which is defined by the energy difference between the Gutzwiller correlated BCS state $|G\rangle$ and the Gutzwiller correlated Fermi sea,

$$|GFS\rangle = \left[\prod_l (1 + (g-1)\hat{F}_l^+ \hat{F}_l \;)\right] \prod_\alpha \prod_{\mathbf{k}:\epsilon_{\mathbf{k}}<\epsilon_F} \hat{c}^+_{\mathbf{k}\alpha}|0\rangle. \tag{3.142}$$

The energy of the state $|GFS\rangle$ can be evaluated when one substitutes $\Delta_0 = 0$ in the selfconsistency equations and in the expression of the variational energy.

If we extrapolate the curves in Fig. 3.9, we can see that within numerical accuracy, g diverges at the same point where the BCS order parameter Δ_0 vanishes. This suggests that the transition between the color superfluid phase and the trionic phase is continuous, and we conclude that the transition point is actually a *quantum critical point* on the phase diagram. A further argument for the second

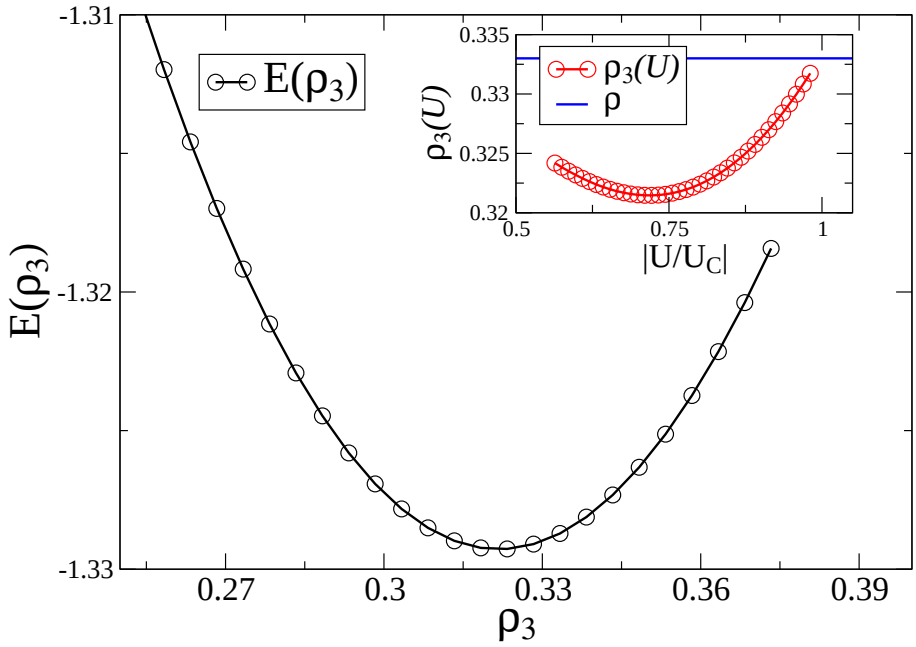

Figure 3.10: The minimum of the energy as a function of ρ_3 is slightly below the total filling, $\rho_3 < \rho$ in the color superfluid phase. This implies that the there is also "ferromagnetic" order: $m_8 \sim \rho_1 + \rho_2 - 2\rho_3 \neq 0$.

order transition is that also the gradient of the energy difference $(E - E_T)$ vanishes. This is usually not the case if the transition is of first order, i.e. a simple level crossing in the ground state.

We can also confirm the coexistence of "ferromagnetism" and superfluidity, since the optimal value of the filling fraction of the unpaired color is slightly below the average filling, $\rho > \rho_3$, in the color superfluid phase, and the difference scales to zero as one approaches the critical point (see Fig. 3.10). This implies that in a homogeneous system with fixed numbers of atoms in each color, domains will form, where the superconducting order parameter points to different directions in the different domains, as shown in Fig. 3.5. The lengthscale of these domains is very likely set by residual, long range interactions, which are not incorporated in the Hamiltonian in Eq. (3.30).

The trion – color superfluid transition does not depend on a particular filling, and Fig. 3.11 shows the critical interaction strengths $U_C(\rho)$ as a function of the filling. In the region we investigated, $\rho < 1/2$, the position of the transition depends weakly on the filling.

3.3.6 Generalization to more realistic models

We expect that the infinite dimensional approximation to the ground state of the SU(3) Hubbard model gives a qualitative insight to the behavior of more realistic systems. However, we shall modify our calculations in two ways, both of which might be considered as generalizations towards systems with more enhanced experimental relevance.

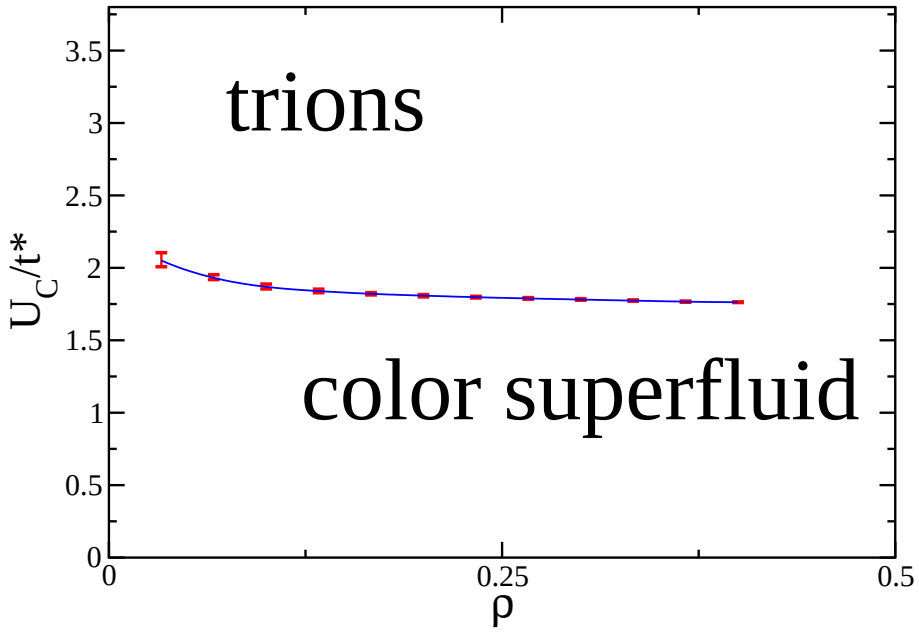

Figure 3.11: The transition point U_C depends weakly on the filling ρ, away from half filling. Therefore weak confining trap potentails should not affect the superfluid-trion transition qualitatively in a future experiment.

Results with semielliptical density of states

As a first approximation to finite dimensional systems, we can carry out the calculations with the semicircular density of states, defined by

$$D(\epsilon) = \frac{2}{\pi}\sqrt{1-\epsilon^2/t^2}\,. \tag{3.143}$$

The Gaussian DOS defined by Eq. (3.76) gives an infinite band, in contrast to the bounded spectrum of finite dimensional systems. As shown in Fig. 3.12, the continuous transition seems to persist. We remark, however, that the main qualitative difference between the finite dimensional and the infinite dimensional calculations is rather the contributions from the off-diagonal ($i \neq j$) terms of the proper self-energy.

Results for anisotropic interaction strengths

So far we assumed that the scattering lengths are the same in all scattering channels. In most systems, however, the three scattering lengths are not equal, and can vary with an external magnetic field. As we proposed, a possible candidate for realizing the trionic – color superfluid phase transition is ^{6}Li. In this system, the magnetic field dependence of the three scattering lengths has been determined numerically, and the position of the resonance is in very good agreement with the experiments [Abr97, Bar05, Moe95]. According to the results of Ref. [Bar05], the interaction strengths can be approximated in the magnetic field region 60 mT - 120

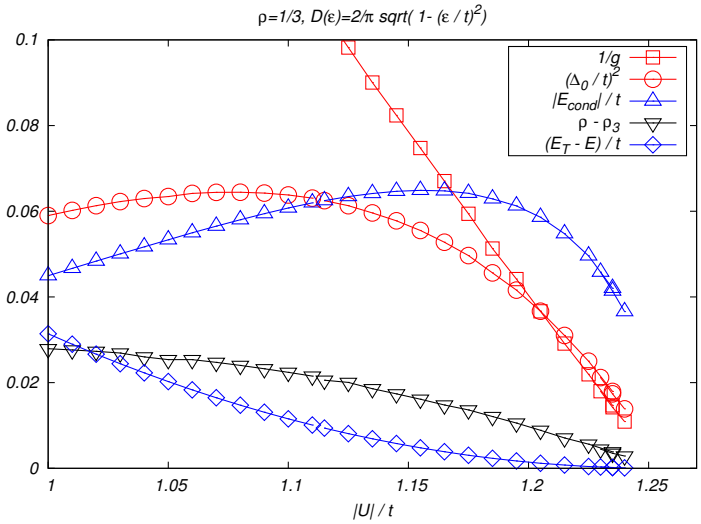

Figure 3.12: Optimal values of the variational parameters with a semicircular density of states, defined by Eq. (3.143).

mT as

$$U_{\beta\gamma} \approx U_0^{\beta\gamma} \left[1 + \frac{\Delta^{\beta\gamma}}{B - B_0^{\beta\gamma}}\right] \left[1 + \alpha^{\beta\gamma}(B - B_0^{\beta\gamma})\right] , \tag{3.144}$$

where the parameters B_0, Δ and α in this equation can be taken from Ref. [Bar05], and $U_0^{12} \equiv U_0$, $U_0^{13} = 1.23\, U_0$ and $U_0^{23} = 1.06\, U_0$. The interaction amplitude $U_0 = U_0^{12}$ can be changed by tuning the potential depth. For fixed magnetic field strengths $B \gg B_r \equiv B_0^{12} = 83.41\mathrm{mT}$, all three interaction strengths become approximately the same, and are negative, $U_{\alpha\beta} < 0$. On the other hand, if we increase the interaction strengths by approaching the Feshbach resonance at B_r, then the interaction becomes rather anisotropic in "color" space.

Experimentally, there are thus several ways to drive the system close to the phase transition regime, $t^*/|U_0| \sim 1$. The first possibility is to change the intensity of the laser beams, and thereby tune mostly the hopping amplitude t^*. In this case one can apply a large magnetic field in which the interaction is almost SU(3) symmetrical, although it is somewhat stronger in channel '12' than in the others. The other possibility is to tune the ratio $t^*/|U_0| \sim 1$ by changing the magnetic field and approaching a Feshbach resonance. In this second case the interactions can strongly break SU(3) symmetry.

In both cases, the anisotropic interaction has an important effect: it locks the superconducting order parameter so that only $\Delta_{12} \neq 0$. The color superfluid phase thus becomes a more or less standard U(1) superfluid with an additional decoupled Fermi liquid. However, as we show, the trionic phase transition can survive in this anisotropic limit.

Let us now investigate the superfluid - trion transition, assuming that $B > B_r$. In this region all interactions are attractive, $U_{\alpha\beta} < 0$. Perturbation theory tells us that the weak-coupling ground state is the color superfluid state $|BCS\rangle$ formed in the channels '12', and in the strong coupling limit, the ground state is a trionic state. Thus we can use the same type of ansatz for the ground state as

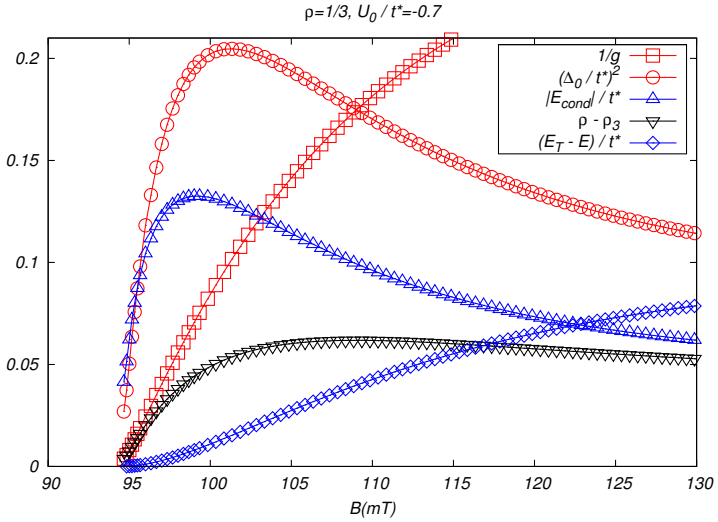

Figure 3.13: Optimal values of the variational parameters with anisotropic interaction strengths $U_{\alpha\beta}$ given by Eq. (3.144), at a fixed lattice depth as a function the magnetic field.

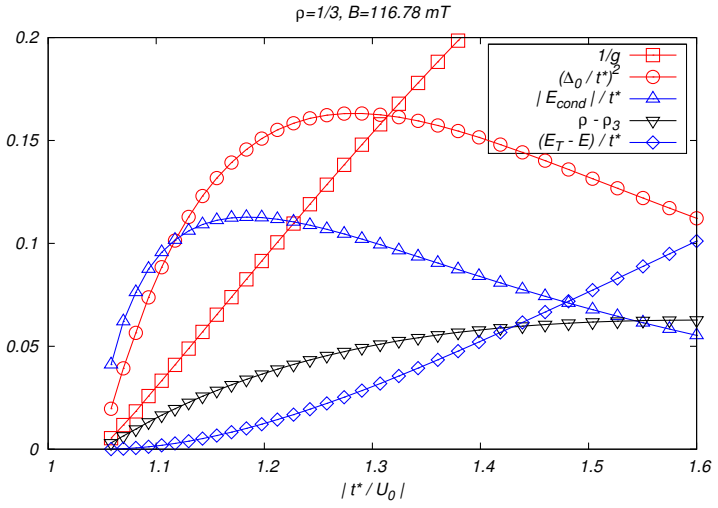

Figure 3.14: Optimal values of the variational parameters with anisotropic interaction strengths $U_{\alpha\beta}$ given by Eq. (3.144), at a fixed magnetic field corresponding to $B = 116.78$mT.

in the SU(3) case, given by Eq. (3.79). Since the structure of the effective theory is uniquely determined by the Gutzwiller ansatz state, the effective action, the Ward identities and the selfconsistency relations for the local effective action are invariant. The only difference is in the expression of the variational energy that we need to minimize:

$$\begin{aligned} E(g,\Delta_0,\rho_3) &= K(g,\Delta_0,\rho_3) \\ &+ \sum_i [U_{12}\langle \hat{n}_{i1}\hat{n}_{i2}\rangle_G + U_{13}\langle \hat{n}_{i1}\hat{n}_{i3}\rangle_G + U_{23}\langle \hat{n}_{i2}\hat{n}_{i3}\rangle_G] \ . \end{aligned} \tag{3.145}$$

The previously used numerical procedure can be modified to match this case, and we find that the quantum phase transition persists even with the anisotropy in the interaction strengths. We use the Gaussian DOS for this calculation, defined by Eq. (3.76).

The anisotropy in $U_{\alpha\beta}$ has also an important secondary effect: it induces somewhat different chemical potentials for the colors "1" and "2", which corresponds to an SU(3) "Zeeman field". Deep in the superfluid phase, this chemical potential difference is not sufficient to create a charge imbalance $\rho_1 \neq \rho_2$, since breaking Cooper pairs requires a finite energy [Sar63]. In principle, close to the transition point U_C, the BCS gap vanishes $\Delta_{12} \to 0$, therefore the chemical potential difference could create a first order transition to the trionic state. This would invalidate our restriction $\rho_1 = \rho_2$ in our calculations. However, at the critical point, trionic correlations also diverge $g \to \infty$, and therefore the effects of this 'Zeeman field' are suppressed. In fact, within the Gutzwiller approach, the phase transition seems to be continuous even for anisotropic interactions, as shown in Fig. 3.13 and Fig. 3.14. In Fig. 3.13, we show different physical quantities computed for the ground state as a function of B at $\rho = 1/3$ and at fixed lattice depth $t^*/|U_0| = 1.43$. The observed phase transition occurs at $B \approx 94.5\mathrm{mT}$, and all parameters behave similarly to the case with SU(3) symmetrical Hamiltonian. In Fig. 3.14, we show the similar transition happening with varying lattice depth and the magnetic field fixed. Despite these results, it is still possible that in $d = 3$ dimensions with anisotropic interactions, the trion - color superfluid transition becomes of first order.

3.4 Summary

In this chapter we investigated the ground state of the SU(3) symmetric attractive Hubbard model, which describes local interactions of itinerant fermions with three inner quantum numbers or colors. We analyzed the weak and strong coupling limits, and an SU(3) symmetry breaking color superfluid and a trionic phase were found, respectively. To investigate the transition between these limiting phases, we approximated the $d = \infty$ dimensional ground state by a Gutzwiller projected BCS wave function to incorporate the trionic correlations.

We formulated a path integral formalism to evaluate the Gutzwiller expectation values, where the effective action contains three-body interaction terms. While local expectation values have been expressed explicitly in terms of the proper self-energy Σ of the effective field theory, we derived "Ward identities" – valid also in $d < \infty$ dimensions – to relate the kinetic energy with this important quantity. Using the cavity method of dynamical mean field theory, we derived a selfconsistency equation for the proper self-energy, and avoided the cumbersome direct evaluation of an infinite series of self-energy diagrams.

We calculated the proper self-energy and the variational energy numerically. The minimalization with respect to the variational parameters, namely, the trionic Gutzwiller correlator g, the BCS order parameter Δ_0 and the filling fraction of the unpaired color ρ_3, implied that the transition in the ground state is continuous.

As first approximations to more realistic systems, we modified the numerical method. On one hand, we used a semicircular density of states to see the effects of a finite single particle band. On the other hand, we introduced anisotropic interactions between the different colors, with a magnetic field dependence analogous to the field dependence of the s-wave scattering lengths in the lowest three hyperfine states in ^{6}Li. We have not found *qualitatively* different results in these cases compared to SU(3) symmetric calculation, and the transition seemed to be continuous in both cases. However, we cannot exclude by our Gutzwiller calculation the possibility that in $d = 3$ dimensions, the trionic – color superfluid phase transition is of first order. It is also not clear whether the Gutzwiller ansatz could also be a good approximation in finite dimensions, although it is adequate to describe the $d = \infty$ dimensional ground state. In low dimensions that is certainly the case, since in $d = 1$ and $d = 2$ dimensions, the ground state is disordered and the weak coupling ground state cannot be approximated by a BCS wave function.

Since the critical value of U/t^* depends weakly on the density away from half filling, it is expected that weak confining potentials will not change qualitatively the transition and the phases. For strong anisotropies in the interaction and stronger harmonic potentials, i.e., $a_s^{(12)} \approx a_{\mathrm{HO}}^{\mathrm{trap}}$, our results certainly shall not apply.

Let us now discuss the experimental possibilities to identify the phases. The color superfluid phase could be detected by recently developed methods, e.g., by observing distinct interference peaks when the superfluid is released from a lattice [Chi06]. As we proposed in Sec. 3.3.6, the transition could be observed by increasing the lattice depth at a fixed, strong magnetic field $B > B_r$. In the trionic phase, periodic amplitude modulations (shaking) of the optical lattice would give a resonance at a characteristic frequency $\omega = |U_{13} + U_{23}|$, where trions break up.

We construct the phase diagram, shown in Fig. 3.15, based on the Gutzwiller calculations and the strong coupling perturbation theory. We find some similarities to the color superfluid - hadronic phase transition of quantum chromodynamics (QCD) [Alf98, Alf99, Fod02]. As pointed out by Wilczek [Wil07], these similarities imply that cold atomic systems might also serve as quantum simulations for QCD. Nevertheless there are certain differences between the three-component Hubbard model and QCD. In cold atomic systems, the fermions have only a single quantum number, namely, the hyperfine angular momentum, while quarks, on the other hand, have charge, flavor, etc., quantum numbers. The local interaction corresponding to massive "gluons" in the Hubbard model is also a weak approximation to the long-range strong interaction between the quarks.

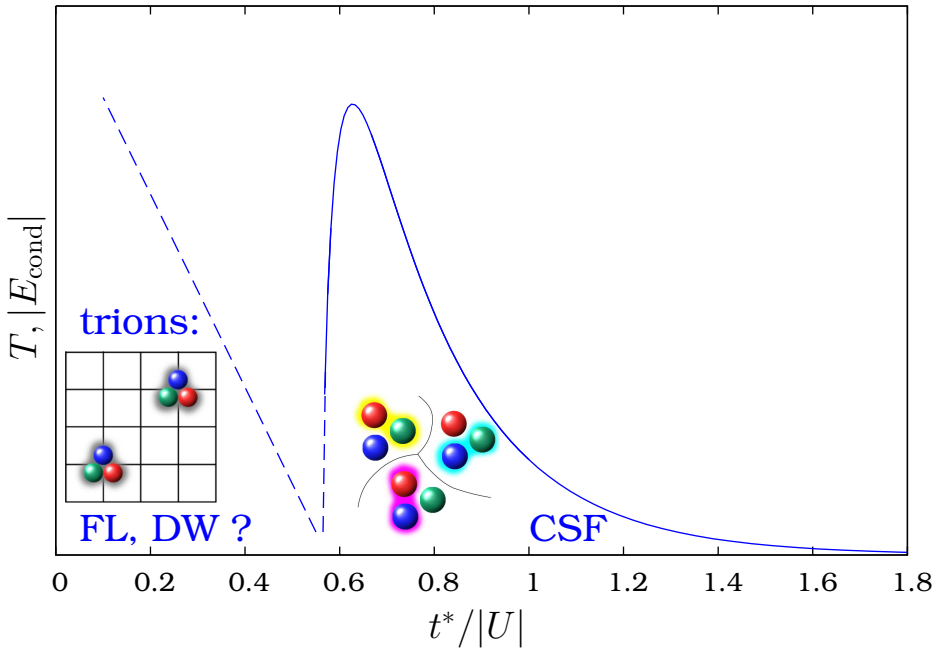

Figure 3.15: Phase diagram of th SU(3) attractive Hubbard model, based on the Gutzwiller calculations and the strong coupling perturbation theory. There are some similarities with corresponding phases in quantum chromodynamics, where a color superfluid phase has also been found [Alf98, Alf99], while the trions correspond to the baryons. The trionic phase in an optical lattice can be decorated by a Fermi liquid phase (FL) or a density wave phase (DW) of trions.

Chapter 4

Summary

Numerous materials and physical systems exhibiting strong correlations show anomalous behavior at low temperatures. In many cases, the origin of these anomalies is a second order quantum phase transition at zero temperature. The complete understanding of the quantum critical behavior emerging from this transition represents one of the most challenging problems in modern condensed matter physics.

Quantum phase transitions can be investigated efficiently in one dimension, since models in low dimensions can be analyzed using powerful mathematical tools. The ground state dynamics of one-dimensional spin models has been studied extensively, and in many cases, finite temperature static properties have also been discussed. On the other hand, the finite temperature dynamical behavior of gapped one-dimensional models is much less understood. The aim of part of the present work was to understand dynamical properties of gapped systems in one dimension, with a particular emphasis on the role of internal degrees of freedom.

The other focus of this work was the quantum phase transitions in ultracold atomic systems. Recently it became possible to trap both bosonic and fermionic atoms in optical lattices in ultracold environments, furthermore, one can also create mixtures with both particle species. The hyperfine quantum numbers of these atoms offer a large number of variational possibilities for experiments, and provide new fields for theoretical investigations. In the experiments with ultracold atomic gases, it is possible to realize systems of locally interacting particles on a lattice, where the number of "spin components" is not limited to two. A generalization of the Hubbard model with multiple spin components provides a good description of such systems. Although the two-component Hubbard model has been the subject of intense research, the ground states of its general, multi-component versions have not been investigated in great detail.

In this thesis, I investigated two models, the $Q = 3$ state quantum Potts model in $d = 1$ dimension, and the attractive SU(3) Hubbard model in $d = \infty$ dimensions. In both cases, the quantum phase transition is driven by strong correlations: in case of the Hubbard model, on-site interactions drive the system to a phase with singlet three-body bound states, while in the Potts model, intersite correlations lead to a ferromagnetically ordered state. The main results of my Ph.D. thesis are summarized in the following points:

I. Using the critical exponents of the $Q = 3$ state classical Potts model in $d = 2$

dimensions, I constructed the correlation function of the $d = 1$ dimensional quantum Potts model at the critical point, $g = g_c$ and $T = 0$. I applied a conformal mapping to obtain the imaginary time dynamical correlation function at finite temperature. Based on the analytic properties of this expression, I performed a Fourier transformation and analytic continuation on the complex frequency plain to obtain the dynamical susceptibility in the quantum critical region, at $g = g_c$ and $T > 0$ [Rap06].

II. I provided two arguments that the small - momentum limit of the two-particle scattering matrix in the gapped phases of the $Q = 3$ quantum Potts model is of purely exchange type. Based on this structure of the $\mathcal{S}$-matrix, I calculated the dynamical correlation functions analytically in the semiclassical limit $T \ll \Delta$. The relaxation function of correlations showed universal diffusive behavior both on the ferromagnetic and on the paramagnetic sides. I reproduced the semiclassical results for the Ising model in a transverse magnetic field in a simple way, in the limit $Q = 2$ [Rap06].

III. Using the semiclassical method, I calculated the $n^z - n^z$ dynamical correlation function of the O(3) quantum rotor model, which is related to the inelastic neutron-scattering lineshape of the S=1 antiferromagnetic Heisenberg chain at wave number $q \approx \pi$. I generalized the method to $O(N)$ quantum rotor models and also showed that the same relaxation function describes the correlations in the sine-Gordon model in the semiclassical limit. I thus found that the relaxation function derived analytically for the quantum Potts model applies to a variety of systems. I found for long timescales an exponential decay of correlations for the parameter $Q = 2$ in the relaxation function, while I found diffusive decay for $Q > 2$ [Rap08b].

IV. Based on symmetry arguments, I showed that there is a phase transition in the SU(3) attractive Hubbard model at zero temperature as a function of the interaction strength. Analyzing the strong coupling limit, I found that the most important correlations can be captured in a Gutzwiller type wave function (in the limit of $d = \infty$ dimensions) to describe the color superfluid – trionic phase transition. I constructed a mapping to an effective field theory to calculate the Gutzwiller expectation values. This functional integral formalism could be generalized to other Gutzwiller calculations as well [Rap07, Rap08a].

V. Based on the cavity method of dynamical mean field theory, I solved the effective field theory in the $d = \infty$ dimensional limit. I evaluated the Gutzwiller expectation values exactly in infinite dimensions in terms of the proper self-energy matrix of the effective field theory. I solved the selfconsistency equations for the self-energy matrix numerically. The results of the Gutzwiller calculation showed that a second order quantum phase transition appears between the color superfluid and the trionic phase, away from half filling. I determined the critical values of the interaction strength as a function of the filling factor. I also observed that the spontaneous breaking of SU(3) symmetry by the superfluid order is accompanied by "ferromagnetism" [Rap07, Rap08a].

VI. I performed modified Gutzwiller calculations using a semicircular single - particle density of states or with anisotropic interactions between the different hyperfine components that explicitly break the SU(3) symmetry. I observed that there are no qualitative differences compared to the case with SU(3) symmetry

and a Gaussian density of states, and that the continuous phase transition seems to persist. These results indicated that the phase transition found is robust and could be observed experimentally [Rap08a].

Appendix A

Appendix for the Potts model

A.1 Quantum critical region of the *Q*=3 quantum Potts model

A.1.1 Conformal mapping

In this section we shall derive the imaginary time correlation function, defined by Eq. (2.9), of the quantum Potts model at $g = g_c$. A conformal mapping $z' = w(z)$ has the following transformation rule for the correlation function in the scaling region [Car96]:

$$\langle \tilde{P}^{\mu}(z_1, \bar{z}_1)\tilde{P}^{\mu}(z_2, \bar{z}_2)\rangle = [w'(z_1)\bar{w}'(z_1)w'(z_2)\bar{w}'(z_2)]^{x_h/2} \langle \tilde{P}^{\mu}(z_1', \bar{z}_1')\tilde{P}^{\mu}(z_2', \bar{z}_2')\rangle \ , \tag{A.1}$$

with the exponents $x_h = 1/8$ and $x_h = 2/15$ for $Q = 2$ and $Q = 3$, respectively [DiF99]. If we use the particular conformal mapping in Eq. (1.23), the correlation function on the left hand side of Eq. (A.1) with $\mathrm{Re}z \in [0, 1/T]$ is related to the finite temperature correlation function

$$C^{\mu\mu}(x,\tau)_{T>0,g=g_c} = \left(1 - \frac{1}{Q}\right) C(x,\tau)_{T>0,g=g_c} \ , \tag{A.2}$$

while the correlation function on the right hand side of Eq. (A.1) with $\mathrm{Re}z' \in \mathcal{R}$ is the $T = 0$ correlation function given explicitely by the expression

$$C^{\mu\mu}(x,\tau)_{T=0,g=g_c} = \left(1 - \frac{1}{Q}\right) C(x,\tau)_{T=0,g=g_c} = \frac{\mathcal{W}}{(z_1' - z_2')^{x_h}(\bar{z}_1' - \bar{z}_2')^{x_h}} \ , \tag{A.3}$$

where $\mathcal{W}$ is a nonuniversal constant. Substituting Eq. (1.23) in Eq. (A.1) gives

$$\frac{w'(z_1)^{1/2}w'(z_2)^{1/2}}{z_1' - z_2'} = \frac{\pi T}{\sin(\pi T(z_1 - z_2))} \ , \tag{A.4}$$

therefore we find that the imaginary time correlation function of the $Q = 2, 3$-state quantum Potts model in the quantum critical region is given by

$$C(x,\tau)_{T>0,g=g_c} = \frac{\mathcal{W}\pi^{2x_h}T^{2x_h}}{\sin^{x_h}(\pi T(\tau + ix))\sin^{x_h}(\pi T(\tau - ix))}. \tag{A.5}$$

A.1.2 Fourier transformation in imaginary time

Let us now focus on the Fourier transformation of Eq. (A.5). We shall refer to certain formulas in Ref. [Abr65] as AS/... and to Ref. [Gra94] as GR/... throughout this subsection. We start by rewriting Eq. (A.5) as

$$C(x,\tau)_{T>0,g=g_c} = \frac{\mathcal{W}2^{x_h}\pi^{2x_h}T^{2x_h}}{[\cosh(2\pi Tx)-\cos(2\pi T\tau)]^{x_h}} \ . \tag{A.6}$$

In order to factorize the integrals in Eq. (2.60), we use the identity

$$\frac{1}{[\cosh(2\pi Tx)-\cos(2\pi T\tau)]^{x_h}} = \frac{1}{\Gamma(x_h)}\int_0^\infty dy\ y^{x_h-1}e^{-y[\cosh(2\pi Tx)-\cos(2\pi T\tau)]} \ . \tag{A.7}$$

Let us now perform the integration over the positions and over the imaginary times separately. By introducing the dimensionless variable $\bar{\tau} = 2\pi T\tau$, the integral over imaginary time can be written as

$$\int_0^\beta d\tau\ e^{i\omega_n\tau + y\cos(2\pi T\tau)} = \frac{1}{2\pi T}\int_0^{2\pi} d\bar{\tau}\ e^{in\bar{\tau}+y\cos(\bar{\tau})} \ , \tag{A.8}$$

and $\bar{\omega}_n = \frac{1}{2\pi T}\omega_n = n$. Using the formulas AS/9.1.21 and GR/8.406.3, we can find

$$\int_0^\beta d\tau\ e^{i\omega_n\tau + y\cos(2\pi T\tau)} = \frac{1}{T}(-1)^{|n|}I_{|n|}(-y) \ , \tag{A.9}$$

where $I_\nu(x)$ is the modified (imaginary argument) Bessel function of the first kind. Next we introduce the dimensionless position as $\bar{x} = 2\pi Tx$, so that

$$\int_{-\infty}^\infty dx\ e^{-ikx - y\cosh(2\pi Tx)} = \frac{1}{2\pi T}\int_{-\infty}^\infty d\bar{x}\ e^{-i\bar{k}\bar{x}-y\cosh(\bar{x})} \ . \tag{A.10}$$

We observe that this integral is convergent for any $y > 0$. Using GR/3.337.1, the integral can be written as

$$\int_{-\infty}^\infty dx\ e^{-ikx - y\cosh(2\pi Tx)} = \frac{1}{2\pi T}2K_{i\bar{k}}(y) \ , \tag{A.11}$$

where $K_\nu(x)$ is the modified Bessel function of the second kind. Another approach to derive this result is that it can be seen that the integral in Eq. (A.10) satisfies the differential equation GR/8.494.1 and vanishes as $y \to \infty$.

To obtain the Fourier transform of Eq. (A.5), we shall perform one last integral:

$$C(k,i\omega_n) = \frac{\mathcal{W}2^{x_h}\pi^{2x_h-1}T^{2x_h-2}}{\Gamma(x_h)}(-1)^{|n|}\int_0^\infty dy y^{-(1-x_h)}K_{i\bar{k}}(y)I_{|n|}(-y) \ . \tag{A.12}$$

According to GR/6.576.5, this can be calculated analytically by using the complicated formula

$$\int_0^\infty dy\, y^{-\lambda} K_\mu(ay) I_\nu(by)$$
$$= \frac{b^\nu \Gamma(\frac{1}{2} - \frac{1}{2}\lambda + \frac{1}{2}\mu + \frac{1}{2}\nu)\Gamma(\frac{1}{2} - \frac{1}{2}\lambda - \frac{1}{2}\mu + \frac{1}{2}\nu)}{2^{\lambda+1}\Gamma(\nu+1)a^{-\lambda+\nu+1}}$$
$$\times F(\frac{1}{2} - \frac{1}{2}\lambda + \frac{1}{2}\mu + \frac{1}{2}\nu, \frac{1}{2} - \frac{1}{2}\lambda - \frac{1}{2}\mu + \frac{1}{2}\nu; \nu+1; \frac{b^2}{a^2}) \,, \tag{A.13}$$

if $Re(\nu + 1 - \lambda \pm \mu) > 0$ and $a > b$, and $F(x_1, x_2; x_3; x_4)$ is the hypergeometric function. Since the parameters in Eq.(A.12) correspond to

$$a = 1 \,; \tag{A.14}$$
$$b = -1 \,; \tag{A.15}$$
$$\lambda = 1 - x_h \,; (x_h = 2/15) \,; \tag{A.16}$$
$$\mu = i\bar{k} = i\frac{1}{2\pi T}k \,; \tag{A.17}$$
$$\nu = |n| = \frac{1}{2\pi T}|\omega_n| \,, \tag{A.18}$$

we see that the conditions of GR/6.576.5 are met. Furthermore, since $b^2/a^2 = 1$, we can simplify Eq. (A.13) according to AS/15.1.20, exploiting the fact that

$$F(a', b'; c'; 1) = \frac{\Gamma(c')\Gamma(c' - b' - a')}{\Gamma(c' - a')\Gamma(b' - a')} \,. \tag{A.19}$$

To summarize, the final form of the Fourier transform of the imaginary time correlation function is

$$C(k, i\omega_n) = \frac{\mathcal{W}}{2^{2-2x_h}\pi^{1-2x_h}T^{2-2x_h}} \frac{\Gamma(1-x_h)}{\Gamma(x_h)}$$
$$\times \frac{\Gamma\left(\frac{x_h}{2} - i\frac{i|\omega_n|+k}{4\pi T}\right)\Gamma\left(\frac{x_h}{2} - i\frac{i|\omega_n|-k}{4\pi T}\right)}{\Gamma\left(1 - \frac{x_h}{2} - i\frac{i|\omega_n|+k}{4\pi T}\right)\Gamma\left(1 - \frac{x_h}{2} - i\frac{i|\omega_n|-k}{4\pi T}\right)} . \tag{A.20}$$

A.2 Derivation of the scattering matrices

A.2.1 Scattering matrix - ferromagnetic side

To obtain the two-particle scattering matrix in leading order in g we make the following simple ansatz for the two-particle wave function $|\Psi\rangle$,

$$|\Psi\rangle = \sum_{\theta,\theta'} \Big\{ A_{\theta,\theta'} \sum_{i<j} \left(e^{i(kx_i + k'x_j)} |i, \theta; j, \theta'\rangle_{\tilde{\mu}} \right) +$$
$$B_{\theta,\theta'} \sum_{i>j} \left(e^{i(kx_i + k'x_j)} |i, \theta; j, \theta'\rangle_{\tilde{\mu}} \right) \Big\} \,, \tag{A.21}$$

where $\tilde{\mu}$ is the orientation of the chain on the far left, and θ and θ' denote the two kinks corresponding to the two domain walls. In leading order in g and for coordinates $|i-j| \gg 1$, $\hat{H}_1 = -Jg\sum_i \tilde{P}_i$ just moves the two domain walls independently, and $|\Psi\rangle$ is clearly an eigenstate of the total Hamiltonian with an eigenvalue

$$\hat{H}_P|\Psi\rangle = (E_0 + \epsilon(k) + \epsilon(k'))\,|\Psi\rangle\ , \tag{A.22}$$

E_0 being the ground state energy, and $\epsilon(k)$ the quasiparticle energy in Eq. (2.16). However, $|\Psi\rangle$ must satisfy Eq. (A.22) also for $j = i+1$, *i.e.* for nearest neighbors. Observing that the operator $\hat{H}_1$ just flips each spin to some other direction,

$$\begin{aligned}
&\sum_n \tilde{P}_n|\tilde{\mu}, i, \mu, i+1, \mu'\rangle \\
= \;& \langle\tilde{\mu}|\tilde{P}|\mu\rangle\ |\tilde{\mu}, i-1, \mu, i+1, \mu'\rangle \\
+ \;& \langle\mu|\tilde{P}|\mu'\rangle\ |\tilde{\mu}, i, \mu, i+2, \mu'\rangle \\
+ \;& \sum_{\mu''\neq\mu} \langle\mu''|\tilde{P}|\mu\rangle\ |\tilde{\mu}, i, \mu'', i+1, \mu'\rangle + \dots\ ,
\end{aligned} \tag{A.23}$$

where $\theta = (\mu - \tilde{\mu}) \mod Q$, $\theta' = (\mu' - \mu) \mod Q$, and we neglected all other terms involving more than two domain wall excitations, since these are high up in energy. Since the off-diagonal matrix elements of $\tilde{P}_n$ are all equal to $1/Q$, we can write this in the 'kink' representation as:

$$\begin{aligned}
&\sum_n \tilde{P}_n|i, \theta;\ i+1, \theta'\rangle_{\tilde{\mu}} \qquad\qquad (A.24)\\
= \;& \frac{1}{Q}\Bigg[|i-1, \theta;\ i+1, \theta'\rangle_{\tilde{\mu}} + |i, \theta;\ i+2, \theta'\rangle_{\tilde{\mu}} \\
&\qquad + \sum_{\tilde{\theta},\tilde{\theta}'} \hat{\delta}^{\tilde{\theta}+\tilde{\theta}'}_{\theta+\theta'}\ (1-\delta^{\tilde{\theta}'}_{\theta})\ |i, \tilde{\theta}';\ i+1, \tilde{\theta}\rangle_{\tilde{\mu}}\Bigg] + \dots\ ,
\end{aligned}$$

where $\hat{\delta}$ denotes the Kronecker-delta modulo Q. Projecting out the $i+1 = j$ component of the Schrödinger equation Eq. (A.22), we obtain the following constraint for the coefficients $A_{\theta,\theta'}$ and $B_{\theta,\theta'}$,

$$\begin{aligned}
&\sum_{\tilde{\theta},\tilde{\theta}'}\left[\delta^{\tilde{\theta}}_{\theta}\delta^{\tilde{\theta}'}_{\theta'} + \frac{1}{e^{ik'}+e^{-ik}}\hat{\delta}^{\tilde{\theta}+\tilde{\theta}'}_{\theta+\theta'}(1-\delta^{\tilde{\theta}'}_{\theta})\right] B_{\tilde{\theta}',\tilde{\theta}} = \\
&-\sum_{\tilde{\theta},\tilde{\theta}'}\left[\delta^{\tilde{\theta}}_{\theta}\delta^{\tilde{\theta}'}_{\theta'} + \frac{1}{e^{ik}+e^{-ik'}}\hat{\delta}^{\tilde{\theta}+\tilde{\theta}'}_{\theta+\theta'}(1-\delta^{\tilde{\theta}'}_{\theta})\right] A_{\tilde{\theta},\tilde{\theta}'}\ .
\end{aligned} \tag{A.25}$$

This equation can clearly be inverted to give the two-particle $\mathcal{S}$-matrix in leading order in g, but the solution is rather complicated even for $Q = 3$. Eq. (A.25) simplifies, however, in the limit $k, k' \to 0$, relevant for low temperatures, $T \ll \Delta$.

For $Q = 3$ we obtain in this way the scattering matrix

$$\mathcal{S}^{\tilde{\theta},\tilde{\theta}'}_{\theta,\theta'}(k, k' \to 0) = (-1)\ \delta^{\tilde{\theta}'}_{\theta}\ \delta^{\tilde{\theta}}_{\theta'}\ , \tag{A.26}$$

which is identical to the expression in Eq. (2.74).

We remark that the above result holds for any $Q \neq 4$. The $Q = 4$ case, however, seems to be special: then the operator in front of the coefficients $A_{\tilde{\theta},\tilde{\theta}'}$ and $B_{\theta,\theta'}$ in Eq. (A.25) has zero eigenvalues for $k = k' = 0$, the inversion is problematic, and the $\mathcal{S}$-matrix does not take the form Eq. (2.74).

A.2.2 Scattering matrices - paramagnetic side

To obtain the two-particle scattering matrix in leading order in $1/g$, we follow similar steps as for the ferromagnetic case. The ansatz for the two-particle wave function can be written as follows:

$$|\tilde{\Psi}\rangle = \sum_{\lambda,\lambda'} \left\{ A_{\lambda,\lambda'} \sum_{i<j} \left(e^{i(kx_i+k'x_j)} |i,\lambda;j,\lambda'\rangle \right) + B_{\lambda,\lambda'} \sum_{i>j} \left(e^{i(kx_i+k'x_j)} |i,\lambda;j,\lambda'\rangle \right) \right\} . \tag{A.27}$$

For $|i-j| \gg 1$ $|\tilde{\Psi}\rangle$ must satisfy a similar two-particle Schrödinger equation as Eq. (A.22), and so it must be valid for $j = i+1$ too. Let us now calculate the effect of $H_{\text{ferro}} = -j \sum_n \sum_\mu \tilde{P}^\mu_n \tilde{P}^\mu_{n+1}$ on the $i+1 = j$ term of $|\tilde{\Psi}\rangle$. If we neglect the high energy terms with multiple quasiparticles we get

$$\begin{aligned} \sum_n \sum_\mu \tilde{P}^\mu_n \tilde{P}^\mu_{n+1} \, |i,\lambda;i+1,\lambda'\rangle &= \frac{1}{Q}|i-1,\lambda;i+1,\lambda'\rangle \\ &+ \frac{1}{Q}|i,\lambda;i+2,\lambda'\rangle \\ &+ \sum_{\tilde{\lambda}\tilde{\lambda}'} \sum_\mu \langle\tilde{\lambda}'|\tilde{P}^\mu|\lambda\rangle\langle\tilde{\lambda}|\tilde{P}^\mu|\lambda'\rangle |i,\tilde{\lambda}';i+1,\tilde{\lambda}\rangle . \end{aligned} \tag{A.28}$$

Substituting this to the two-particle Schrödinger equation leads to a constraint for the coefficients similar to the ferromagnetic case:

$$\begin{aligned} \sum_{\tilde{\lambda},\tilde{\lambda}'} \left[\delta^{\tilde{\lambda}}_{\lambda} \delta^{\tilde{\lambda}'}_{\lambda'} + \frac{1}{e^{ik'}+e^{-ik}} M^{\tilde{\lambda}\tilde{\lambda}'}_{\lambda\lambda'} \right] B_{\tilde{\lambda}',\tilde{\lambda}} = \\ - \sum_{\tilde{\lambda},\tilde{\lambda}'} \left[\delta^{\tilde{\lambda}}_{\lambda} \delta^{\tilde{\lambda}'}_{\lambda'} + \frac{1}{e^{ik}+e^{-ik'}} M^{\tilde{\lambda}\tilde{\lambda}'}_{\lambda\lambda'} \right] A_{\tilde{\lambda},\tilde{\lambda}'} , \end{aligned} \tag{A.29}$$

where the matrix $M^{\tilde{\lambda}\tilde{\lambda}'}_{\lambda\lambda'}$ is given by

$$M^{\tilde{\lambda}\tilde{\lambda}'}_{\lambda\lambda'} = \sum_\mu \langle\tilde{\lambda}'|\tilde{P}^\mu|\lambda\rangle\langle\tilde{\lambda}|\tilde{P}^\mu|\lambda'\rangle. \tag{A.30}$$

In the limit of vanishing quasiparticle momenta $k, k' \to 0$, this equation can be solved to obtain the $\mathcal{S}$-matrix for $Q = 3$, which gives the result

$$\mathcal{S}^{\tilde{\lambda},\tilde{\lambda}'}_{\lambda,\lambda'}(k,k' \to 0) = (-1)\, \delta^{\tilde{\lambda}'}_{\lambda}\, \delta^{\tilde{\lambda}}_{\lambda'} . \tag{A.31}$$

A.3 Dynamical correlations in the Potts model

A.3.1 Ferromagnetic side

As discussed in Section 2.4.3, we have to evaluate the thermal average

$$C^{\mu_1\mu_2}(x,t) = \prod_\nu \left[\int_{-L/2}^{L/2} \frac{dx_\nu}{L} \int_{-\infty}^{\infty} dv_\nu P(v_\nu) \sum_{\theta_\nu} \frac{1}{Q-1} \right]$$

$$\times\Bigg\{\sum_{m,l}\chi(x_{l-1}\le 0\le x_l)\chi(X_{m-1}\le x\le X_m)$$
$$\sum_{\mu\mu'}\chi(m\mathrm{th}:\mu)(\delta_{\mu\mu_1}-\frac{1}{Q})\chi(l\mathrm{th}:\mu')(\delta_{\mu'\mu_2}-\frac{1}{Q})\Bigg\} \qquad \text{(A.32)}$$

For fixed indeces m and l, we can carry out the average over the kink quantum numbers θ_ν. To this end, let us examine the expression

$$F(\mu_1,\mu_2,l,m)=\sum_{\mu\mu'}(\delta_{\mu\mu_1}-\frac{1}{Q})(\delta_{\mu'\mu_2}-\frac{1}{Q})\sum_{\{\theta_\nu\}}\chi(m\mathrm{th}:\mu)\chi(l\mathrm{th}:\mu')\ . \qquad \text{(A.33)}$$

There are three cases, depending on the value of m and l. For $l=m$, we can simply find

$$F(\mu_1,\mu_2,l,m)=\sum_{\mu\mu'}(\delta_{\mu\mu_1}-\frac{1}{Q})(\delta_{\mu'\mu_2}-\frac{1}{Q})\delta_{\mu\mu'}=\delta_{\mu_1\mu_2}-\frac{1}{Q}\ . \qquad \text{(A.34)}$$

For $l<m$, we can use that the difference in the orientations of l'th and m'th domains, $\mu-\mu'$ has to be the same as the sum of the steps (mod$Q$) at the kinks between them:

$$\sum_{\{\theta_\nu\}}\chi(m\mathrm{th}:\mu)\chi(l\mathrm{th}:\mu')=\sum_{\{\theta_\nu\}}\hat{\delta}_{\mu',\mu+\theta_l+\theta_{l+1}+\ldots+\theta_{m-1}}\ , \qquad \text{(A.35)}$$

since the difference between the domains is given by the net kink step size, and $\hat{\delta}$ is the Kronecker-delta modulo Q. Summing up for $\nu<l$ and $\nu\ge m$ leads to the expression

$$\begin{aligned}\langle\hat{\delta}_{\mu,\mu'+\theta_l+\theta_{l+1}+\ldots+\theta_{m-1}}\rangle_{\{\theta_\nu\}} &= \Big[\frac{1}{Q-1}\Big]^M\sum_{\{\theta_\nu\}}\hat{\delta}_{\mu,\mu'+\theta_l+\theta_{l+1}+\ldots+\theta_{m-1}} \qquad \text{(A.36)}\\ &= \Big[\frac{1}{Q-1}\Big]^{m-l}\sum_{\theta_l,\ldots,\theta_{m-1}}\hat{\delta}_{\mu,\mu'+\theta_l+\theta_{l+1}+\ldots+\theta_{m-1}}\ .\end{aligned}$$

Let us introduce new sum indeces as $\mu_{l+1}=(\mu'+\theta_l)\mathrm{mod}Q$, $\mu_{l+k+1}=(\mu_{l+k}+\theta_{l+k})\mathrm{mod}Q$, and finally $\mu_m=(\mu_{m-1}+\theta_{m-1})\mathrm{mod}Q$. Exploiting these definitions, we can write

$$\begin{aligned}&\sum_{\theta_l,\theta_{l+1},\ldots,\theta_{m-1}}\hat{\delta}_{\mu,\mu'+\theta_l+\theta_{l+1}+\ldots+\theta_{m-1}}\\ &=\sum_{\mu_{l+1}}(1-\delta_{\mu'\mu_{l+1}})\sum_{\mu_{l+2}}(1-\delta_{\mu_{l+1}\mu_{l+2}})\ldots\sum_{\mu_m}(1-\delta_{\mu_{m-1}\mu_m})\hat{\delta}_{\mu\mu_m}\ . \qquad \text{(A.37)}\end{aligned}$$

Therefore, it is possible to eliminate the last of the $m-l$ summations. The summations over the other indeces can be interpreted as row-vs-column compositions at matrix multiplications, which enables us to rewrite Eq. (A.38) in a more compact form:

$$\sum_{\theta_l,\theta_{l+1},\ldots,\theta_{m-1}}\hat{\delta}_{\mu,\mu'+\theta_l+\theta_{l+1}+\ldots+\theta_{m-1}}=\langle\mu'|[Q\hat{P}-1]^{m-l}|\mu\rangle\ , \qquad \text{(A.38)}$$

where $\hat{P} = |C\rangle\langle C|$ is a projector and the corner state $|C\rangle$ is defined by Eq. (2.2). We can compute the power $m-l$ of the matrix $Q\hat{P}-1$ using the binomial identity as

$$\begin{aligned}
[Q\hat{P}-1]^{m-l} &= \sum_{k=0}^{m-l}\binom{m-l}{k}Q^k\hat{P}^k(-1)^{m-l-k} \\
&= (-1)^{m-l}+\hat{P}\sum_{k=1}^{m-l}\binom{m-l}{k}Q^k(-1)^{m-l-k} \\
&= (-1)^{m-l}+\hat{P}[(Q-1)^{m-l}-(-1)^{m-l}]\,. \qquad \text{(A.39)}
\end{aligned}$$

This allows us to simplify the expression in Eq. (A.38) as

$$\begin{aligned}
\left(\frac{1}{Q-1}\right)^{m-l}\langle\mu'|[Q\hat{P}-1]^{m-l}|\mu\rangle &= \left(\frac{-1}{Q-1}\right)^{m-l}\delta_{\mu\mu'} \\
&\quad +\frac{1}{Q}\left[1-\left(\frac{-1}{Q-1}\right)^{m-l}\right]\,. \qquad \text{(A.40)}
\end{aligned}$$

Finally, for $m>l$ we can write

$$\begin{aligned}
F(\mu_1,\mu_2,l,m) &= \sum_{\mu\mu'}(\delta_{\mu\mu_1}-\frac{1}{Q})(\delta_{\mu'\mu_2}-\frac{1}{Q}) \\
&\quad \left\{\left(\frac{-1}{Q-1}\right)^{m-l}\delta_{\mu\mu'}+\frac{1}{Q}\left[1-\left(\frac{-1}{Q-1}\right)^{m-l}\right]\right\} \\
&= \left(\delta_{\mu_1\mu_2}-\frac{1}{Q}\right)\left(\frac{-1}{Q-1}\right)^{m-l}, \qquad \text{(A.41)}
\end{aligned}$$

since the second term in the second equation. For $l>m$, we observe that the roles of μ and μ' are simply exchanged, which can be transferred to the sum variables. To summarize, for any l and m we can write

$$F(\mu_1,\mu_2,l,m) = \left(\delta_{\mu_1\mu_2}-\frac{1}{Q}\right)\left(\frac{-1}{Q-1}\right)^{|m-l|}\,. \qquad \text{(A.42)}$$

We see that the expression for the correlation function on the ferromagnetic side can be written as:

$$\begin{aligned}
C^{\mu_1\mu_1}(x,t) &= \sum_{m,l}\left(\delta_{\mu_1\mu_2}-\frac{1}{Q}\right)\left(\frac{-1}{Q-1}\right)^{|m-l|} \\
&\quad \langle\chi(x_{l-1}\le 0\le x_l)\chi(X_{m-1}(t)\le x\le X_m(t))\rangle_{\{x_\nu,v_\nu\}}\,, \qquad \text{(A.43)}
\end{aligned}$$

where

$$\begin{aligned}
&\langle\chi(x_{l-1}\le 0\le x_l)\chi(X_{m-1}(t)\le x\le X_m(t))\rangle_{\{x_\nu,v_\nu\}} \qquad \text{(A.44)} \\
&=\prod_\nu\left[\int_{-L/2}^{L/2}\frac{dx_\nu}{L}\int_{-\infty}^{\infty}dv_\nu P(v_\nu)\right]\chi(x_{l-1}\le 0\le x_l)\chi(X_{m-1}(t)\le x\le X_m(t))\,.
\end{aligned}$$

Let us now focus on the average over the positions and velocities. First we can exploit the identity

$$\begin{aligned} & \chi(x_{l-1} \le 0 \le x_l)\chi(X_{m-1}(t) \le x \le X_m(t)) \\ = \; & \chi(x_{l-1} \le 0 \le x_l)\delta_{m-l,\sum_{\nu'}[\Theta(x-x_{\nu'}(t))-\Theta(-x_{\nu'})]} \; , \end{aligned} \tag{A.45}$$

since x will be $n = m - l$ particles to the right if and only if the line $(0,0) \to (x,t)$ is crossed by a net number of $m - l$ lines from the right. We shall introduce the variable $n = l - m$. We can also perform the summation over l, since there is allways precisely a single term giving a non-zero contribution $\chi(x_{l-1} \le 0 \le x_l) = 1$. Thus we can write

$$\begin{aligned} C^{\mu_1\mu_2}(x,t) \; = \; & \sum_n \left(\delta_{\mu_1\mu_2} - \frac{1}{Q}\right)\left(\frac{-1}{Q-1}\right)^{|n|} \\ & \left\langle \delta_{n,\delta_{n,\sum_{\nu'}[\Theta(x-x_{\nu'}(t))-\Theta(-x_{\nu'})]}} \right\rangle_{\{x_\nu,v_\nu\}} \end{aligned} \tag{A.46}$$

Let us rewrite the Kronecker-delta in an integral representation to factorize the integrals over the positions and the velocities of the different quasiparticles:

$$\begin{aligned} & \delta_{n,\sum_{\nu'}\Theta(x-x_{\nu'}(t))-\Theta(-x_{\nu'})} \\ & = \int_0^{2\pi} \frac{d\phi}{2\pi} \exp\left\{ i\phi \left(n - \delta_{n,\sum_{\nu'}[\Theta(x-x_{\nu'}(t))-\Theta(-x_{\nu'})]} \right) \right\} \; , \end{aligned} \tag{A.47}$$

Therefore, we have to evaluate the expression

$$C^{\mu_1\mu_2}(x,t) = \sum_n \int_0^{2\pi} \frac{d\phi}{2\pi} e^{i\phi n} \left(\delta_{\mu_1\mu_2} - \frac{1}{Q}\right)\left(\frac{-1}{Q-1}\right)^{|n|} \prod_{\nu=1}^{M} I_\nu \; , \tag{A.48}$$

where the integral I_ν is given by

$$I_\nu = \int_{-L/2}^{L/2} \frac{dx_\nu}{L} \int_{-\infty}^{\infty} dv_\nu P(v_\nu) e^{-i\phi\Theta(x-x_\nu(t))+i\phi\Theta(-x_{\nu'})} \; . \tag{A.49}$$

We can safely assume that $x, t \ge 0$, since symmetries implie

$$C(x,t) = C(\pm x, \pm t) \; . \tag{A.50}$$

The integration range in Eq. (A.49) can be divided to six regions, where the Heaviside functions can be evaluated giving

$$\begin{aligned} I_\nu \; = \; & 1 + \frac{t}{L}\left(e^{-i\phi} - 1\right) \int_{-\infty}^{x/t} dv_\nu \; P(v_\nu) \left(\frac{x}{t} - v_\nu\right) \\ & + \frac{t}{L}\left(1 - e^{i\phi}\right) \int_{x/t}^{\infty} dv_\nu \; P(v_\nu) \left(\frac{x}{t} - v_\nu\right) \; . \end{aligned} \tag{A.51}$$

We can now introduce dimensionless variables, defining the dimensionless velocity

$$\bar{v} = \sqrt{\frac{\Delta}{2c^2T}} v_\nu \ , \tag{A.52}$$

while using the definition of the semiclassical characteristic length

$$\xi_c \equiv \frac{1}{\rho} = \frac{1}{Q-1}\sqrt{\frac{2\pi c^2}{T\Delta}} e^{\Delta/T} \ , \tag{A.53}$$

we define the semiclassical characteristic time

$$\tau_c = \xi_c \sqrt{\frac{\Delta}{2c^2T}} = \frac{1}{Q-1}\frac{\sqrt{\pi}}{T} e^{\Delta/T} \ . \tag{A.54}$$

We define the dimensionless variables $\bar{t} = t/\tau_c, \bar{x} = x/\xi_c$ and $\bar{L} = L/\xi_c \equiv M$. Using these definitions, we can evaluate the integrals in Eq. (A.51) as

$$\begin{aligned} I_\nu &= 1 + \frac{\bar{t}}{\bar{L}}\left(e^{-i\phi}-1\right)\int_{-\infty}^{\bar{x}/\bar{t}} d\bar{v}\ P(\bar{v})\left(\frac{\bar{x}}{\bar{t}} - \bar{v}\right) \\ &\quad + \frac{\bar{t}}{\bar{L}}\left(1-e^{i\phi}\right)\int_{\bar{x}/\bar{t}}^{\infty} d\bar{v}\ P(\bar{v})\left(\frac{\bar{x}}{\bar{t}} - \bar{v}\right) \\ &= 1 - \frac{\bar{t}}{\bar{L}}\left\{G(\bar{x}/\bar{t}) + G(-\bar{x}/\bar{t}) - e^{i\phi}G(\bar{x}/\bar{t}) - e^{-i\phi}G(-\bar{x}/\bar{t})\right\} \ , \end{aligned} \tag{A.55}$$

where

$$G(u) = \frac{1}{2\sqrt{\pi}} e^{-u^2} - \frac{u}{2}\mathrm{erfc}(u) \ . \tag{A.56}$$

In the thermodynamic limit,

$$\prod_\nu I_\nu = I_\nu^M \to e^{-\bar{t}\left(G(\bar{x}/\bar{t}) + G(-\bar{x}/\bar{t}) - e^{i\phi}G(\bar{x}/\bar{t}) - e^{-i\phi}G(-\bar{x}/\bar{t})\right)} \ . \tag{A.57}$$

We can further simplify this expression exploiting that only the even part in ϕ gives contribution to the integral, which is given by the following expression:

$$\begin{aligned} &\frac{1}{2}[I_\nu^M(\phi) + I_\nu^M(-\phi)] \\ &\quad = e^{-\bar{t}(1-\cos\phi)(G(\bar{x}/\bar{t}) + G(-\bar{x}/\bar{t}))} \cos\left(\bar{t}(G(\bar{x}/\bar{t}) - G(-\bar{x}/\bar{t}))\ \sin\phi\right) \ . \end{aligned} \tag{A.58}$$

Furthermore, we define the function

$$F(u) \equiv G(u) + G(-u) = \frac{1}{\sqrt{\pi}} e^{-u^2} + u\mathrm{erf}u \ , \tag{A.59}$$

and it is easy to see that

$$G(u) - G(-u) = -u \ . \tag{A.60}$$

We can now perform the sum over n as

$$\sum_{n=-\infty}^{\infty} e^{i\phi n}\left(\frac{-1}{Q-1}\right)^{|n|} = \frac{(Q-1)^2 - 1}{(Q-1)^2 + 2(Q-1)\cos(\phi) + 1} \ . \tag{A.61}$$

Therefore the correlation function can be written as

$$C^{\mu_1\mu_2}(x,t) = \left(\delta_{\mu_1\mu_2} - \frac{1}{Q}\right) R(\bar{x},\bar{t}) \tag{A.62}$$

where the relaxation function is given by

$$\begin{aligned} R(\bar{x},\bar{t}) &= \int_0^{2\pi} \frac{d\phi}{2\pi} \frac{(Q-1)^2 - 1}{(Q-1)^2 + 2(Q-1)\cos(\phi) + 1} \\ & \qquad e^{-|\bar{t}|(1-\cos\phi)F(\bar{x}/\bar{t})} \cos(\bar{x}\sin\phi) \ . \end{aligned} \tag{A.63}$$

Appendix B

Appendix for the Hubbard model

B.1 Evaluation of a Matsubara-sum

Let us focus in this section on the $\mathcal{O}(\Delta_0^4)$ term in the effective BCS action S_{BCS} in Eq. (3.49). We have to calculate the Matsubara sum and the integral

$$\sum_n |\omega_n|^{-3} \int_0^\infty dy \frac{1}{(1+y^2)^2} \,. \tag{B.1}$$

We shall first compute integrals of the form

$$J_p = \int dy \frac{1}{(1+y^2)^p} \,. \tag{B.2}$$

To this end, we set up a recursion relation:

$$\begin{aligned} J_{p+1} &= \int dy \frac{1}{(1+y^2)^{p+1}} = \int dy \frac{1+y^2-y^2}{(1+y^2)^{p+1}} \\ &= J_p - \int dy\, y \frac{y}{(1+y^2)^{p+1}} = J_p + \frac{-1}{2p} J_p = \frac{2p-1}{2p} J_p \,, \end{aligned} \tag{B.3}$$

and we know that $J_1 = [\arctan y]_{-\infty}^{\infty} = \pi$. Thus

$$J_2 = \frac{1}{2}\pi \,;\, J_3 = \frac{3}{8}\pi \,;\, J_4 = \frac{5}{16}\pi \,. \tag{B.4}$$

We use that the modulus of the Matsubara frequencies is given by $|\omega_n| = |\pi(2n+1)T|$ to have

$$\sum_n |\omega_n|^{-\nu} = (\pi T)^{-\nu} \left[2 \sum_{n=0} \frac{1}{(2n+1)^\nu} - 1 \right] \tag{B.5}$$

We can now evaluate the Matsubara sums using the following identity:

$$\sum_{n=0} \frac{1}{(2n+1)^\nu} = \sum_{n=1} \frac{1}{n^\nu} - \sum_{n=1} \frac{1}{(2n)^\nu} = \frac{2^\nu - 1}{2^\nu} \zeta(\nu) > 0 \,. \tag{B.6}$$

We can substitute the result in Eq. (B.4) and Eqs. (B.5) and (B.6) to obtain the last expression in Eq. (3.53).

B.2 Diagonalization and symmetry properties of the cavity action

In this section we shall show that the matrix $\mathcal{U}$ that diagonalizes the bare cavity propagator, $\mathcal{D}_0$, has a special symplectic symmetry, which implies that one can evaluate the Green's functions by performing a variable transformation with this matrix. We first observe that the Nambu spinors Ψ satisfy the relation $\bar{\Psi} = \Psi^T \tau_1$ where $\tau_1 = \sigma_1 \otimes \delta_{\alpha\beta}$ and σ_1 is the first Pauli matrix acting in Nambu space. Therefore, we can parameterize $\mathcal{D}_0^{-1}$ in the following way,

$$\mathcal{D}_0^{-1} = \begin{pmatrix} H & A \\ A^+ & -H^T \end{pmatrix} , \tag{B.7}$$

where H is hermitian and A is antisymmetric. Thus the following identity holds:

$$\tau_1 \mathcal{D}_0^{-1} \tau_1 = -\mathcal{D}_0^{-1*} , \tag{B.8}$$

This structure of $\mathcal{D}_0^{-1}$ enables us to discuss its eigenvectors. Let us assume that $\underline{\mathbf{v}}_i$ is a righthand side eigenvector of $\mathcal{D}_0^{-1}$ (a column vector),

$$\mathcal{D}_0^{-1} \underline{\mathbf{v}}_i = \epsilon_i \underline{\mathbf{v}}_i . \tag{B.9}$$

Then $\underline{\mathbf{w}}_i = \tau_1 \underline{\mathbf{v}}_i^*$ is also an eigenvector:

$$\mathcal{D}_0^{-1} \tau_1 \underline{\mathbf{v}}_i^* = \tau_1 (\tau_1 \mathcal{D}_0^{-1} \tau_1) \underline{\mathbf{v}}_i^* = -\tau_1 \mathcal{D}_0^{-1*} \underline{\mathbf{v}}_i^* = -\epsilon_i \tau_1 \underline{\mathbf{v}}_i^* , \tag{B.10}$$

since the eigenvalues are real. We shall construct the unitary matrix using the eigenvectors

$$\mathcal{U}^+ = (\underline{\mathbf{v}}_1, \underline{\mathbf{v}}_2, \underline{\mathbf{v}}_3, \tau_1 \underline{\mathbf{v}}_1^*, \tau_1 \underline{\mathbf{v}}_2^*, \tau_1 \underline{\mathbf{v}}_3^*) . \tag{B.11}$$

which transforms $\mathcal{D}_0^{-1}$ to a diagonal form,

$$\mathcal{U} \mathcal{D}_0^{-1} \mathcal{U}^+ = \begin{pmatrix} \mathrm{d}^{-1} & 0 \\ 0 & -\mathrm{d}^{-1} \end{pmatrix} , \tag{B.12}$$

with d is a real diagonal matrix. Now we shall show that $\mathcal{U}$ is a well-defined transformation for the Nambu vector Ψ in the sense that the identity $\bar{\Psi} = \Psi^T \tau_1$ also holds for the transformed eigenvectors defined by $\Phi = \mathcal{U}\Psi, \bar{\Phi} = \bar{\Psi}\mathcal{U}^+$, as

$$\bar{\Phi} = \Phi^T \tau_1 . \tag{B.13}$$

Note that this identity is necessary to carry out the functional integral in terms of the components of the transformed field Φ as new independent variables. Eq. (B.13) is satisfied if

$$\bar{\Psi}\mathcal{U}^+ = \bar{\Phi} = \Phi^T \tau_1 = (\mathcal{U}\Psi)^T \tau_1 = \Psi^T \mathcal{U}^T \tau_1 , \tag{B.14}$$

i.e., if the matrix $\mathcal{U}$ satisfies the condition

$$\mathcal{U}^+ = \tau_1 \mathcal{U}^T \tau_1 . \tag{B.15}$$

Eq. (B.15) can readily be verified using the properties of the eigenvectors

$$\begin{aligned} \tau_1 \mathcal{U}^T \tau_1 &= \tau_1 (\underline{\mathbf{v}}_1^*, \underline{\mathbf{v}}_2^*, \underline{\mathbf{v}}_3^*, \tau_1 \underline{\mathbf{v}}_1, \tau_1 \underline{\mathbf{v}}_2, \tau_1 \underline{\mathbf{v}}_3) \tau_1 \\ &= \tau_1 (\tau_1 \underline{\mathbf{v}}_1, \tau_1 \underline{\mathbf{v}}_2, \tau_1 \underline{\mathbf{v}}_3, \underline{\mathbf{v}}_1^*, \underline{\mathbf{v}}_2^*, \underline{\mathbf{v}}_3^*) \\ &= (\underline{\mathbf{v}}_1, \underline{\mathbf{v}}_2, \underline{\mathbf{v}}_3, \tau_1 \underline{\mathbf{v}}_1^*, \tau_1 \underline{\mathbf{v}}_2^*, \tau_1 \underline{\mathbf{v}}_3^*) \\ &= \mathcal{U}^+ . \end{aligned} \tag{B.16}$$

Relation Eq. (B.12) therefore implies that the cavity functional integrals can be computed by first transforming to the diagonal basis of $\mathcal{D}_0^{-1}$ and then transforming back the Green's function to the original basis using the transformation $\mathcal{U}$. Importantly, the interaction term of the local action is invariant under the transformation $\Psi \to \Phi$. This follows simply from the fact that the interaction can be also expressed as $\sim \prod_{\alpha=1}^{6} \eta_\alpha$, and that the determinant of $\mathcal{U}$ is just 1.

B.3 Ward identities

In this section we shall connect certain expectation values with the self energy S defined by Eq. (3.95), which shall be used to express the kinetic energy in terms of the self energy itself. First we shift the integration variables of Γ in Eq. (3.119) following the transformation Eq. (3.121), which automatically applies for the conjugate fields as

$$\bar{\Psi}_i \to \bar{\Phi}_i = \bar{\Psi}_i + \lambda \sum_p \bar{I}_p \tau_3 D^0_{pi} \; . \tag{B.17}$$

Using the transformed expressions, the linear and quadratic terms in the generatic action become

$$\begin{aligned} &\frac{1}{2}\sum_{ij} \bar{\Psi}_i D^{0-1}_{ij} \Psi_j + \sum_i \bar{I}_i \tau_3 \Psi_i \\ &= \frac{1}{2}\sum_{ij} \bar{\Phi}_i D^{0-1}_{ij} \Phi_j + (1-\lambda)\sum_i \bar{I}_i \tau_3 \Phi_i \\ &\quad + \frac{\lambda^2 - 2\lambda}{2} \sum_{ij} \bar{I}_i \tau_3 D^0_{ij} \tau_3 I_j \; . \end{aligned} \tag{B.18}$$

Transforming the interaction term is more complicated, therefore let us first consider the on-site density:

$$\begin{aligned} \bar{\Psi}_i \tau_3 \Psi_i \;\; &= \;\; \bar{\Phi}_i \tau_3 \Phi_i - 2\lambda \bar{\Phi}_i \tau_3 \sum_m D^0_{im} \tau_3 I_m \\ &+ \;\; \lambda^2 \sum_{nm} \bar{I}_n \tau_3 D^0_{ni} \tau_3 D^0_{im} \tau_3 I_m \; , \end{aligned} \tag{B.19}$$

where we used that $\bar{\Phi}_i \tau_3 D^0_{ij} \tau_3 I_j = \bar{I}_j \tau_3 D^0_{ji} \tau_3 \Phi_i$. We note that all terms here behave like scalars with respect to both the Grassmann algebra and the color matrices; and they commute with each other. When performing the functional derivation, we also need to expand the exponential in terms of I to the order $\mathcal{O}(I^2)$. Thus, when calculating the third power of Eq. (B.19), we can drop certain higher order terms. Following these arguments, the interaction term can be written as follows:

$$\begin{aligned} \sum_r (\bar{\Psi}_r \tau_3 \Psi_r)^3 \;\; = \;\; &\sum_r (\bar{\Phi}_r \tau_3 \Phi_r)^3 \\ &-6\lambda \sum_{r,m} (\bar{\Phi}_r \tau_3 \Phi_r)^2 (\bar{\Phi}_r \tau_3 M^{-1}_{rm} \tau_3 I_m) \\ &+12\lambda^2 \sum_{r,n,m} (\bar{I}_n \tau_3 M^{-1}_{nr} \tau_3 \Phi_r)(\bar{\Phi}_r \tau_3 \Phi_r)(\bar{\Phi}_r \tau_3 M^{-1}_{rm} \tau_3 I_m) \\ &+3\lambda^2 \sum_{r,n,m} (\bar{\Phi}_r \tau_3 \Phi_r)^2 (\bar{I}_n \tau_3 M^{-1}_{nr} \tau_3 M^{-1}_{rm} \tau_3 I_m) + \dots \; , \end{aligned}$$

where the ellipsis stands for terms of order $\mathcal{O}(I^3)$. Now we can expand the exponential in the definition of the generating functional. Introducing the abbreviation $u = g^2 - 1$ we obtain the following long expression

$$\begin{aligned}
\Gamma &= \ln \int \mathcal{D}\bar{\eta}\mathcal{D}\eta \; e^{-\mathcal{S}+\sum_i \bar{I}_i \tau_3 \Psi_i} \approx \\
&\approx \ln \int \mathcal{D}\bar{a}\mathcal{D}a \; e^{-\mathcal{S}} \left(1 + \frac{\lambda^2 - 2\lambda}{2} \sum_{rr'} \bar{I}_r \tau_3 M^{-1}_{rr'} \tau_3 I_{r'} \right. \\
&\quad + \frac{1}{2}\lambda^2 u \sum_{rr'r"} (\bar{I}_{r'} \tau_3 M^{-1}_{r'r} \tau_3 n^F_r \Phi_r)(\bar{\Phi}_r \tau_3 M^{-1}_{rr"} \tau_3 I_{r"}) \\
&\quad + \frac{1}{2}\lambda^2 u \sum_{rr'r"} (\bar{I}_{r'} \tau_3 M^{-1}_{r'r} d^F_r \tau_3 M^{-1}_{rr"} \tau_3 I_{r"}) \\
&\quad + \frac{1}{2}(1-\lambda)^2 \sum_{rr'} (\bar{I}_r \tau_3 \Phi_r)(\bar{\Phi}_{r'} \tau_3 I_{r'}) \\
&\quad + \frac{1}{2}\lambda^2 u^2 \sum_{rr'pp'} (\bar{I}_{r'} \tau_3 M^{-1}_{r'r} \tau_3 \Phi_r d^F_r)(d^F_p \bar{\Phi}_p \tau_3 M^{-1}_{pp'} \tau_3 I_{p'}) \\
&\quad - \frac{1}{2}\lambda(1-\lambda) u \sum_{rr'r"} (\bar{I}_r \tau_3 \Phi_r)(d^F_{r'} \Phi_{r'} \tau_3 M^{-1}_{r'r"} \tau_3 I_{r"}) \\
&\quad \left. - \frac{1}{2}\lambda(1-\lambda) u \sum_{rr'r"} (\bar{I}_r \tau_3 M^{-1}_{rr'} \tau_3 d^F_{r'} \Phi_{r'})(\bar{\Phi}_r" \tau_3 I_r") \right) ,
\end{aligned} \tag{B.20}$$

where $\bar{\Phi} = (\bar{a}_1, \bar{a}_2, \bar{a}_3, a_1, a_2, a_3)$ are the transformed Grassmann fields. Now one can perform the functional derivation to obtain the dressed propagator:

$$\begin{aligned}
D_{ij} &= \begin{pmatrix} \frac{\delta^2\Gamma}{\delta J_i \delta J_j} & -\frac{\delta^2\Gamma}{\delta J_i \delta J_j} \\ -\frac{\delta^2\Gamma}{\delta J_i \delta J_j} & \frac{\delta^2\Gamma}{\delta J_i \delta J_j} \end{pmatrix} = \\
&= "\tau_3 \frac{\delta^2\Gamma}{\delta\bar{I}\delta I} \tau_3" = \\
&= (2\lambda - \lambda^2) D^0_{ij} - (1-\lambda)^2 \langle \Phi_i \bar{\Phi}_j \rangle_{\mathcal{S}} \\
&\quad - \lambda^2 u \sum_r D^0_{ir} \tau_3 \langle n^F_r \Phi_r \bar{\Phi}_r \rangle_{\mathcal{S}} \tau_3 D^0_{rj} \\
&\quad - \lambda^2 u \sum_r D^0_{ir} \tau_3 \langle d^F_r \rangle_{\mathcal{S}} \tau_3 D^0_{rj} \\
&\quad - \lambda^2 u^2 \sum_{rr'} D^0_{ir} \tau_3 \langle \Phi_r d^F_r d^F_{r'} \bar{\Phi}_{r'} \rangle_{\mathcal{S}} \tau_3 D^0_{r'j} \\
&\quad + (1-\lambda)\lambda u \sum_r \langle \Phi_i d^F_r \bar{\Phi}_r \rangle_{\mathcal{S}} \tau_3 D^0_{rj} \\
&\quad + (1-\lambda)\lambda u \sum_r D^0_{ir} \tau_3 \langle \Phi_r d^F_r \bar{\Phi}_j \rangle_{\mathcal{S}} \; .
\end{aligned} \tag{B.21}$$

Using that $D = -\langle \Phi \bar{\Phi} \rangle_{\mathcal{S}}$, we can rewrite this expression in the following form:

$$D_{ij} = D^0_{ij} - \frac{\lambda}{2-\lambda} u \sum_r D^0_{ir} \tau_3 \langle n^F_r \Phi_r \bar{\Phi}_r \rangle_{\mathcal{S}} \tau_3 D^0_{rj}$$

$$
\begin{aligned}
&-\frac{\lambda}{2-\lambda}u\sum_r D^0_{ir}\tau_3\langle d^F_r\rangle_{\mathcal{S}} D^0_{rj}\\
&-\frac{\lambda}{2-\lambda}u^2\sum_{rr'} D^0_{ir}\tau_3\langle \Phi_r d^F_r d^F_{r'}\bar{\Phi}_{r'}\rangle_{\mathcal{S}}\tau_3 D^0_{r'j}\\
&+\frac{1-\lambda}{2-\lambda}u\sum_r\langle\Phi_i d^F_r\bar{\Phi}_r\rangle_{\mathcal{S}}\tau_3 D^0_{rj}\\
&+\frac{1-\lambda}{2-\lambda}u\sum_r D^0_{ir}\tau_3\langle\Phi_r d^F_r\bar{\Phi}_j\rangle_{\mathcal{S}}\ . \qquad \text{(B.22)}
\end{aligned}
$$

Substituting $\lambda = 1$ leads to

$$
\begin{aligned}
D_{ij} &= D^0_{ij} - u\sum_r D^0_{ir}\tau_3\langle n^F_r\Phi_r\bar{\Phi}_r\rangle_{\mathcal{S}}\tau_3 D^0_{rj}\\
&\quad - u\sum_r D^0_{ir}\tau_3\langle d^F_r\rangle_{\mathcal{S}} D^0_{rj} +\\
&\quad - u^2\sum_{rr'} D^0_{ir}\tau_3\langle\Phi_r d^F_r d^F_{r'}\bar{\Phi}_{r'}\rangle_{\mathcal{S}}\tau_3 D^0_{r'j}\ , \qquad \text{(B.23)}
\end{aligned}
$$

while setting $\lambda = 0$ we obtain another interesting identity,

$$
\begin{aligned}
D_{ij} &= D^0_{ij} + \frac{u}{2}\sum_r(\langle\Phi_i d^F_r\bar{\Phi}_r\rangle_{\mathcal{S}}\tau_3 D^0_{rj}\\
&\quad + \frac{u}{2}\sum_r D^0_{ir}\tau_3\langle\Phi_r d^F_r\bar{\Phi}_j\rangle_{\mathcal{S}}\ . \qquad \text{(B.24)}
\end{aligned}
$$

Comparing these with the the definition of the self energy Eq. (3.95), one finds the Ward identities given by Eqs. (3.122)-(3.124) and thus the expression Eq. (3.129) of the kinetic energy in terms of the self energy.

B.4 Kinetic energy in the Gutzwiller ansatz

According to Section 3.3.5, the expectation value of the kinetic energy in the Gutzwiller ansatz ground state can be written

$$
K = \langle -\sum_{ij\alpha} c^+_{i\alpha}c_{j\alpha}\rangle_G = \sum_k \epsilon_k \mathrm{tr}P(k)\ . \qquad \text{(B.25)}
$$

Using Eq. (3.129) and Dyson's equation, we can calculate the Fourier transform of the density matrix

$$
\begin{aligned}
P(k)^T &= \Big[D^0(k)[1-D^0(k)\Sigma]^{-1} - \frac{1}{1+g}\big(D^0(k)[1-D^0(k)\Sigma]^{-1}\Sigma +\\
&\quad + [1-D^0(k)\Sigma]^{-1}\Sigma D^0(k)\big) + \frac{1}{(1+g)^2}[1-D^0(k)\Sigma]^{-1}\Sigma\Big]^{11}\ . \qquad \text{(B.26)}
\end{aligned}
$$

The trace operation enables us to relocate some of the matrices:

$$
\begin{aligned}
\mathrm{tr}P(k) &= \mathrm{tr}\Big[[D^{0-1}(k)-\Sigma]^{-1} - \frac{2}{1+g}[D^{0-1}(k)-\Sigma]^{-1}\Sigma +\\
&\quad + \frac{1}{(1+g)^2}D^{0-1}(k)[D^{0-1}(k)-\Sigma]^{-1}\Sigma\Big]^{11}\ . \qquad \text{(B.27)}
\end{aligned}
$$

The kinetic energy of the third color is thus

$$\begin{aligned}
K_3 &= \sum_k \epsilon_k \Big[[D^{0-1}(k)-\Sigma]^{-1} - \frac{2}{1+g}[D^{0-1}(k)-\Sigma]^{-1}\Sigma \\
&\qquad + \frac{1}{(1+g)^2} D^{0-1}(k)[D^{0-1}(k)-\Sigma]^{-1}\Sigma \Big]_{33} \\
&= \sum_k \epsilon_k \Bigg[\frac{\Theta(\epsilon_F-\epsilon_k)}{1+u\Theta(\epsilon_F-\epsilon_k)(a^2+c^2)} \\
&\qquad + \frac{2}{1+g}\frac{\Theta(\epsilon_F-\epsilon_k)u(a^2+c^2)}{1+u\Theta(\epsilon_F-\epsilon_k)(a^2+c^2)} \\
&\qquad - \frac{1}{(1+g)^2}\frac{u(a^2+c^2)}{1+u\Theta(\epsilon_F-\epsilon_k)(a^2+c^2)} \Bigg] \\
&= N\int_{-\infty}^{\epsilon_F} d\epsilon D(\epsilon)\epsilon \Bigg[\frac{1}{1+u(a^2+c^2)} + \frac{2}{1+g}\frac{u(a^2+c^2)}{1+u(a^2+c^2)} \\
&\qquad - \frac{1}{(1+g)^2}\frac{u(a^2+c^2)}{1+u(a^2+c^2)} \Bigg] \\
&\quad + \int_{\epsilon_F}^{\infty} d\epsilon D(\epsilon)\epsilon \Big[-\frac{1}{(1+g)^2}u(a^2+c^2) \Big] \\
&= N\int_{-\infty}^{\epsilon_F} d\epsilon D(\epsilon)\epsilon \Bigg[\frac{1}{1+u(a^2+c^2)} + \frac{2}{1+g}\frac{u(a^2+c^2)}{1+u(a^2+c^2)} \\
&\qquad - \frac{1}{(1+g)^2}\frac{u(a^2+c^2)}{1+u(a^2+c^2)} \Bigg] \\
&\quad - \int_{-\infty}^{\epsilon_F} d\epsilon D(\epsilon)\epsilon \Big[-\frac{1}{(1+g)^2}u(a^2+c^2) \Big] \\
&= N\frac{\big[1+(g-1)(a^2+c^2)\big]^2}{1+u(a^2+c^2)} \int_{-\infty}^{\epsilon_F} d\epsilon D(\epsilon)\epsilon \\
&= \frac{\big[1+(g-1)(a^2+c^2)\big]^2}{1+u(a^2+c^2)} K_3^0 \,, \qquad \text{(B.28)}
\end{aligned}$$

where K_3^0 is the unperturbed kinetic energy of the third color. To obtain these results, we used that with nearest neighbor hopping, the density of states defines a symmetric band.

We can also express the kinetic energy of the other colors in terms of the proper self energy:

$$K_1 = \sum_k \epsilon_k \Big[[D^{0-1}(k)-\Sigma]^{-1} - \frac{2}{1+g}[D^{0-1}(k)-\Sigma]^{-1}\Sigma$$

$$
\begin{aligned}
&+ \frac{1}{(1+g)^2} D^{0-1}(k)[D^{0-1}(k)-\Sigma]^{-1}\Sigma\Big]_{11} \\
= \sum_k \epsilon_k \Bigg[& \frac{1-\Sigma_1}{(1-\Sigma_1)^2+(\theta_k-\Sigma_3)^2} \\
& - \frac{2}{1+g}\frac{\Sigma_1(1-\Sigma_1)+\Sigma_3(\theta_k-\Sigma_3)}{(1-\Sigma_1)^2+(\theta_k-\Sigma_3)^2} \\
& + \frac{1}{(1+g)^2}\frac{\Sigma_1(1-\Sigma_1)+\theta_k^2\Sigma_1-\Sigma_3^2}{(1-\Sigma_1)^2+(\theta_k-\Sigma_3)^2}\Bigg] ,
\end{aligned}
\tag{B.29}
$$

where $\theta_k = \Sigma_3 + f_k(1-\Sigma_1)$ is defined below Eq. (3.132). By symmetry, the kinetic energy of the second color is simply equivalent to $K_2 = K_1$. We shall use some algebraic identities when writing

$$
\begin{aligned}
K_1 &= \sum_k \epsilon_k \Bigg[\frac{1}{1-\Sigma_1}\frac{1}{1+f_k^2} - \frac{2}{1+g}\frac{1}{1-\Sigma_1}\frac{\Sigma_1+\Sigma_3 f_k}{1+f_k^2} \\
&\qquad + \frac{1}{(1+g)^2}\frac{1}{1-\Sigma_1}\frac{\Sigma_1(1+f_k^2)-(\Sigma_3-\Sigma_1 f_k)^2}{1+f_k^2}\Bigg] \\
&= \sum_k \epsilon_k \left[\frac{1}{1-\Sigma_1}\frac{1}{1+f_k^2}\right] \\
&\qquad \times \left[1-2\tilde{\Sigma}_1 - 2\tilde{\Sigma}_3 f_k - \tilde{\Sigma}_3^2 + 2\tilde{\Sigma}_3\tilde{\Sigma}_1 f_k - \tilde{\Sigma}_1^2 f_k^2\right] \\
&= \sum_k \epsilon_k \left[\frac{1}{1-\Sigma_1}\frac{1}{1+f_k^2}\right] \\
&\qquad \times \Big[1-2\tilde{\Sigma}_1 - 2\tilde{\Sigma}_3 f_k - \tilde{\Sigma}_3^2(f_k^2+1-f_k^2) \\
&\qquad\qquad + 2\tilde{\Sigma}_3\tilde{\Sigma}_1 f_k - \tilde{\Sigma}_1^2(f_k^2+1-1)\Big] \\
&= \sum_k \epsilon_k \left[\frac{1}{1-\Sigma_1}\frac{1}{1+f_k^2}\right] \\
&\qquad \times \left[1-2\tilde{\Sigma}_1 - 2\tilde{\Sigma}_3 f_k + \tilde{\Sigma}_3^2 f_k^2 + 2\tilde{\Sigma}_3\tilde{\Sigma}_1 f_k + \tilde{\Sigma}_1^2\right] \\
&= \sum_k \epsilon_k \left[\frac{1}{1-\Sigma_1}\frac{[\tilde{\Sigma}_1+\tilde{\Sigma}_3 f_k - 1]^2}{1+f_k^2}\right] ,
\end{aligned}
\tag{B.30}
$$

where $\tilde{\Sigma} = \Sigma/(1+g)$ and exploiting that the constant(k-independent) terms shall vanish. In terms of the parameters a, b, c, the kinetic energy of the first color can be written as

$$
\begin{aligned}
K_1 &= \sum_k \epsilon_k \frac{1}{1+uab}\frac{[1+(g-1)ab+(g-1)cbf_k]^2}{1+f_k^2} \\
&= N\frac{2}{1+uab}\int d\epsilon D(\epsilon)\epsilon\frac{[1+(g-1)ab+(g-1)cbf(\epsilon)]^2}{1+f(\epsilon)^2} .
\end{aligned}
\tag{B.31}
$$

Bibliography

[Abr97] E. R. I. Abraham, W. I. McAlexander, J. M. Gerton, R. Cotéand, A. Dalgarnoand, and R. G. Hulet, *Triplet s-wave resonance in ^{6}Li collisions and scattering lengths of ^{6}Li and ^{7}Li*, Phys. Rev. A **55**, R3299 - R3302 (1997).

[Abr65] M. Abramowitz and I. A. Stegun: *Handbook of Mathematical Functions* (Dover Publications, Inc., New York, 1965).

[Aff88] I. Affleck and J. B. Marston, *Large-n limit of the Heisenberg-Hubbard model: Implications for high-T_c superconductors*, Phys. Rev. B **37**, 3774 - 3777 (1988).

[Aff89] I. Affleck, *Quantum spin chains and the Haldane gap*, J. Phys.: Condens. Matter: **1**, 3047-3072 (1989).

[Alf98] M. Alford, K. Rajagopal, and F. Wilczek, *QCD at finite baryon density: nucleon droplets and color superconductivity*, Phys. Lett. B **422**, 247-256 (1998).

[Alf99] M. Alford, K. Rajagopal, and F. Wilczek, *Color-flavor locking and chiral symmetry breaking in high density QCD*, Nucl. Phys. B **537**, 443-458 (1999).

[And95] M. H. Anderson, J. R. Ensher, M. R. Matthews, C. E. Wieman, and E. A. Cornell, *Observation of Bose-Einstein Condensation in a Dilute Atomic Vapor*, Science **269**, 198-201 (1995).

[Ari77] E. Arimondo, M. Inguscio, and P. Violino, *Experimental determinations of the hyperfine structure in the alkali atoms*, Rev. Mod. Phys. 49, 31 - 75 (1977).

[Ave89] J. Avery: *Hyperspherical Harmonics: Applications in Quantum Theory*, (Springer, 1989).

[Axi43] B. M. Axilrod and E. Teller, *Interaction of the van der Waals Type Between Three Atoms*, J. Chem. Phys. **11**, 299 (1943).

[Bar05] M. Bartenstein, A. Altmeyer, S. Riedl, R. Geursen, S. Jochim, C. Chin, J. Hecker Denschlag, R. Grimm, A. Simoni, E. Tiesinga, C. J. Williams, and P. S. Julienne, *Precise Determination of ^{6}Li Cold Collision Parameters by Radio-Frequency Spectroscopy on Weakly Bound Molecules*, Phys. Rev. Lett. **94**, 103201 (2005).

[Bel66] R. J. Bell and A. E. Kingston, *The van der Waals interaction of two or three atoms*, Proc. Phys. Soc. **88**, 901 (1966).

[Bet31] H. Bethe, *Zur Theorie der Metalle*, Z. Phys. **71**, 205-226 (1931).

[Bit96] D. Bitko, T. F. Rosenbaum, and G. Aeppli, *Quantum Critical Behavior for a Model Magnet*, Phys. Rev. Lett. **77**, 940 - 943 (1996).

[Blo07] I. Bloch, J. Dalibard, W. Zwerger, *Many-Body Physics with Ultracold Gases* (to appear in Rev. Mod. Phys.) arXiv:0704.3011 (2007).

[Bun97] J. Bünemann, F. Gebhard, and W. Weber, J. Phys.: Condens. Matter **9**, 7343-7358 (1997).

[Bun98] J. Bünemann, W. Weber, and F. Gebhard, Phys. Rev. B **57**, 6896 - 6916 (1998).

[Bun05] J. Bünemann, F. Gebhard, K. Radnóczi, and P. Fazekas, *Gutzwiller variational theory for the Hubbard model with attractive interaction*, J. Phys.: Condens. Matter **17**, 3807-3814 (2005).

[Car80] J. L. Cardy, M. Nauenberg, and D. J. Scalapino, *Scaling theory of the Potts-model multicritical point*, Phys. Rev. B **22**, 2560 - 2568 (1980).

[Car96] J. L. Cardy: *Scaling and Renormalization in Statistical Physics* (Cambridge University Press, 1996).

[Cha97] G. Chaboussant, M.-H. Julien, Y. Fagot-Revurat, L. P. Levy, C. Berthier, M. Horvatic, and O. Piovesana, *Identification of Nuclear Relaxation Processes in a Gapped Quantum Magnet:* ^1H *NMR in the* $S = 1/2$ *Heisenberg Ladder* $Cu_2(C_5H_{12}N_2)_2Cl_4$, Phys. Rev. Lett. **79**, 925 (1997).

[Che07] R. W. Cherng, G. Refael, and E. Demler, *Superfluidity and Magnetism in Multicomponent Ultracold Fermions*, Phys. Rev. Lett. **99**, 130406 (2007).

[Chi06] J. K. Chin, D. E. Miller, Y. Liu, C. Stan, W. Setiawan, C. Sanner, K. Xu, and W. Ketterle, *Evidence for superfluidity of ultracold fermions in an optical lattice*, Nature **443**, 961-964 (2006).

[Col05] P. Coleman, and A. J. Schofield, *Quantum criticality*, Nature **433**, 226-229 (2005).

[Dei93] J. Deisz, M. Jarrell, and D. L. Cox, *Dynamical properties of one-dimensional antiferromagnets: A Monte Carlo study*, Phys. Rev. B **48**, 10227 - 10239 (1993).

[Dam98] K. Damle and S. Sachdev, *Spin dynamics and transport in gapped one-dimensional Heisenberg antiferromagnets at nonzero temperatures*, Phys. Rev. B **57**, 8307 - 8339 (1998).

[Dam05] K. Damle and S. Sachdev, *Universal Relaxational Dynamics of Gapped One-Dimensional Models in the Quantum Sine-Gordon Universality Class*, Phys. Rev. Lett. **95**, 187201 (2005).

[DeM99] B. DeMarco and D. S. Jin, *Onset of Fermi Degeneracy in a Trapped Atomic Gas*, Science **285**, 1703-1706 (1999).

[DiF99] P. Di Francesco, P. Mathieu, and D. Sénéchal: *Conformal Field Theory* (Springer-Verlag, New York, Berlin, Heidelberg, corrected second printing, 1999).

[Don01] E. A. Donley, N. R. Claussen, S. L. Cornish, J. L. Roberts, E. A. Cornell, C. E. Wieman, *Dynamics of collapsing and exploding Bose-Einstein condensates*, Nature **412**, 295 - 299 (2001).

[Dot84] V. S. Dotsenko and V. A. Fateev, *Conformal algebra and multipoint correlation functions in 2D statistical models*, Nucl. Phys. B **240**, 312-348 (1984).

[Eis30] R. Eisenschitz and F. London, *Über das Verhältnis der van der Waalsschen Kräfte zu den homöopolaren Bindungskräften*, Z. Phys. **60**, 491-527 (1930).

[Fet71] A. L. Fetter and J. D. Walecka: *Quantum Theory of Many-Particle Systems* (McGraw-Hill Book Company, 1971).

[Fir90] M. E. Firmino, C. A. Faria Leite, S. C. Zilio, and V. S. Bagnato, *Process of stopping atoms with the Zeeman tuning technique with a single laser*, Phys. Rev. A **41**, 4070 - 4073 (1990).

[Fod02] Z. Fodor and S. D. Katz, *Lattice determination of the critical point of QCD at finite T and μ*, J. High Energy Phys. **03** 014 (2002).

[Ful64] P. Fulde and R. A. Ferrel, *Superconductivity in a Strong Spin-Exchange Field*, Phys. Rev. **135**, A550-A563 (1964).

[Geo96] A. Georges, G. Kotliar, W. Krauth, and M. J. Rozenberg, *Dynamical mean-field theory of strongly correlated fermion systems and the limit of infinite dimensions*, Rev. Mod. Phys. **68**, 13 - 125 (1996).

[Ger00] J. M. Gerton, D. Strekalov, I. Prodan and R. G. Hulet, *Direct observation of growth and collapse of a Bose-Einstein condensate with attractive interactions*, Nature **408**, 692-695 (2000).

[Gol98] D. Goldhaber-Gordon, H. Shtrikman, D. Mahalu, D. Abusch-Magder, U. Meirav, and M. A. Kastner, *Kondo effect in a single-electron transistor*, Nature (London) 391, 156-159 (1998).

[Gra94] I. S. Gradshteyn and I. M. Rhyzik: *Table of Integrals, Series, and Products* (Academic Press, Fifth edition, 1994).

[Gre02] M. Greiner, O. Mandel, T. Esslinger, T. W. Hänsch, I. Bloch, *Quantum phase transition from a superfluid to a Mott insulator in a gas of ultracold atoms*, Nature **415**, 39 - 44 (2002).

[Gre03] M. Greiner, C. A. Regal, D. S. Jin, *Emergence of a molecular Bose-Einstein condensate from a Fermi gas*, Nature **426**, 537 - 540 (2003).

[Gub85] J. E. Gubernatis, D. J. Scalapino, R. L. Sugar, and W. D. Toussaint, *Two-dimensional spin-polarized fermion lattice gases*, Phys. Rev. B **32**, 103 - 116 (1985).

[Had02] Z. Hadzibabic, C. A. Stan, K. Dieckmann, S. Gupta, M. W. Zwierlein, A. Grlitz, and W. Ketterle, *Two-Species Mixture of Quantum Degenerate Bose and Fermi Gases*, Phys. Rev. Lett. **88**, 160401 (2002).

[Hal83] A. F. M. Haldane, *Continuum dynamics of the 1-D Heisenberg antiferromagnet: Identification with the O(3) nonlinear sigma model*, Phys. Lett. **93** 464-468 (1983).

[Ham79] C. J. Hamer, J. B. Kogut, and L. Susskind, *Strong-coupling expansions and phase diagrams for the O(2), O(3), and O(4) Heisenberg spin systems in two dimensions*, Phys. Rev. D **19**, 3091 - 3105 (1979).

[Her76] J. A. Hertz, *Quantum critical phenomena*, Phys. Rev. B **14**, 1165 - 1184 (1976).

[Hof02] W. Hofstetter, J. I. Cirac, P. Zoller, E. Demler, and M. D. Lukin, *High-Temperature Superfluidity of Fermionic Atoms in Optical Lattices*, Phys. Rev. Lett. **89**, 220407 (2002).

[Hon04a] C. Honerkamp and W. Hofstetter, *Ultracold Fermions and the SU(N) Hubbard Model*, Phys. Rev. Lett. **92**, 170403 (2004).

[Hon04b] C. Honerkamp and W. Hofstetter, *BCS pairing in Fermi systems with N different hyperfine states*, Phys. Rev. B **70**, 094521 (2004).

[Hub59] J. Hubbard, *Calculation of Partition Functions*, Phys. Rev. Lett. **3**, 77 - 78 (1959).

[Ino98] S. Inouye, M. R. Andrews, J. Stenger, H.-J. Miesner, D. M. Stamper-Kurn, W. Ketterle, *Observation of Feshbach resonances in a Bose-Einstein condensate*, Nature **392**, 151 - 154 (1998).

[Jak98] D. Jaksch, C. Bruder, J. I. Cirac, C. W. Gardiner, and P. Zoller, *Cold Bosonic Atoms in Optical Lattices*, Phys. Rev. Lett. **81**, 3108 - 3111 (1998).

[Jep65] D. W. Jepsen, *Dynamics of a Simple Many-Body System of Hard Rods*, J. Math. Phys. **6**, 405 (1965).

[Joc03] S. Jochim, M. Bartenstein, A. Altmeyer, G. Hendl, S. Riedl, C. Chin, J. Hecker Denschlag, and R. Grimm, *Bose-Einstein Condensation of Molecules*, Science **302**, 2101-2103 (2003).

[Jos77] J. V. José and L. P. Kadanoff, S. Kirkpatrick, and D. R. Nelson, *Renormalization, vortices, and symmetry-breaking perturbations in the two-dimensional planar model*, Phys. Rev. B **16**, 1217 - 1241 (1977).

[Kit96] C. Kittel: *Introduction to Solid State Physics* (John Wiley & Sons, Inc., New York, Chichester, Brisbane, Toronto, Singapore, 1996, Seventh Edition).

[Kob79] R. Köberle and J. A. Swieca, *Factorizable Z(N) models*, Phys. Lett. B **86**, 209 (1979).

[Kob87] R. Köberle and V. Kurak, *The S-matrix of a factorizable supersymmetric Z(N) model*, Phys. Lett. B *191*, 295-298 (1987).

[Koh05] M. Köhl, H. Moritz, T. Stöferle, K. Günter, and T. Esslinger, *Fermionic Atoms in a Three Dimensional Optical Lattice: Observing Fermi Surfaces, Dynamics, and Interactions*, Phys. Rev. Lett. **94**, 080403 (2005).

[Lar64] A. I. Larkin and Y. N. Ovchinnikov, *Inhomogeneous State of Superconductors*, Soviet Physics JETP-USSR **20**, 762-769 (1965) [Zh. Eksp. Teor. Fiz. **47**, 1136, (1964)].

[Leb69] J. L. Lebowitz, J. Sykes, and J. K. Percus, *Kinetic-Equation Approach to Time-Dependent Correlation Functions*, Phys. Rev. **188**, 487 - 504 (1969).

[Len31] J. E. Lennard-Jones, *Cohesion*, Proc. Phys. Soc. **43**, 461-482 (1931).

[Loh94] H. v. Löhneysen, T. Pietrus, G. Portisch, H. G. Schlager, A. Schröder, M. Sieck, and T. Trappmann, *Non-Fermi-liquid behavior in a heavy-fermion alloy at a magnetic instability*, Phys. Rev. Lett. **72**, 3262 - 3265 (1994).

[Mac50] J. E. Mack, *A Table of Nuclear Moments, January 1950*, Rev. Mod. Phys. **22**, 64 - 76 (1950).

[Mar89] J. B. Marston and I. Affleck, *Large-n limit of the Hubbard-Heisenberg model*, Phys. Rev. B **39**, 11538 - 11558 (1989).

[Mar02] A. Marte, T. Volz, J. Schuster, S. Dürr, G. Rempe, E. G. M. van Kempen, and B. J. Verhaar, *Feshbach Resonances in Rubidium 87: Precision Measurement and Analysis*, Phys. Rev. Lett. **89**, 283202 (2002).

[McC68] B. M. McCoy, *Spin Correlation Functions of the X-Y Model*, Phys. Rev. **173**, 531 - 541 (1968).

[Met87] W. Metzner and D. Vollhardt, *Ground-state properties of correlated fermions: Exact analytic results for the Gutzwiller wave function*, Phys. Rev. Lett. **59**, 121 - 124 (1987).

[Met88] W. Metzner and D. Vollhardt, *Analytic calculation of ground-state properties of correlated fermions with the Gutzwiller wave function*, Phys. Rev. B **37**, 7382 - 7399 (1988).

[Met89] W. Metzner and D. Vollhardt, *Correlated Lattice Fermions in $d = \infty$ Dimensions*, Phys. Rev. Lett. **62**, 324 - 327 (1989).

[Mil93] A. J. Millis, *Effect of a nonzero temperature on quantum critical points in itinerant fermion systems*, Phys. Rev. B **48**, 7183 - 7196 (1993).

[Mit71] L. Mittag and M. J. Stephen, *Dual Transformations in Many-Component Ising Models*, J. Math. Phys. **12**, 441 (1971).

[Mod03] G. Modugno, F. Ferlaino, R. Heidemann, G. Roati, and M. Inguscio, *Production of a Fermi gas of atoms in an optical lattice*, Phys. Rev. A **68**, 011601R (2003).

[Moe95] A. J. Moerdijk, B. J. Verhaar, and A. Axelsson, *Resonances in ultracold collisions of ^{6}Li, ^{7}Li, and ^{23}Na*, Phys. Rev. A **51**, 4852 - 4861 (1995).

[Morg88] I. Morgenstern and D. Würtz, *Monte Carlo simulations for two-dimensional quantum systems* , Zeitschrift für Physik B: Cond. Matt. **70**, 115-120 (1988).

[Mora88] R. M. Morra, W. J. L. Buyers, R. L. Armstrong, and K. Hirakawa, *Spin dynamics and the Haldane gap in the spin-1 quasi-one-dimensional antiferromagnet $CsNiCl_3$*, Phys. Rev. B **38**, 543 - 555 (1988).

[Mut89] H. Mutka, J. L. Soubeyroux, G. Bourleaux, P. Colombet, *Support for the Haldane conjecture: Gap for magnetic excitations in the quasi-one-dimensional S=1 Heisenberg antiferromagnet $AgVP_2S_6$*, Phys. Rev. B **39**, 4820 - 4823 (1989).

[Mut91] H. Mutka, C. Payen, P. Molini, J. L. Soubeyroux, P. Colombet, and A. D. Taylor, *Dynamic structure factor [S(Q,ω)] of the S=1 quasi-one-dimensional Heisenberg antiferromagnet: Neutron-scattering study on $AgVP_2S_6$*, Phys. Rev. Lett. **67**, 497 - 500 (1991).

[Neg98] J. W. Negele and H. Orland: *Quantum Many-Particle Systems* (Perseus Books, 1998).

[Neu07] M. Neumann, J. Nyéki, B. Cowan, and J. Saunders, *Bilayer ^{3}He: A Simple Two-Dimensional Heavy-Fermion System with Quantum Criticality*, Science **317**, 1356 - 1359 (2007).

[Nik07] P. Nikolić and S. Sachdev, *Renormalization-group fixed points, universal phase diagram, and 1/N expansion for quantum liquids with interactions near the unitarity limit*, Phys. Rev. A **75**, 033608 (2007).

[Noz80] P. Nozières, and A. Blandin, *Kondo effect in real metals*, J. Phys. **41**, 193211 (1980).

[Par06a] G. B. Partridge, W. Li, R. I. Kamar, Y. Liao, and R. G. Hulet, *Pairing and Phase Separation in a Polarized Fermi Gas*, Science **311**, 503 - 505 (2006).

[Par06b] G. B. Partridge, W. Li, Y. A. Liao, M. Haque, H. T. C. Stoof, and R. G. Hulet, *Deformation of a Trapped Fermi Gas with Unequal Spin Populations*, Phys. Rev. Lett. **97**, 190407 (2006).

[Poto07] R. M. Potok, I. G. Rau, H. Shtrikman, Y. Oreg, and D. Goldhaber-Gordon, *Observation of the two-channel Kondo effect*, Nature **446**, 167-171 (2007).

[Potts52] R. B. Potts, *Some Generalized Order-Disorder Transformations*, Proc. Cambridge Philos. Soc. **48**, 106 (1952).

[Rap06] Ákos Rapp and Gergely Zaránd, *Dynamical correlations and quantum phase transition in the quantum Potts model*, Phys. Rev. B **74**, 014433 (2006).

[Rap07] Ákos Rapp, Gergely Zaránd, Carsten Honerkamp, and Walter Hofstetter, *Color Superfluidity and Baryon Formation in Ultracold Fermions*, Phys. Rev. Lett. **98**, 160405 (2007).

[Rap08a] Ákos Rapp, Walter Hofstetter, Gergely Zaránd, *Trionic phase of ultracold fermions in an optical lattice: a variational study*, Phys. Rev. B **77**, 144520 (2008).

[Rap08b] Ákos Rapp and Gergely Zaránd, *Universal Diffusive Decay of Correlations in Gapped One-Dimensional Systems*, preprint (2008).

[Rap08c] Ákos Rapp, Lars Fritz and Gergely Zaránd, *Possibility of Topological Excitations in a Three-Component, SU(2)xU(1) Attractive Hubbard Model*, unpublished (2008).

[Rap08d] Ákos Rapp, Csaba Tőke, Walter Hofstetter and Gergely Zaránd, *Effective Hamiltonian and Density Waves in the Attractive SU(3) Hubbard Model*, unpublished (2008).

[Rega04] C. A. Regal, M. Greiner, and D. S. Jin, *Observation of Resonance Condensation of Fermionic Atom Pairs*, Phys. Rev. Lett. **92**, 040403 (2004).

[Regn94] L. P. Regnault, I. Zaliznyak, J. P. Renard, and C. Vettier, *Inelastic-neutron-scattering study of the spin dynamics in the Haldane-gap system* $Ni(C_2H_8N_2)_2NO_2ClO_4$, Phys. Rev. B **50**, 9174 - 9187 (1994).

[Rei98] L. E. Reichl: *A modern course in statistical physics* (John Wiley and Sons, Inc., 2nd edition, 1998).

[Sac94] S. Sachdev, T. Senthil, and R. Shankar, *Finite-temperature properties of quantum antiferromagnets in a uniform magnetic field in one and two dimensions*, Phys. Rev. B **50**, 258 - 272 (1994).

[Sac97a] S. Sachdev and K. Damle, *Low Temperature Spin Diffusion in the One-Dimensional Quantum O(3) Nonlinear Model*, Phys. Rev. Lett. **78**, 943 - 946 (1997).

[Sac97b] S. Sachdev and A. P. Young, *Low Temperature Relaxational Dynamics of the Ising Chain in a Transverse Field*, Phys. Rev. Lett. **78**, 2220 - 2223 (1997).

[Sac99] S. Sachdev: *Quantum Phase Transitions* (Cambridge University Press, 1999).

[Sal97] J. Salas and A. D. Sokal, *Logarithmic Corrections and Finite-Size Scaling in the Two-Dimensional 4-State Potts Model*, J. Stat. Phys. **88**, 567-615 (1997).

[Sar63] G. Sarma, *On the influence of a uniform exchange field acting on the spins of the conduction electrons in a superconductor*, J. Phys. Chem. Solids **24**, 1029-1032 (1963).

[Sen04a] T. Senthil, A. Vishwanath, L. Balents, S. Sachdev, and M. P. A. Fisher, *Deconfined Quantum Critical Points*, Science **303**, 1490 - 1494 (2004).

[Sen04b] T. Senthil, L. Balents, S. Sachdev, A. Vishwanath, and M. P. A. Fisher, *Quantum criticality beyond the Landau-Ginzburg-Wilson paradigm*, Phys. Rev. B **70**, 144407 (2004).

[Shi06] Y. Shin, M. W. Zwierlein, C. H. Schunck, A. Schirotzek, and W. Ketterle, *Observation of Phase Separation in a Strongly Interacting Imbalanced Fermi Gas*, Phys. Rev. Lett. **97**, 030401 (2006).

[Shi08] Y. Shin, C. H. Schunck, A. Schirotzek, W. Ketterle, *Phase diagram of a two-component Fermi gas with resonant interactions*, Nature **451**, 689 - 693 (2008).

[Sol03] A. V. Sologubenko, S. M. Kazakov, H. H. Ott, T. Asano, and Y. Ajino, *Diffusive energy transport in the S=1 Haldane chain compound* $AgVP_2S_6$, Phys. Rev. B **68**, 094432 (2003).

[Sol81a] J. Sólyom and P. Pfeuty, *Renormalization-group study of the Hamiltonian version of the Potts model*, Phys. Rev. B 24, 218 - 229 (1981).

[Sol81b] J. Sólyom, *Duality of the block transformation and decimation for quantum spin systems*, Phys. Rev. B 24, 230 - 243 (1981).

[Sta98] D. M. Stamper-Kurn, M. R. Andrews, A. P. Chikkatur, S. Inouye, H.-J. Miesner, J. Stenger, and W. Ketterle, *Optical Confinement of a Bose-Einstein Condensate*, Phys. Rev. Lett. **80**, 2027 - 2030 (1998).

[Swe81] R. H. Swendsen, D. Andelman, and A. Nihat Berker, *Critical exponents and marginality of the four-state Potts model: Monte Carlo renormalization group*, Phys. Rev. B **24**, 6732 - 6735 (1981).

[Tak96] M. Takigawa, T. Asano, Y. Ajiro, M. Mekata, and Y. J. Uemura, *Dynamics in the $S = 1$ One-Dimensional Antiferromagnet $AgVP_2S_6$ via ^{31}P and ^{51}V NMR*, Phys. Rev. Lett. **76**, 2173 - 2176 (1996).

[Tie91] E. Tiesinga, S. J. M. Kuppens, B. J. Verhaar, and H. T. C. Stoof, *Collisions between cold ground-state Na atoms*, Phys. Rev. A **43**, 5188 - 5190 (1991).

[Tru01] A. G. Truscott, K. E. Strecker, W. I. McAlexander, G. B. Partridge, and R. G. Hulet, *Observation of Fermi Pressure in a Gas of Trapped Atoms*, Science **291**, 2570-2572 (2001).

[Uhr93] G. S. Uhrig and R. Vlaming, *Inhibition of phase separation and appearance of new phases for interacting spinless fermions*, Phys. Rev. Lett. **71**, 271 - 274 (1993).

[Vog97] J. M. Vogels, C. C. Tsai, R. S. Freeland, S. J. J. M. F. Kokkelmans, B. J. Verhaar, and D. J. Heinzen, *Prediction of Feshbach resonances in collisions of ultracold rubidium atoms*, Phys. Rev. A **56**, R1067 - R1070 (1997).

[Voj03] M. Vojta, *Quantum phase transitions*, Rep. Prog. Phys. **66**, 2069-2110 (2003).

[Wil07] F. Wilczek, *Quantum chromodynamics: Lifestyles of the small and simple*, Nature Physics **3**, 375 - 376 (2007).

[Wu82] F. Y. Wu, *The Potts model*, Rev. Mod. Phys. **54**, 235 - 268 (1982).

[Xu96] G. Xu, J. F. DiTusa, T. Ito, K. Oka, H. Takagi, C. Broholm, and G. Aeppli, *Y_2BaNiO_5: A nearly ideal realization of the S=1 Heisenberg chain with antiferromagnetic interactions*, Phys. Rev. B **54**, R6827 - R6830 (1996).

[Zam78] A. B. Zamolodchikov and Al. B. Zamolodchikov, *Relativistic factorized S-matrix in two dimensions having O(N) isotopic symmetry*, Nuclear Physics B **133**, 525-535 (1978).

[Zaw80] A. Zawadowski, *Kondo-like State in a Simple Model for Metallic Glasses*, Phys. Rev. Lett. **45**, 211214 (1980).

[Zwi03] M. W. Zwierlein, C. A. Stan, C. H. Schunck, S. M. F. Raupach, S. Gupta, Z. Hadzibabic, and W. Ketterle, *Observation of Bose-Einstein Condensation of Molecules*, Phys. Rev. Lett. **91**, 250401 (2003).

[Zwi04] M. W. Zwierlein, C. A. Stan, C. H. Schunck, S. M. F. Raupach, A. J. Kerman, and W. Ketterle, *Condensation of Pairs of Fermionic Atoms near a Feshbach Resonance*, Phys. Rev. Lett. **92**, 120403 (2004).

[Zwi06a] M. W. Zwierlein, A. Schirotzek, C. H. Schunck, and W. Ketterle, *Fermionic Superfluidity with Imbalanced Spin Populations*, Science **311**, 492-496 (2006).

[Zwi06b] M. W. Zwierlein, C. H. Schunck, A. Schirotzek, W. Ketterle, *Direct observation of the superfluid phase transition in ultracold Fermi gases*, Nature **442**, 54 - 58 (2006).